University of Nottingham

School of Mathematical Sciences

Quantum communication and metrology in curved spacetime

Jan Kohlrus

A thesis submitted to the University of Nottingham for the degree of

Doctor of Philosophy

January 2019

Abstract

In this thesis we study relativistic effects on quantum systems. Quantum physics in curved spacetime is reviewed in a first place, with a focus on continuous variables formalism, quantum metrology techniques, and the relativistic treatment of polarised photons. Then, three topics of interest are studied. The first one is the phononic gravitational wave detector, where resonant mode-mixing and particle creation are triggered in a Bose-Einstein condensate by the passing of a gravitational wave, which can then be measured thanks to quantum metrology techniques. The theory for the phonons' transformation is developed in details in different resonance scenarios and some sources of noise are considered, like shaking of the cavity where the condensate is trapped and thermal noise. The second topic adressed is quantum communication and metrology in space. In this part, we describe quantum experiments involving communications between Earth and satellites using frequency modes of photons. The propagated and measured photons encode parameters of the spacetime background that can be measured using quantum metrology. Several satellite schemes are discussed, such as satellite to satellite radial communications in Kerr spacetime or Earth to satellite communications in Schwarzschild spacetime. The last topic of this thesis is the evolution of helicity states of photons in a relativistic picture. Two experiments are considered: one where the photons propagate between Earth and satellites through the curved spacetime background surrounding the Earth. The other experiment looks at quantum states of polarised photons as seen by centrifuged observers. For each of these parts, we provide the theory for novel experimental proposals, within the frameworks of either (or both) quantum communications and quantum metrology, that, we believe, would lead to a better understanding in the overlap of quantum mechanics and the relativity theories.

Acknowledgements

I would like to address my thanks to everyone who helped me in any way to carry out the research that lead to this thesis. In particular:

To the university of Nottingham for having made this possible, and to the university of Vienna for welcoming me for almost two years.

To Ivette Fuentes for giving me the chance to do this work in a first place. I am very grateful for your enthusiasm, the opportunities you gave me to meet new people and to start numerous projects, and for the confidence I received from you. To Jorma Louko, I am very grateful for the help you provided me with the calculations, the physical insights, and for the numerous discussions we had about my projects. To (Master) David Bruschi for sharing the satellite projects with me and for the guidance you offered all along the way. I hope our work will inspire many satellite experiments!

To my examiners Daniel Oi and Madalin Guta for the careful reading of this thesis and the useful advices and suggested corrections.

To the whole Fuentes group, and in particular: Richard Howl for the numerous discussions on the gravitational wave detector and Dennis Rätzel for your advices and help regarding academia. To everyone I met in academia who helped me get new ideas, or simply with whom I shared nice moments.

To M. Laguerre, for giving me the interest I have for physics since then. To M. Oury, for making me develop the same interest for mathematics. To the fundamental physics department in Orsay and the mathematical physics Master in Marseille for perpetuating this appeal in me. To Alejandro Perez for the help and advices, in particular for telling me about Ivette's works.

To my parents, thank you for the warm welcome whenever I felt the need to come back home. To my friends in Toulouse and elsewhere, thank you for still being the same to me despite my long absences! Finally I would like to thank Ana. Without you life would be very different, and I am not sure I would have been able to achieve what I did. Thank you!

CONTENTS

PUBLICATIONS

The work carried out in this thesis lead to the following publications.

As first author (most of the work done by me):

1. *Quantum communications and quantum metrology in the spacetime of a rotating planet* [1]
2. *Quantum metrology of spacetime parameters of the Earth beating classical precision* [2]
3. *Wigner phase of photonic helicity states in the spacetime of the Earth* [3]

As a co-author (most of the work done by other authors):

4. *Thermal noise in BEC-phononic gravitational wave detectors* [4]
5. *Ultimate precision: Gaussian parameter estimation in flat and curved spacetime* [5]

LIST OF FIGURES

1

INTRODUCTION

General relativity and quantum physics are the two fundamental theories of modern physics that have been widely proven correct since their creation. The former predicts how length and duration change with respect to moving observers and by the presence of mass-energy, while the latter describes microphysics where concepts such as localisation and particles become hazy. Their respective mathematical foundations are very different: general relativity is based on Riemannian geometry while the quantum theotry works on Hilbert spaces. In quantum theory, time and space are absolute, while in relativity these are relative concepts. These and many other fundamental differences explain why the search for a theory encompassing both general relativity and quantum physics has been so challenging.

Each of these two theories has been proven extensively successful, and they keep being proven correct through new experiments. An anomaly of Newton's mechanics, the perihelion precession of Mercury noticed in 1859, has only been explained when general relativity was completed [6], which gave credit to the theory even before dedicated experimental demonstration. Still, a wide range of experimental tests in different regimes have been passed since then, from the deflection of light by the sun measured by Eddington in 1919 [7] to the measurement of gravitational waves from a binary black hole merger in 2016 [8]. Quantum theory was also introduced thanks to the failure of previous theories to explain a physical system that, it seemed, should have belonged to classical physics. It's only thanks to the

introduction of the quantum of energy by Planck [9] that the black body radiation could be understood. The other quantum features that we are now familliar with have been witnessed later on, like the wave-particle nature of electrons which has been measured in 1928 [10], and the Bell experiments that have now definitely proven the non local-realistic nature of the theory [11, 12].

It is generally believed that the quantum and relativity theories are relevant only at very distinct scales: quantum physics is interesting to study microscopic systems, while general relativity acts on macroscopic scales. However, there are already many examples of physical situations where special relativity and quantum physics overlap, for example in particle accelerators [13] or in quantum chemistry where the behaviour of heavy elements cannot be explained without taking relativistic effects into account [14]. The overlap between general relativity and quantum physics is also investigated, despite the widespread belief of the mismatch of their domains of applicability. Recent examples include the alteration of wave functions due to spacetime curvature changes along the arms of an optical interferometer [15] and a test of the equivalence principle using quantum superpositions [16]. Small scale general relativistic experiments such as the measurement of time dilation of clocks separated by a few tens of centimeters [17] together with the observation of quantumness at a macroscopic scale [18] and for large molecules [19] also indicate the need to find a way to use the features of both theories together. There is now a large variety of modern quantum experiments where relativistic effects play a role that cannot be ignored, that could be tested in the lab [20] or using satellites [21].

Satellite experiments are very promising for the exploration of relativistic effects on quantum states. Communications with satellites permit to propagate quantum states over large distances, where changes caused by the curved spacetime background are important. Quantum communication has already been established in a first place with schemes using satellites with retroreflectors [22, 23, 24, 25]. The loss of quantum coherence of laser

signals sent from a geostationary satellite, due to both the Earth's gravity and atmosphere, was measured and characterised in [26]. Within the last couple of years, a lot happened in the field of quantum experiments with satellites. Correlated pairs of photons were generated aboard a nanosatellite in 2016 [27] and entangled ones in 2017 [28]. An example of practical implementation of a quantum scheme necessitating satellites are quantum key distritribution (QKD) protocols. Such protocols would in principle enable secure communications thanks to the use of quantum features. A feasibility study for such protocols was carried out in [29] and a review on the progress made was published last year [30]. Last year has also seen the first QKD protocol between space and Earth [31] being established thanks to the Chinese satellite Micius. The Chinese group lead by Jian-Wei Pan also successfully established quantum teleportation [32] and entanglement distribution [32] protocols. They also established the first intercontinental quantum network [33], between China and Austria, at the end of last year. These recent successes show how relevant is the search for a theory that deals with both quantum features and relativistic effects at the same time: we are entering the era of large scale quantum communications, which means that spacetime curvature effects can no longer be ignored from the usual quantum communication theory. A proper theoretical description of these relativistic effects will be required in order to compensate for them, such that the usual protocols of quantum communications keep working properly.

These technological advances bring as well the possibility to use satellite communications for fundamental research purposes, i.e. to probe the effects of curved spacetime and motion of observers on the measurement of quantum systems [34]. Some proposals are aiming in the direction of taking advantage of these effects, for example for metrology purposes [35, 1]. Such schemes are developed in this thesis, in chapters 6 and 7. Other proposals are also considering space quantum experiments yet outside of the scope of communications, e.g. a test of the weak equivalence principle using atom interferometers in space [36], or a measurement of entanglement between

two Bose Einstein condensates (BEC) in satellites when they change their orbits around the Earth [37].

The overlap between quantum and relativistic theories is also sought theoretically in the extreme cases of cosmological [38] and black hole spacetime singularities [39], but these require a complete theory of quantum gravity where the notions of spacetime and quantum become very closely intertwined. In our work, we are not interested in such regimes, we rather focus our attention on possible relativistic deviations from known results of (Galilean) quantum physics. To do so, we use the framework of the semi-classical theory that incorporates both the quantum and relativity theories: Quantum Field Theory (QFT) in Curved Spacetime (QFTCS) [40].

Within this framework was proposed a new experimental scheme to detect gravitational waves: squeezed states of phonons in a BEC resonate with the gravitational wave and undergo strong alterations due to the passing of the wave [41]. Contrarily to the setup that lead the spectacular direct measurement of gravitational waves two years ago [8], such a scheme would be much more compact, movable and cheap. The theory between this proposal is developed in chapter 4, and some possible sources of noise are studied in chapter 5.

Whether with the phononic gravitational wave detector or with the satellite communications considered in chapters 6 and 7, the quantum states considered are frequency modes of phonons and photons respectively. Phonons are spinless particles, but what about the photons' helicity? In the last part of this thesis, we address other quantum experiments but now focusing on the polarisation degree of freedom of light: in chapter 8 we develop the theory for a quantum experiment proposal using again satellite communication links, but here exchanging wavepackets of momentum-helicity states of photons between Earth and satellites. This is motivated by the extensive use of polarisation states of light in satellite experiments [31, 32, 42, 33, 22, 29], mainly because of their stronger resilience to noise, in particular caused by the atmosphere. Motivated by the recent experiment [43] using polarised

light to proble the entanglement of photons in a centrifuge, we worked out the theory for a similar experimental proposal in chapter 9. However, we consider different helicity states than in [43], which should enable a measurable effect to arise at measurement by the centrifuged observer.

To sum up, the structure of the thesis is as follows:

In part I, we introduce frameworks required to carry out the computations performed in this thesis. First, we briefly review quantum physics in curved spacetime in chapter 2. After a brief review of the fundamental concepts of quantum physics in 2.1, we introduce general relativity in 2.2 and provide the mathematical treatment for observers and light rays in the Schwarzschild and Kerr spacetimes. Then we give a brief summary of quantum field theory in curved spacetime in 2.3. The following chapter 3 aims at introducing some more advanced formalisms that will be used throughout the thesis: the covariance matrix formalism introduced in 3.1 will be the framework we will use to describe frequency modes of phonons and photons, quantum metrology tools given in 3.2 will help us evaluate possible quantum experiments in space, and finally the polarisation rotation of light and its induced photonic Wigner phase are described in 3.3.

In part II, we study the proposal for a phononic gravitational wave detector. The theory for the transformation of the phononic field due to the presence of a gravitational wave is reviewed and extended in chapter 4. Characterisation of the effects of shaking and thermal noises on the phonon field is carried out in chapter 5.

In part III, we look at quantum communication and quantum metrology schemes between Earth and satellites using frequency modes of photons. Previous results are extended in chapter 6 by taking into account the Earth's rotation, special relativistic effects, and by considering quantum communications between satellites. General quantum communications in Schwarzschild spacetime are considered in chapter 7, together with the proposal for a quantum experiment beating the state-of-the-art precision for the measurement of the Earth's Schwarzschild radius.

In part IV, we investigate relativistic effects on helicity states of photons. In chapter 8, such effects are investigated within the scope of satellite quantum communications with the Earth. Similar effects are discussed within the picture of a centrifuge experiment in chapter 9.

Finally, we conclude on the results of the thesis in chapter 10.

1.1 NOTATIONS

We employ geometrical units where the gravitational constant $G = 1$ and the speed of light in the vacuum $c = 1$. We also sometimes set the reduced Planck constant $\hbar$ to unity as well. Constants are restored when required for the sake of clarity.

Quantum operators are denoted with a hat: for example, the Hamiltonian operator is $\hat{H}$.

The Einstein summation convention is implied for repeated indices, i.e. $\psi^\mu k_\mu = \sum_{\mu=0}^{3} \psi^\mu k_\mu = \sum_{\mu,\nu=0}^{3} \psi^\mu k^\nu g_{\mu\nu}$, where $g_{\mu\nu}$ are the components of the metric tensor $\boldsymbol{g}$.

Vectors, matrices, and in general tensors expressed in spacetime coordinates are denoted in bold characters. Vectors are written using the usual differential geometry notation [44], namely

$$\boldsymbol{X} = (X^t, X^r, X^\theta, X^\phi) = X^\mu \partial_\mu = X^t\, \partial_t + X^r\, \partial_r + X^\theta\, \partial_\theta + X^\phi\, \partial_\phi.$$

The notation $O(\epsilon^n)$ designates a term of order n in the parameter ϵ.

Functions appearing with a prime denote the function derived with respect to its single variable, i.e. $f'(x) = \frac{df(x)}{dx}$. Time or affine parameter derivatives are denoted by a dot above the quantity derived: $\frac{dx}{dt} = \dot{x}$.

The Pauli matrices are denoted by: $\boldsymbol{\sigma_x} = \boldsymbol{\sigma_1} = \left(\begin{smallmatrix} 0 & 1 \\ 1 & 0 \end{smallmatrix}\right)$, $\boldsymbol{\sigma_y} = \boldsymbol{\sigma_2} = \left(\begin{smallmatrix} 0 & -i \\ i & 0 \end{smallmatrix}\right)$ and $\boldsymbol{\sigma_z} = \boldsymbol{\sigma_3} = \left(\begin{smallmatrix} 1 & 0 \\ 0 & -1 \end{smallmatrix}\right)$.

The identity is denoted by $\mathbb{1}$ in general, and the identity matrix of dimension n by $\mathbb{1}_n$.

1.2 TABLE OF SYMBOLS AND STANDARD VALUES

Quantity	Symbol	Value (S.I. u.)	Value (natural u.)
Newton's gravitational constant	G	6.67408×10^{-11} $m^3.kg^{-1}.s^{-2}$	1
Speed of light in the vacuum	c	299792458 m/s	1
Reduced Planck constant	$\hbar$	$1.054571800 \times 10^{-34}$ J.s	/
Average radius of the Earth	R_E	6371 km	/
Average equatorial radius of the Earth	r_A	6378 km	/
Mass of the Earth	M	5.97×10^{24} kg	4.43×10^{-3} m
Schwarzschild radius of the Earth	r_S	8.87×10^{-3} m	/
Kerr parameter of the Earth	a	3.26 m	/
Angular velocity of the Earth	ω_A	7.29×10^{-5} rad/s	2.43×10^{-13} rad/m

Table 1.: Quantities used throughout the thesis with their symbols and standard values (in S.I. and natural units).

Part I.

Preliminary considerations and formalisms

2

QUANTUM PHYSICS IN CURVED SPACETIME

In this chapter we introduce all the basic formalisms and mathematical tools we will employ to describe the physical situtations we will encounter. In general, we will need to characterise the behaviour of quantum systems evolving on curved spacetime and as seen by observers in motion.

2.1 QUANTUM PHYSICS

In this section, we provide a brief review of the basic theory for the description of quantum states. The quantum theory is only Galilean relativistic, i.e. the quantum states are assumed to evolve in Euclidean space and absolute time, which is the same for the different observers at different locations and with different motions, keeps track of this evolution. The underlying Galilean symmetry of the theory is therefore incompatible with the relativistic theories (in the Einsteinian sense) which are constructed upon Lorentz invariance, and that will be introduced in the next section. In a subsequent section, we will provide a theory that manages to combine these relativistic theories with the quantum theory presented in the current section.

2.1.1 *Quantum systems*

States and observables

The information of a quantum system is contained in a quantum state. When this state can be written as a vector $|\psi\rangle$ belonging to a Hilbert space $\mathcal{H}$, the state is said pure. The vector space structure of the Hilbert space ensures that superpositions of quantum states remain in the Hilbert space, namely $a|\phi\rangle + b|\varphi\rangle = |a\phi + b\varphi\rangle \in \mathcal{H}$ for $(a, b) \in \mathbb{C}^2$. For any state vectors $|\psi\rangle, |\phi\rangle \in \mathcal{H}$ and respective dual vectors $\langle\psi|, \langle\phi| \in \mathcal{H}^* = L(\mathcal{H}, \mathbb{C})$, there is a Hermitian product $\langle\psi|\phi\rangle \doteq \langle\psi, \phi\rangle \in \mathbb{C}$. Quantum states are normalised to unity, namely $\langle\psi, \psi\rangle = 1$, such that we can give them a statistical interpretation. Then, the product $\langle\psi, \phi\rangle$ represents the overlap of the two states and the modulus square $|\langle\psi, \phi\rangle|^2$ gives the probability of transition amplitude from one state to the other.

In general, the quantum state is in a statistical mixture of pure states. We know the state vectors that could possibly represent the system but we lack knowledge to determine which one it actually is. We say that the quantum state is mixed and it is defined by a density operator: $\hat{\rho} = \sum_j p_j |\psi_j\rangle \langle\psi_j|$ where the p_j are the probabilities for the quantum state to be in the pure state $|\psi_j\rangle$, thus $\sum_j p_j = 1$. The density operator is Hermitian, has trace equal to one, and is positive semi-definite, i.e. $\langle\phi|\hat{\rho}|\phi\rangle \geq 0$, for any $|\phi\rangle \in \mathcal{H}$.

Physical quantities are represented by Hermitian operators, called observables. A Hermitian operator satisfies $\hat{O}^\dagger = \hat{O}$, where the dagger operation transposes and complex conjugates the operator. The value of the physical quantity represented by the observable $\hat{O}$ is given by $\langle\hat{O}\rangle_{|\psi\rangle} = \langle\psi|\hat{O}|\psi\rangle$ for a pure state and by $\mathrm{tr}(\hat{\rho}\hat{O})$ for a mixed state. A quantum system is therefore characterized by a Hilbert space of states together with an algebra of Hermitian operators describing the physical quantities.

Measurements

Measurements are described by a familly of operators $\{\hat{M}_n\}_{n\in\mathbb{N}}$. If m_n is the outcome of measurement $\hat{M}_n$ on the pure state $|\psi\rangle$, the probability to get this outcome is $q_n = \langle\psi|\,\hat{M}_n^\dagger\hat{M}_n\,|\psi\rangle$, with $\sum_n q_n = 1$ and therefore $\sum_n \hat{M}_n^\dagger\hat{M}_n = \mathbb{1}_{\mathcal{H}}$. Immediately after the measurement, the quantum state is changed: $|\psi'\rangle = \frac{1}{\sqrt{q_n}}\hat{M}_n\,|\psi\rangle$. For a mixed state, these relations read: $q_n = \mathrm{tr}(\hat{M}_n\,\hat{\rho}\,\hat{M}_n^\dagger)$ and $\hat{\rho}' = \frac{\hat{M}_n\,\hat{\rho}\,\hat{M}_n^\dagger}{\mathrm{tr}(\hat{M}_n\,\hat{\rho}\,\hat{M}_n^\dagger)}$. The measurement mechanism therefore makes the quantum state evolve discontinuously.

The Heisenberg uncertainty relations give bounds for the precision one can achieve for simultaneous measurements of conjugate quantities. For example, the position-momentum uncertainty relation is:

$$\Delta\hat{x}\,\Delta\hat{p}_x \geq \frac{\hbar}{2}, \tag{1}$$

where $\Delta\hat{O} = \sqrt{\langle\hat{O}^2\rangle_{|\psi\rangle} - \langle\hat{O}\rangle^2_{|\psi\rangle}}$ is the variance of the operator $\hat{O}$. This relation is purely quantum since the precisions can be arbitrary in the $\hbar \to 0$ limit. This inequality arises from the non-commutativity of the conjugate operators $\hat{x}$ and $\hat{p}_x$: $[\hat{x}, \hat{p}_x] = i\hbar\mathbb{1}_{\mathcal{H}}$. In general, for any two operators $\hat{O}_1$ and $\hat{O}_2$, we have $\Delta\hat{O}_1\,\Delta\hat{O}_2 \geq \frac{1}{2}\left|\langle[\hat{O}_1, \hat{O}_2]\rangle_{|\psi\rangle}\right|$.

2.1.2 *Entanglement*

A quantum state in $\mathcal{H} = \bigotimes_j \mathcal{H}_j$ is separable if $|\psi\rangle = \bigotimes_j |\psi_j\rangle$ for a pure state and if $\hat{\rho} = \sum_k p_k \bigotimes_j \hat{\rho}_j^k$ for a mixed state. When the state is not separable, then it said to be entangled. Entanglement is a quantum feature that has no classical equivalent.

Pure states

There are several ways to characterise the entanglement of a quantum state. In order to introduce measures of entanglement we need to first define the von Neumann entropy, which measures the mixedness of a state: $\mathrm{S}(\hat{\rho}) =$

$-\mathrm{tr}(\hat{\rho}\ln\hat{\rho}) = -\sum_j \lambda_j \ln\lambda_j$, where the λ_j are the eigenvalues of $\hat{\rho}$. A pure state has eigenvalues 0 or 1, which means that its von Neumann entropy vanishes. A pure and bipartite quantum state $|\psi\rangle \in \mathcal{H}_{AB} = \mathcal{H}_A \otimes \mathcal{H}_B$ with $\dim(\mathcal{H}_{AB}) < \infty$ has Schmidt decomposition $|\psi\rangle = \sum_{j=1}^{n} \alpha_j |\psi_j^A\rangle |\psi_j^B\rangle$, where $\alpha_j \geq 0$ for all j, $\sum_j^n \alpha_j^2 = 1$, and $n = \min(\dim\mathcal{H}_A, \dim\mathcal{H}_B)$. The $\{|\psi_j^A\rangle\}$, $\{|\psi_j^B\rangle\}$ form an orthonormal basis for $\mathcal{H}_A$ and $\mathcal{H}_B$, respectively. The reduced density operators for the two subsystems then read: $\hat{\rho}_A = \sum_{j=1}^{n} \alpha_j^2 |\psi_j^A\rangle \langle\psi_j^A|$ and $\hat{\rho}_B = \sum_{j=1}^{n} \alpha_j^2 |\psi_j^B\rangle \langle\psi_j^B|$. These reduced states are diagonal and they share the same spectrum of eigenvalues. Thanks to this feature we will be able to use one or the other reduced state indistinctively. Now, the argument goes as follows: If only one of the Schmidt coefficients α_j is non zero, say for $j = j_0$, it implies that $\alpha_{j_0} = 1$ and thus $\hat{\rho}_A = |\psi^A\rangle \langle\psi^A|$ is pure. This also implies that $|\psi\rangle$ is separable. Therefore, the entanglement of the state $|\psi\rangle$ is quantified by the mixedness of its reduced state. We can thus define our first measure of entanglement, the entropy of entanglement, as the von Neumann entropy of the reduced states:

$$\mathrm{E}(|\psi\rangle) = \mathrm{S}(\hat{\rho}_A) = \mathrm{S}(\hat{\rho}_B) = -\sum_j^n \alpha_j^2 \ln\alpha_j^2. \tag{2}$$

The state $|\psi\rangle$ is entangled if $0 < \mathrm{E}(|\psi\rangle) \leq \ln n$, and separable if $\mathrm{E}(|\psi\rangle) = 0$

Mixed states

There is no Schmidt decomposition for mixed or tripartite states, we can therefore not use the same argument. Yet there is another way for mixed states, using the partial transpose negativity criterion [45]. To begin, let's take the separable state $\hat{\rho} = \sum_j \omega_j \hat{\rho}_j^A \otimes \hat{\rho}_j^B$ with $\hat{\rho} \in \mathcal{H}_{AB} = \mathcal{H}_A \otimes \mathcal{H}_B$, $\hat{\rho}^A \in \mathcal{H}_A$ and $\hat{\rho}^B \in \mathcal{H}_B$. Let us now define the partial transposed state:

$$\hat{\rho}^{\mathrm{pt}} = \sum_j \omega_j \left(\hat{\rho}_j^A\right)^{\mathrm{t}} \otimes \hat{\rho}_j^B \tag{3}$$

Since $\left(\hat{\rho}_i^A\right)^{\mathrm{t}} = \left(\hat{\rho}_i^A\right)^*$ is non-negative and with unit trace, it is also a density operator. Therefore, $\hat{\rho}^{\mathrm{pt}}$ has only non-negative eigenvalues. By con-

traposition, we obtain the partial transpose negativity criterion: if the partial transpose of the state has negative eigenvalues, then the state is entangled. When $\dim \mathcal{H}_A \leq 2$ and $\dim \mathcal{H}_B \leq 3$ (or the other way round), the criterion is also sufficient, which means that the criterion becomes an equivalence instead of a simple implication. The equivalence is not true in general, there are entangled states that have partial transposed states with positive eigenvalues. To quantify the entanglement, we define a norm: $\|\hat{\rho}^{\mathrm{pt}}\| = \mathrm{tr}\sqrt{(\hat{\rho}^{\mathrm{pt}})^2} = \sum_j |\lambda_j| = \sum_k \lambda_k^+ - \sum_l \lambda_l^-$, where the λ_j, λ_k^+ and λ_l^- are the partial transpose's eigenvalues, the positive ones and the negative ones, respectively. We define the negativity of the state $\hat{\rho}$ as:

$$\mathcal{N}(\hat{\rho}) \doteq \frac{\|\hat{\rho}^{\mathrm{pt}}\| - 1}{2} = \frac{\|\hat{\rho}^{\mathrm{pt}}\| - \mathrm{tr}\,\hat{\rho}^{\mathrm{pt}}}{2} = \sum_k |\lambda_k^-|, \tag{4}$$

The more the partial transpose has negative eigenvalues of large amplitudes, the more the state $\hat{\rho}$ is entangled and the larger is the negativity. Another related measure of entanglement is the logarithmic negativity $\mathcal{E}_{\mathcal{N}}(\hat{\rho}) = \ln\|\hat{\rho}^{pt}\|$.

2.1.3 *Time evolution*

Schrödinger first introduced the time evolution description of a quantum system, where quantum states are time dependent but observables aren't. For a pure state, the equation that bears his name reads:

$$i\hbar \frac{d}{dt} |\psi_S(t)\rangle = \hat{H}_S |\psi_S(t)\rangle . \tag{5}$$

where it was assumed that the quantum system is an isolated system (which we will assume in general). For a system that is only closed, the Hamiltonian $\hat{H}_S(t)$ evolves in time, which is not convenient in this representation. One could then prefer the Heisenberg picture, where the quantum states are time independent but not the observables. In this representation, an observable $\hat{O}_H(t)$ evolves in time according to the Heisenberg equation:

$$i\hbar \frac{d}{dt}\hat{O}_H(t) = [\hat{H}_H(t), \hat{O}_H(t)] + i\hbar \frac{\partial \hat{O}_H(t)}{\partial t}. \tag{6}$$

Nonetheless, both evolution equations are only invariant under Galilean transformations. We are however interested in regimes with possible deviations from this classical quantum physics models. In order to establish such a relativistic formalism (in the sense of Lorentz symmetries), we will introduce the relativity theories in the next section.

2.2 RELATIVITY

In this section we introduce the concepts of general relativity that are important for the calculations performed in this thesis. Most aspects of special relativity are also introduced within the general relativistic framework. Special relativity introduced new concepts by working out the implications of the constancy of the speed of light in the vacuum: spacetime as a single entity, duration dilation and contraction of distances as seen by observers in motion, a new definition for the notion of simultaneity, and thus the relativity of the notions of time and space. General relativity enables to describe gravity in a completely novel framework. Newtonian mechanics was built in the same framework as the quantum theory described in the previous section: it is Galilean relativistic, it describes particles and observers evolving on Euclidean space and in absolute time due to the gravitational field of massive objects. General relativity took the reverse picture: the spacetime background itself is the gravitational field. In general relativity, the spacetime is a non-trivial field, it is in general dynamic, and it is shaped by the mass and energy distribution of the objects living in it. These latter objects then evolve according to the curvature of the spacetime. The present section will define explicitly curved spacetime backgrounds describing the neighbourhood of the Earth (i.e. the space around the Earth and far enough from other mass-energy objects). From there we can work out the relativistic trajectories of observers and of light rays in such curved backgrounds. This will enable us to describe in the next section the evolution of quantum states in curved spacetime backgrounds according to observers in motion.

2.2.1 *Spacetime*

The notions of spacetime and curvature

The theories of relativity established by Einstein at the beginning of the twentieth century brought a complete change of paradigm with respect to previous theories in physics. Special relativity showed in a first place that space and time are notions that become intertwined and cannot be separated in various situations. For example, the frequency of particles of light (photons) is different depending on the motion of the observer measuring it. Ten years later, general relativity achieved to push this conclusion even further: not only spacetime should be regarded as a single entity, but it is also a dynamic field. The equations of general relativity show how the spacetime curves under the presence of a mass-energy density, like the Earth for example. In the illustration with the light's frequency, this also leads to a new effect: two observers with the same motion, say two static observers for example, will measure the frequency of photons to be different at two different spacetime points in general. Such changes are very important for example for the quantum communications using photons that are studied in this thesis. In the next paragraph, we show how the non relativistic picture of Euclidean space and linear time are replaced by a dynamic Riemannian spacetime in order to account for this relativistic physics picture.

The spacetime and its metric

In the relativity theories, the spacetime can be defined as a differentiable manifold of dimension 4 embedded with a Lorentzian metric $\boldsymbol{g}$, that is a symmetric non-degenerate bilinear form with signature $(-,+,+,+)$. The metric defines a scalar product $\boldsymbol{g}(\boldsymbol{X},\boldsymbol{Y}) = g_{\mu\nu}X^\mu Y^\nu = X^\mu Y_\mu$, where $\boldsymbol{X}$ and $\boldsymbol{Y}$ are arbitrary 4-vectors, and in particular a line element $ds^2 = g_{\mu\nu}dx^\mu dx^\nu$, where $\boldsymbol{dx}$ is the infinitesimal 4-distance in the spacetime coordinates.

The special case of flat spacetime is given by the Minkowski metric, which has a matrix representation in the usual Cartesian coordinates of the simple form $\boldsymbol{g} = \boldsymbol{\eta} = \mathrm{diag}(-1, 1, 1, 1)$. Locally (within infinitesimal distances), neighbourhoods of points on the manifold of a curved spacetime can be mapped to such a Minkowski flat picture.

2.2.2 *Curves in spacetime*

Vectors and curves

Contrarily to the Euclidean space where the distances are positive, the spacetime's metric tensor yields a scalar product that is not positive definite due to the Lorentzian signature of the spacetime. Vectors are then classifield in three different categories depending on the sign of their norm squared. If $\boldsymbol{g}(\boldsymbol{X}, \boldsymbol{X}) < 0$, the vector $\boldsymbol{X}$ is timelike, if $\boldsymbol{g}(\boldsymbol{X}, \boldsymbol{X}) = 0$ it is null (also sometimes named lightlike), and if $\boldsymbol{g}(\boldsymbol{X}, \boldsymbol{X}) > 0$ it is spacelike. A curve $\gamma(\lambda)$ in the spacetime is said to be timelike, null or spacelike when its tangent vector $\gamma'(\lambda) = \frac{d\gamma(\lambda)}{d\lambda}$ is timelike, null or spacelike along the whole curve parametrised by λ, respectively. Timelike curves are the curves followed by massive particles while massless particles follow null curves. Timelike and null curves are called causal curves. Spacelike curves are the non causal curves. The length of a spacelike curve, also called proper length, is the curved generalisation of the usual concept of distance in Euclidean space.

Geodesic curves

The principle of stationary action applied to the arc length

$$S = \int ds = \int_\gamma \sqrt{g_{\mu\nu} \frac{dx^\mu}{d\lambda} \frac{dx^\nu}{d\lambda}}\, d\lambda, \tag{7}$$

where $\frac{d\boldsymbol{x}(\lambda)}{d\lambda}$ is the tangent vector at each point $\gamma(\lambda)$ along the curve, yields the following geodesic equations:

$$\frac{d^2 x^\mu}{d\lambda^2} + \Gamma^\mu{}_{\rho\sigma} \frac{dx^\rho}{d\lambda} \frac{dx^\sigma}{d\lambda} = 0, \tag{8}$$

with the Christophel symbols:

$$\Gamma^{\mu}{}_{\rho\sigma} = \frac{1}{2} g^{\mu\alpha} \left(\frac{\partial g_{\alpha\rho}}{\partial x^{\sigma}} + \frac{\partial g_{\alpha\sigma}}{\partial x^{\rho}} - \frac{\partial g_{\rho\sigma}}{\partial x^{\alpha}} \right), \tag{9}$$

and λ the chosen affine parameter along the geodesic. A common choice of affine parameter for a timelike curve γ_t is the proper time:

$$\tau = \int_{\gamma_t} \sqrt{-ds^2}. \tag{10}$$

The proper time is the time as seen by an observer following the timelike curve. Proper time is the relativistic generalisation of the classical concept of time for massive particles (and thus for physical observers).

Killing fields

Killing fields are fields of vectors or tensors that can be found in spacetimes that have some symmetry. A tensor K of order two is a Killing tensor if $\nabla_\mu K_{\nu\rho} + \nabla_\nu K_{\rho\mu} + \nabla_\rho K_{\mu\nu} = 0$, with $\boldsymbol{\nabla}$ the covariant derivative associated to the spacetime's metric, namely $\boldsymbol{\nabla g} = \mathbf{0}$. Similarly, a Killing vector field $\boldsymbol{K}$ obeys $\nabla_\mu K_\nu + \nabla_\nu K_\mu = 0$. The Lie derivative of the metric tensor vanishes along the curves followed by the Killing vector fields: the Killing vector field is an isometry for the metric.

Timelike Killing vector fields are necessary to define the notion of particles in curved spacetime. Such vector fields enable to split the positive and negative frequencies, and therefore to have a well defined tracking of the particles' time evolution. In a general spacetime, there is no guarantee of having such a vector field. Nevertheless, in the stationary spacetimes we are interested in and which we will introduce starting in the following paragraph, there is always the $\boldsymbol{\xi} = \boldsymbol{\partial_t}$ timelike Killing vector field to preserve a well defined notion of particles.

2.2.3 *Schwarzschild spacetime around the static Earth*

The Schwarzschild metric can be used to model the spacetime background of the vacuum surrounding the Earth if we assume our planet to be a static

spherical mass distribution, namely without any asperity or angular momentum. There are more refined spacetime metrics like the Hartle-Thorne metric [46], or the Kerr metric [47] that we'll introduce later on, that can take into account such features, at the price of a significant increase in the complexity of the analytical computations. In the usual Schwarzschild (i.e., asymptotically spherical) coordinates $(t, r, \theta, \phi) \in \mathbb{R}\times]2M, \infty[\times[0, \pi] \times [0, 2\pi[$, the matrix representation of the Schwarzschild metric reads:

$$g = \text{diag}\left(-\left(1 - \frac{2M}{r}\right), \frac{1}{1 - \frac{2M}{r}}, r^2, r^2 \sin^2\theta\right). \tag{11}$$

We adopt the following convention for the polar angle (latitude): $\theta = 0$ and $\theta = \pi$ indicate the Earth's North and South poles respectively, and we therefore have the equatorial plane placed at $\theta = \pi/2$. Notice that this latter convention, which is widely used in physics, is different from the geographic convention used for coordinates on our globe, where the latitude zero is given by the equator. Note that the only parameter in the metric is the mass of the Earth M. In the natural units $G = c = 1$ we are using, the Earth's mass M has the dimension of a length. The quantities of the form M/r have a value of $GM/r\,c^2$ in SI units, and for all the cases considered in our calculations this quantity will be very small. That is because all the radii we consider are larger than the Earth's radius R_E. Values $r \sim O(M)$ are only relevant for the study of very compact objects like black holes. We remain very far from these regimes, that means that we do not need to worry about the changes and singularities that can occur when $r \leq 2M$.

Because the metric does not depend on the time and azimuthal angle (longitude) coordinates t and ϕ, the spacetime has two Killing vector fields ∂_t and ∂_ϕ. This feature provides the photons and the observers with two conserved quantities, related to their energy and azimuthal angular momentum respectively. Due to the spherical symmetry of the Schwarzschild spacetime, the metric has two other spacelike Killing vector fields: $\sin\phi\,\partial_\theta + \cot\theta\cos\phi\,\partial_\phi$ and $\cos\phi\,\partial_\theta - \cot\theta\sin\phi\,\partial_\phi$, which with the already mentioned ∂_ϕ are the generators of the SO(3) rotations. The spherical symmetry pro-

vides us with a third conserved quantity that is linked to the square of the total angular momentum. More details will be given on these conserved quantities when we will define explicitely the null vectors later on.

Relevant observers in Schwarzschild spacetime

In the communication schemes considered in this thesis, two families of observers are of particular interest: the observers standing on Earth's surface, who are static and therefore accelerated in Schwarzschild spacetime, and the circularly and geodesically orbiting satellites. The motion of this first family of observers, the static observers, is given by the 4-velocity:

$$\boldsymbol{v_E} = \frac{1}{\sqrt{1-\frac{2M}{r}}}\,\boldsymbol{\partial_t}. \tag{12}$$

Such observers only evolve in time. Being at a fixed point in space, these observers are accelerated due to the presence of the gravitational field of the Earth. Their 4-acceleration reads: $\boldsymbol{a}(\boldsymbol{v_E}) = \left(1-\frac{2M}{r}\right)^{-\frac{1}{2}}\frac{M}{r^2}\,\boldsymbol{\partial_r}$. Let us now turn to the circularly orbiting observers. Such observers have a 4-velocity of the form $\boldsymbol{v_s} = \Gamma(\,\boldsymbol{\partial_t} + \omega\,\boldsymbol{\partial_\theta} + \zeta\,\boldsymbol{\partial_\phi})$ and they can be either accelerated or geodesic. Note that the static observer is a particular case of circularly orbiting observer, simply with vanishing angular velocities $\omega = \zeta = 0$. Then $\Gamma = \left(1-\frac{2M}{r}\right)^{-\frac{1}{2}}$ for the static case is obtained thanks to the constraint $\boldsymbol{g}(\boldsymbol{v_s},\boldsymbol{v_s}) = -1$ for the velocity that is an affinely parametrised timelike vector. Using this latter constraint for the general circularly orbiting observer, we obtain:

$$\boldsymbol{v_s} = \frac{1}{\sqrt{1-\frac{2M}{r}-r^2(\omega^2+\zeta^2\sin^2\theta)}}\left(\,\boldsymbol{\partial_t} + \omega\,\boldsymbol{\partial_\theta} + \zeta\,\boldsymbol{\partial_\phi}\right). \tag{13}$$

If we require the satellite to follow a geodesic, which means that the satellite doesn't need to use any fuel to remain on its orbit, the angular coordinate velocities for the satellite must have the following values:

$$\omega = \epsilon_\omega\sqrt{\frac{M}{r^3}}\sqrt{1-\frac{\sin^2\alpha}{\sin^2\theta}}, \quad \zeta = \epsilon_\zeta\sqrt{\frac{M}{r^3}}\frac{\sin\alpha}{\sin^2\theta}. \tag{14}$$

The angle $\alpha \in [0, \pi]$ indicates the inclination of the satellite's plane of orbit with respect to the Earth's polar axis. For all the values taken by the satellite's polar coordinate θ during its orbit, we thus always have $\alpha \leq \theta$. The constants $\epsilon_\omega = \pm 1$ and $\epsilon_\zeta = \pm 1$ give the sign of the satellite's angular velocities. Notice that we recover the usual Keplerian frequency $\sqrt{M/r^3}$ for the θ and ϕ motions when considering polar ($\alpha = 0\,[\pi]$) and equatorial ($\alpha = \theta = \pi/2$) orbits, respectively.

Null vectors in Schwarzschild spacetime

The trajectory followed by photons that propagate in the Schwarzschild spacetime can be represented by a classical light ray to a very good approximation. This light ray follows a null geodesic curve, which is defined by the field of null vectors tangent to it. In the Schwarzschild spacetime, at each point along this curve a light ray has a null vector of the form:

$$\boldsymbol{k} = E_p \left(\frac{1}{f(r)}\, \boldsymbol{\partial_t} + \epsilon_r \sqrt{1 - f(r)\frac{l_\phi^2 + \kappa}{r^2}}\, \boldsymbol{\partial_r} + \frac{\epsilon_\theta}{r} \sqrt{\frac{\kappa - l_\phi^2 \cot^2\theta}{r^2}}\, \boldsymbol{\partial_\theta} + \frac{l_\phi}{r^2 \sin^2\theta}\, \boldsymbol{\partial_\phi} \right), \tag{15}$$

with $f(r) = 1 - \frac{2M}{r}$, and $\epsilon_r = \pm 1$ and $\epsilon_\theta = \pm 1$ giving the sign of the radial and polar components of the null vector, respectively. Thanks to the staticity and spherical symmetry of the Schwarzschild spacetime, we have three constants of motion for each geodesic. The first one is E_p, which is the energy of the photon as it would be measured by an inertial observer at space infinity. In (15), we introduced the rescaled angular momentum and Carter constants $l_\phi = L_\phi / E_p$ and $\kappa = K/E_p^2$, in order to factor out the energy constant of the photon E_p. These two rescaled constants l_ϕ and κ are independent on the energy of the photon. The constants L_ϕ and $K \geq 0$ are the azimuthal angular momentum and the Carter constant -a quantity related to the square of the total angular momentum [48] of the photon-, respectively, as seen by an inertial observer at spatial infinity. Notice that from (15) we can see that $\kappa \geq l_\phi^2 \cot^2\theta \geq 0$. The energy constant of motion $E_p > 0$ can be expressed in terms of the photon's frequency Ω measured by

an observer with velocity $\boldsymbol{v}$ through the relation $\hbar\Omega = -\boldsymbol{k}\cdot\boldsymbol{v}$. For the static observer (12) on Earth, we thus have:

$$E_p = \hbar\Omega_E\sqrt{1-\frac{2M}{R_E}}, \tag{16}$$

with the frequency of the photon Ω_E measured by a static observer on Earth's surface $r = R_E$. Unfortunately, the two angular constants of motion l_ϕ and κ cannot be obtained explicitly that easily. However there are some special cases where one can obtain at least a simple relation between them: for a trajectory constrained to the equatorial plane we have $\kappa = 0$, and for any radial light ray namely with $\theta = cst.$ and $\phi = cst.$, we have $l_\phi = \kappa = 0$. For a trajectory with a constant azimuthal angle ϕ but varying polar angle θ, $l_\phi = 0$ and $\kappa \geq 0$. The general procedure to obtain the constants l_ϕ and κ is the integration of the relations $\frac{dr}{k^r} = \frac{d\theta}{k^\theta}$ and $\frac{d\theta}{k^\theta} = \frac{d\phi}{k^\phi}$, respectively. From (15), these constraints are respectively:

$$\epsilon_r\int_{r_1}^{r_2}\frac{dr}{r^2\sqrt{1-\left(1-\frac{2M}{r}\right)\frac{\kappa+l_\phi^2}{r^2}}} = \epsilon_\theta\int_{\theta_1}^{\theta_2}\frac{d\theta}{\sqrt{\kappa-l_\phi^2\cot^2\theta}}, \tag{17}$$

$$\epsilon_\theta\, l_\phi\int_{\theta_1}^{\theta_2}\frac{d\theta}{\sin^2\theta\sqrt{\kappa-l_\phi^2\cot^2\theta}} = \phi_2-\phi_1 \equiv \Delta\phi, \tag{18}$$

where the spatial coordinates (r_1,θ_1,ϕ_1) and (r_2,θ_2,ϕ_2) denote the start and the end of the null geodesic, respectively. These coupled integral equations are not easily solvable analyticaly. To solve them requires either to make some approximation or to do it numerically.

2.2.4 *Kerr spacetime around the rotating Earth*

If the Earth's rotation about its polar axis is taken into account, the spacetime background surrounding the Earth is different from the Schwarzschild spacetime considered previously. The rotation of the mass distribution of the Earth actually drags the spacetime around it, which thus rotates as well. Such a spacetime is not static anymore but it is still stationary. Mathematically, this spacetime is implemented through the Kerr metric [47]. In

Boyer-Lindquist coordinates (t, r, θ, ϕ), which are asymptotically spherical coordinates, the line element for the Kerr spacetime reads:

$$\begin{aligned} ds^2 = &- \left(1 - \frac{2Mr}{\Sigma}\right) dt^2 + \frac{\Sigma}{r^2\,\Delta}\, dr^2 + \Sigma\, d\theta^2 \\ &+ \left(r^2 + a^2 + \frac{2Mra^2}{\Sigma} \sin^2\theta\right) \sin^2\theta\, d\phi^2 - \frac{4Mra}{\Sigma} \sin^2\theta\, dt\, d\phi, \end{aligned} \tag{19}$$

where $\Sigma = r^2 + a^2 \cos^2\theta$ and $\Delta = 1 - \frac{2M}{r} + \frac{a^2}{r^2}$. The Kerr parameter a is the Earth's self rotation angular momentum divided by its mass M, also called specific angular momentum. The Kerr solution reduces to the Schwarzschild one (11) when taking the static limit $a \to 0$. The Kerr metric admits two Killing vector fields ∂_t and ∂_ϕ, which arise respectively due to the metric's stationarity and axial symmetry. Also, the metric is invariant under the reflection $(t, \phi) \to (-t, -\phi)$. We broke the Schwarzschild spacetime's spherical symmetry by introducing the Earth's rotation, which means that we have lost the two other spacelike Killing vectors. However, there is a Killing tensor in Kerr spacetime which also provides a conserved quantity, the Carter constant. As in the Schwarzschild case, we will work at radii large enough to ignore all the issues arising from coordinate and physical singularities, that are relevant only for objects with considerably higher mass-energy densities than the Earth has.

In this thesis we will focus on the equatorial plane $\theta = \frac{\pi}{2}$ when considering the Kerr spacetime, in order to work with simpler analytical formulas. The reduced metric in the Boyer-Lindquist coordinates (t, r, ϕ) then reads:

$$ds^2 = -\left(1 - \frac{2M}{r}\right) dt^2 + \frac{1}{\Delta} dr^2 + \left(r^2 + a^2 + \frac{2Ma^2}{r}\right) d\phi^2 - \frac{4Ma}{r}\, dt\, d\phi. \tag{20}$$

Relevant observers in Kerr spacetime

In the Kerr spacetime, the observer on Earth's surface is not a static observer anymore: the Earth's rotation makes it follow a circular path of the form:

$$v_E = \frac{1}{\sqrt{1 - \zeta_0^2 \sin^2\theta (r^2 + a^2) - \frac{2Mr}{\Sigma}(1 - a\zeta_0 \sin^2\theta)^2}} \left(\partial_t + \zeta_0\, \partial_\phi\right), \tag{21}$$

where $\zeta_0 = aM/I$ is the Earth's (azimuthal) angular coordinate velocity about its axis, with I the Earth's moment of inertia. In the Schwarzschild limit $a \to 0$, the velocity (21) reduces to the one of the static observer (12). Like the static observers, our Earth observer (21) is accelerated. Another observer of interest is the geodesic satellite orbiting circularly in the Earth's equatorial plane. Its 4-velocity reads:

$$v_s = \frac{1}{\sqrt{1-\zeta_s^2(r^2+a^2)-\frac{2M}{r}(1-a\,\zeta_s)^2}}\left(\partial_t + \zeta_s\,\partial_\phi\right), \tag{22}$$

with $\zeta_s = \left[a + \epsilon_\zeta\sqrt{r^3/M}\right]^{-1}$ and $\epsilon_\zeta = \pm 1$ for co-rotating and counter-rotating orbits, respectively.

Null vectors in Kerr spacetime

In Kerr spacetime, the null vectors are given by [49]:

$$k^t = \frac{E_p}{\Sigma}\left[-a\left(a\sin^2\theta - l_\phi\right) + \frac{r^2+a^2}{r^2\Delta}\left(r^2+a^2-a\,l_\phi\right)\right], \tag{23a}$$

$$k^r = \epsilon_r\frac{E_p}{\Sigma}\sqrt{\left(r^2+a^2-a\,l_\phi\right)^2 - r^2\Delta\left(\kappa+(l_\phi-a)^2\right)}, \tag{23b}$$

$$k^\theta = \epsilon_\theta\frac{E_P}{\Sigma}\sqrt{\kappa - \cos^2\theta\left(\frac{l_\phi^2}{\sin^2\theta} - a^2\right)}, \tag{23c}$$

$$k^\phi = \frac{E_p}{\Sigma}\left[\frac{l_\phi}{\sin^2\theta} + \frac{2Mr - a\,l_\phi}{r^2\Delta}a\right]. \tag{23d}$$

The conserved quantities are here defined in the same way as they were already in the Schwarzschild spacetime.

2.3 QUANTUM FIELDS ON CURVED SPACETIME

After having given the description of quantum physics on one side and of the relativity theory on the other side, we would like to incorporate the two together in order to look at the evolution of quantum systems on a curved spacetime background and as seen by observers in motion. This is achieved within the framework of Quantum Field Theory (QFT) on Curved Spacetimes (QFTCS) [40] which we describe in the present section.

2.3.1 *Quantum fields*

In QFT, we study quantum fields whose excitations are the usual quantum particles. For example, photons propagating in curved spacetime are here viewed as excitations of a bosonic (or scalar, when we ignore the polarisation degree of freedom) field defined upon the spacetime's metric field. In order to describe a field of quantum particles, we first derive the field equations for the classical field ϕ, which will be quantised later on. Using Hamilton's variational principle on the Lagrangian density $\mathcal{L}(\phi, \partial\phi)$ of the field, namely $\delta S = \delta\left\{\int \mathcal{L}\left(\phi(\boldsymbol{x}), \partial\phi(\boldsymbol{x})\right) d\boldsymbol{x}\right\} = 0$, where $\partial\phi$ is the field's conjugate variable, we obtain the Euler-Lagrange equation:

$$\frac{\partial\mathcal{L}}{\partial\phi} - \partial_\mu\left(\frac{\partial\mathcal{L}}{\partial(\partial_\mu\phi)}\right) = 0. \tag{24}$$

From there, we can specialise to a particular field in order to obtain explicit field equations. In what follows we will take the example of the simplest possible field: the scalar field, also called Klein-Gordon field.

2.3.2 *Quantisation in curved spacetime*

Free real scalar field in Minkowski spacetime

The Lagrangian density for a free (real) scalar field in flat spacetime is $\mathcal{L} = \frac{1}{2}\left(\eta^{\mu\nu}(\partial_\mu\phi)(\partial_\nu\phi) + m^2\phi^2\right)$, where m is the mass of the field's elementary particles. The Euler-Lagrange equation then reads:

$$\partial^\mu\partial_\mu\phi - m^2\phi = (\Box - m^2)\phi = 0. \tag{25}$$

This equation is called Klein-Gordon equation and it admits a simple set of solutions, the plane waves:

$$u_{\vec{k}}(\boldsymbol{x}) = \frac{1}{(2\pi)^{\frac{3}{2}}\sqrt{2\omega_k}} e^{i(\vec{k}.\vec{x} - \omega_k t)} \tag{26}$$

with $\omega_k = \sqrt{\vec{k}^2 + m^2}$. Since we are in flat spacetime, the particles are defined on the whole Minkowski spacetime thanks to the global timelike

Killing vector field $\xi = \partial_t$. This set of solutions are eigenfunctions of the timelike Killing vector field: $\partial_t u_{\vec{k}} = -i\omega_k u_{\vec{k}}$. Antiparticles are given by the complex conjugate of the particles' mode functions, and we thus have: $\partial_t u^*_{\vec{k}} = i\omega_k u^*_{\vec{k}}$. Therefore, it is as if the antiparticles were particles with opposite frequency (and thus energy). We can define a scalar product for this space of solutions:

$$(\phi_1, \phi_2) = -i \int_{\Sigma_t} d\vec{x} \, (\phi_1(\partial_t \phi_2^*) - (\partial_t \phi_1)\phi_2^*) \,, \tag{27}$$

where Σ_t is a spacelike hypersurface of simultaneity at time t. With this scalar product, the mode functions are orthogonal: $\left(u_{\vec{k}_1}, u_{\vec{k}_2}\right) = \delta(\vec{k}_1 - \vec{k}_2)$. The antiparticles' mode function have opposite norm to the particles' one: $(u^*_{\vec{k}_1}, u^*_{\vec{k}_2}) = -\delta(\vec{k}_1 - \vec{k}_2)$. Furthermore, particles and antiparticles modes are orthogonal $(u_{\vec{k}_1}, u^*_{\vec{k}_2}) = 0$, they therefore form together a basis for the field.

Free real scalar field in curved spacetime

The Lagrangian density for the free (real) scalar field in curved spacetime is given by:

$$\mathcal{L} = \frac{1}{2}\sqrt{|g|}\left(g^{\mu\nu}(\partial_\mu \phi)(\partial_\nu \phi) + (m^2 + \gamma R)\phi^2\right), \tag{28}$$

where $g = \det \boldsymbol{g}$, R is the spacetime's Ricci scalar, and γ is the coupling constant between the scalar field and the spacetime. Using again the Euler-Lagrange equation (24) together with the Lagrangian density above yields the Klein-Gordon equation in curved spacetime:

$$(\Box - m^2 - \gamma R)\phi = 0 \tag{29}$$

with the d'Alembertian differential operator in curved spacetime:

$$\Box = \frac{1}{\sqrt{|g|}}\partial_\mu(\sqrt{|g|}g^{\mu\nu}\partial_\nu). \tag{30}$$

In this thesis, we will always work in the minimally coupled case $\gamma = 0$ and with massless particles. The Klein-Gordon equation then simplifies to a simple wave equation in curved spacetime $\Box\phi = 0$. The field solutions

can then be obtained in the same fashion as in the flat case, with more or less difficulty depending on the complexity of the spacetime considered. We then define a scalar product on the space of these solutions:

$$(\phi_1, \phi_2) = -i \int_\Sigma d\Sigma^\mu \sqrt{|g_\Sigma|} \left(\phi_1 \partial_\mu \phi_2^* - (\partial_\mu \phi_1)\phi_2^*\right), \tag{31}$$

where $d\Sigma^\mu = n^\mu d\Sigma$, and $\boldsymbol{n}$ is a future-directed unit vector orthogonal to the spacelike hypersurface Σ. $\boldsymbol{g_\Sigma}$ is the metric on this hypersurface and g_Σ denotes its determinant.

Quantisation

In order to proceed with the quantisation of the field, we need to introduce the structure that plays the role of the Hilbert space of particles in QFT: the Fock space. For a definite type of particle, for example the spinless particles associated to our free (real) scalar field, the Fock space is defined as the direct sum of the n particles Hilbert spaces:

$$\mathbb{F}(\mathcal{H}) = \bigoplus_{n=0}^{\infty} S(\mathcal{H})^{\otimes n} = \mathbb{C} \oplus \mathcal{H} \oplus S(\mathcal{H} \otimes \mathcal{H}) \oplus S(\mathcal{H} \otimes \mathcal{H} \otimes \mathcal{H}) \oplus \dots \tag{32}$$

The operator S either symmetrises or antisymmetrises the tensor products of individual particle's quantum states, for bosons and fermions respectively. The need for defining such new structure comes from the change of picture QFT brings about: particles are not absolute entities anymore, they are merely excitations of a quantum field that can be created and annihilated. The Fock space provides the relevant structure for a quantum state of several particles with a changing particle content. The free scalar particles and antiparticles that we found earlier on form together a complete orthonormal basis for our free (real) scalar field, which we can thus decompose:

$$\hat{\phi}(\boldsymbol{x}) = \int d\vec{k} \left[u_{\vec{k}}(\boldsymbol{x})\, \hat{a}_{\vec{k}} + u^*_{\vec{k}}(\boldsymbol{x})\, \hat{a}^\dagger_{\vec{k}}\right], \tag{33}$$

where $\hat{a}_{\vec{k}}$ and $\hat{a}^\dagger_{\vec{k}}$ are respectively the annihilation operator and its Hermitian conjugate the creation operator for particles of the mode $\vec{k}$. If the particles are bosons, these operators fulfil the commutation relation $[\hat{a}_{\vec{k}_1}, \hat{a}^\dagger_{\vec{k}_2}] = \delta(\vec{k}_1 -$

$\vec{k}_2$), together with $[\hat{a}_{\vec{k}_1}, \hat{a}_{\vec{k}_2}] = [\hat{a}^\dagger_{\vec{k}_1}, \hat{a}^\dagger_{\vec{k}_2}] = 0$. This guarantees the following commutation relations for the field $\hat{\phi}$ and its canonical conjugate momentum $\hat{\pi}$: $[\hat{\phi}(\boldsymbol{x}_1), \hat{\phi}(\boldsymbol{x}_2)] = [\hat{\pi}(\boldsymbol{x}_1), \hat{\pi}(\boldsymbol{x}_2)] = 0$ and $[\hat{\phi}(\boldsymbol{x}_1), \hat{\pi}(\boldsymbol{x}_2)] = i\delta(\vec{x}_1 - \vec{x}_2)$. If the particles are fermions, one needs to change the commutators for anticommutators instead. To give the action of such operators on a general Fock state, we need to first define a vacuum state, which is a Fock state that is empty of particles. A vacuum state $|0\rangle$ is defined thanks to the action of the annihilation operator: $\hat{a}_{\vec{k}} |0\rangle = 0$. From this empty state, one can create a state with arbitrary particle content, for example $|1_{\vec{k}_1}, 2_{\vec{k}_2}\rangle = \hat{a}^\dagger_{\vec{k}_2} \hat{a}^\dagger_{\vec{k}_1} \hat{a}^\dagger_{\vec{k}_2} |0\rangle$. In general, the action of the creation and annihilation operators is given by: $\hat{a}_{\vec{k}} |n_{\vec{k}}\rangle = \sqrt{n_{\vec{k}}}\, |n_{\vec{k}} - 1\rangle$ and $\hat{a}^\dagger_{\vec{k}} |n_{\vec{k}}\rangle = \sqrt{n_{\vec{k}} + 1}\, |n_{\vec{k}} + 1\rangle$.

2.3.3 *Bogolyubov transformations*

A Bogolyubov transformation is a change of basis in the Fock space. It is a unitary transformation that maps a Fock state to another Fock state but with a change in the particle content of the quantum state.

The quantum field can be decomposed in two different bases:

$$\hat{\phi}(\boldsymbol{x}) = \int d\vec{k} \left[u_{\vec{k}}(\boldsymbol{x})\, \hat{a}_{\vec{k}} + u^*_{\vec{k}}(\boldsymbol{x})\, \hat{a}^\dagger_{\vec{k}} \right], \tag{34}$$

$$\hat{\phi}(\boldsymbol{x}) = \int d\vec{k} \left[U_{\vec{k}}(\boldsymbol{x})\, \hat{A}_{\vec{k}} + U^*_{\vec{k}}(\boldsymbol{x})\, \hat{A}^\dagger_{\vec{k}} \right]. \tag{35}$$

The field modes and the annihilation and creation operators from each basis are related as follows:

$$U_{\vec{k}} = \int d\vec{k}' \left\{ \alpha_{\vec{k}'\vec{k}} u_{\vec{k}'} + \beta_{\vec{k}'\vec{k}} u^*_{\vec{k}'} \right\}, \tag{36}$$

$$\hat{A}_{\vec{k}} = \int d\vec{k}' \left\{ \alpha^*_{\vec{k}'\vec{k}} \hat{a}_{\vec{k}'} - \beta^*_{\vec{k}'\vec{k}} \hat{a}^\dagger_{\vec{k}'} \right\}, \tag{37}$$

$$u_{\vec{k}} = \int d\vec{k}' \left\{ \alpha^*_{\vec{k}'\vec{k}} U_{\vec{k}'} - \beta_{\vec{k}'\vec{k}} U^*_{\vec{k}'} \right\}, \tag{38}$$

$$\hat{a}_{\vec{k}} = \int d\vec{k}' \left\{ \alpha_{\vec{k}'\vec{k}} \hat{A}_{\vec{k}'} + \beta^*_{\vec{k}'\vec{k}} \hat{A}^\dagger_{\vec{k}'} \right\}. \tag{39}$$

where the $\alpha_{\vec{k}'\vec{k}} = (U_{\vec{k}'}, u_{\vec{k}})$ and $\beta_{\vec{k}'\vec{k}} = -(U_{\vec{k}'}, u^*_{\vec{k}})$ are the Bogolyubov coefficients. Note that the former maps annihilation operators to annihilation

operators and creation operators to creation operators from one basis to the other, it is called mode-mixing coefficient. The $\beta_{\vec{k}'\vec{k}}$ coefficient however maps annihilation (resp. creation) operators of one basis to creation (resp. annihilation) operators of the other basis. It is therefore called particle creation coefficient as it is responsible for the change in the particle content of the field. This implies that in general the vacuum state differs in each different basis, which has important consequences for the physics of quantum fields. Note that the bosonic commutation relations (or fermionic using an anticommutator instead) hold from one basis $\hat{a}_{\vec{k}}, \hat{a}^\dagger_{\vec{k}}$ to the other $\hat{A}_{\vec{k}}, \hat{A}^\dagger_{\vec{k}}$ thanks to the unitarity of the transformation:

$$\int d\vec{k}'' \left\{ \alpha_{\vec{k}\vec{k}''} \alpha^*_{\vec{k}'\vec{k}''} - \beta_{\vec{k}\vec{k}''} \beta^*_{\vec{k}'\vec{k}''} \right\} = \delta(\vec{k} - \vec{k}'), \tag{40}$$

$$\int d\vec{k}'' \left\{ \alpha_{\vec{k}\vec{k}''} \beta_{\vec{k}'\vec{k}''} - \beta_{\vec{k}\vec{k}''} \alpha_{\vec{k}'\vec{k}''} \right\} = 0. \tag{41}$$

In practice, such a change of basis can be motivated by different reasons. It can be for mathematical convenience, for example in order to diagonalise a Hamiltonian operator. It can also be in order to characterise the time evolution of a quantum field in a dynamical spacetime. This is done for example in cosmology where the field's modes at the spacetime's past infinity are compared with those at future infinity using a Bogolyubov transformation. One can also use a Bogolyubov transformation in order to implement a change in the motion of the observer. This is for example the case of the calculation of the Unruh effect: initially, an inertial observer in Minkowski spacetime sees a quantum field in the vacuum state, but when it starts to accelerate the field becomes populated by thermal particles. There, the Bogolyubov transformation enables to compute the change in the particle content of the field when changing from the inertial observer's picture to the accelerated one.

Particle creation occurs due to the presence of non vanishing $\beta_{\vec{k}'\vec{k}}$ coefficients. This can be seen from the vacuum state already: the action of the new annihilation operator on the vacuum state in the initial basis is:

$$\hat{A}_{\vec{k}} |0\rangle = \int d\vec{k}' \left\{ \alpha^*_{\vec{k}'\vec{k}} \hat{a}_{\vec{k}'} - \beta^*_{\vec{k}'\vec{k}} \hat{a}^\dagger_{\vec{k}'} \right\} |0\rangle = - \int d\vec{k}' \beta^*_{\vec{k}'\vec{k}} |1_{\vec{k}'}\rangle \,, \tag{42}$$

which is non zero unless all the $\beta_{\vec{k}'\vec{k}}$ coefficients are zero. Therefore the two bases do not share the same vacuum state, a vacuum state in one basis can be populated by field excitations in the other basis. This leads to the particle creation effects like in the Unruh and Hawking effects. We introduce the number operator $\hat{N}_{\vec{k}} = \hat{A}^\dagger_{\vec{k}} \hat{A}_{\vec{k}}$ for the mode $\vec{k}$ here in the new basis. If the mode was initially empty of particles, the number of particles created in this mode in the new basis is given by $\langle 0|\hat{N}_{\vec{k}}|0\rangle = \int d\vec{k}' |\beta_{\vec{k}'\vec{k}}|^2$.

Note that since the Bogolyubov transformations are unitary transformations, they transform a pure quantum state into another pure state. This is in particular true for the vacuum state. The thermalisation experienced by the field in the Unruh effect is due to the causal structure of the Rindler spacetime, which is the spacetime seen by an initially inertial observer in Minkowski spacetime who starts to accelerate: a part of the spacetime becomes causally disconnected from the observer as he starts to accelerate. This leads to a loss of information on the field and thus turns the quantum state of the field to a mixed state.

3

ADVANCED FORMALISMS

In this chapter we describe the covariance matrix formalism, quantum metrology and the polarisation rotation of light. These three formalism are used in this thesis together with the quantum field theory in curved spacetime that we gave in the previous chapter.

3.1 COVARIANCE MATRIX FORMALISM

The covariance matrix formalism is a powerful framework which can be used for Gaussian quantum states. In this section, we will consider Gaussian states of bosonic fields only. Unpolarised photons can for example be represented by such Gaussian states.

3.1.1 *Continuous variables quantum formalism*

Symplectic geometry

Let us consider a bosonic field with a number of modes N. Each mode has a position and a momentum operator, $\hat{x}_j = \frac{\hat{a}_j^\dagger + \hat{a}_j}{\sqrt{2}}$ and $\hat{p}_j = i\frac{\hat{a}_j^\dagger - \hat{a}_j}{\sqrt{2}}$ respectively, which enables to give a phase space representation. For Gaussian states, all the information is encoded into the first and the second moments. These are respectively the displacement vector $\boldsymbol{d}$ and the covariance matrix $\boldsymbol{\Gamma}$. Their components are given in terms of the position and momentum operators:

$d_j = \langle \hat{X}_j \rangle$ and $\Gamma_{jk} = \langle \hat{X}_j \hat{X}_k + \hat{X}_k \hat{X}_j \rangle - 2 \langle \hat{X}_j \rangle \langle \hat{X}_k \rangle$, where we gathered the operators in a single vector $\hat{\boldsymbol{X}} = (\hat{x}_1, \hat{p}_1, \ldots, \hat{x}_N, \hat{p}_N)^{\mathrm{t}}$ for simplicity. From the usual commutation relations $\left[\hat{x}_j, \hat{p}_k\right] = i\delta_{jk}$, we have that $\left[\hat{X}_j, \hat{X}_k\right] = i\Omega_{jk}$ with $\boldsymbol{\Omega} = \bigoplus_{k=1}^{N} \boldsymbol{\omega}$ the symplectic form and $\boldsymbol{\omega} = \left(\begin{smallmatrix} 0 & 1 \\ -1 & 0 \end{smallmatrix}\right)$.

Covariance matrix

The first moments encoded in the displacement vector can be changed arbitrarily by the action of unitary displacement operators [50]. Such unitary operations do change the state of our system but not its correlations: these are encoded in the covariance matrix. When working with measures of entanglement we can therefore set the displacement vector $\boldsymbol{d} = \boldsymbol{0}$ without loss of generality.

The covariance matrix fulfils $\boldsymbol{z}^{\dagger}(\boldsymbol{\Gamma} + i\boldsymbol{\Omega})\boldsymbol{z} \geq 0$, for any $\boldsymbol{z} \in \mathbb{C}^{2N}$. The purity of the state can be estimated thanks to the determinant of the covariance matrix $\det(\boldsymbol{\Gamma}) \geq 1$, where the equality is reached for pure states. The covariance matrix encodes information about the N modes of the state. When one can only work with $n < N$ modes of the field, it is easy to trace out the $N - n$ inaccessible modes: to do so, it suffices to simply remove the components of these $N - n$ modes from the covariance matrix. This procedure can be repeated at will as it preserves the Gaussian nature of the states.

Symplectic transformations

The action of unitary operators on the quantum state, usually performed on the density operator as $\hat{\rho}' = \hat{U}^{\dagger}\hat{\rho}\hat{U}$, is given in the continuous variables formalism by $\boldsymbol{d'} = \boldsymbol{S}\boldsymbol{d}$ and $\boldsymbol{\Gamma'} = \boldsymbol{S}\boldsymbol{\Gamma}\boldsymbol{S}^{t}$, where $\boldsymbol{S}$ is the symplectic matrix that is the analogue of the unitary operator $\hat{U}$ in the covariance matrix formalism. Only unitary transformations at most quadratic in the mode operators preserve the Gaussian nature of the state, we therefore restrict ourselves to such transformations in the present formalism. A real symplectic matrix verifies the symplectic identity $\boldsymbol{S}\boldsymbol{\Omega}\boldsymbol{S}^{t} = \boldsymbol{\Omega}$, with $\boldsymbol{\Omega}$ the symplectic form that

we have defined previously. These real symplectic matrices are square matrices of dimension $(2N)^2$ that form the group $\mathrm{Sp}(2N, \mathbb{R})$. They are block matrices with square blocks of dimension 4. From the symplectic identity, we clearly see that $\det(\boldsymbol{S}) = \pm 1$. Using the Pfaffian together with the symplectic identity, we have $\mathrm{Pf}(\boldsymbol{\Omega}) = \mathrm{Pf}(\boldsymbol{S}\boldsymbol{\Omega}\boldsymbol{S}^t) = \det(\boldsymbol{S})\mathrm{Pf}(\boldsymbol{\Omega})$, and therefore actually $\det(\boldsymbol{S}) = +1$.

3.1.2 *Other representations*

Several respresentations are used in the covariance matrix formalism. In this subsection we describe the quadrature and complex representations.

Quadrature representation

By simply changing the order of the basis vector's components, we can switch to the quadrature representation. The new basis vector is then given by $\hat{\boldsymbol{Y}} = (\hat{x}_1, \ldots, \hat{x}_N, \hat{p}_1, \ldots, \hat{p}_N)^{\mathrm{t}} = \boldsymbol{L}_{(q)}\hat{\boldsymbol{X}}$. This choice is particularly convenient as the symplectic matrices and the symplectic form take a square block matrix form, where each block is a square matrix of dimension N^2:

$$\boldsymbol{S}_{(q)} = \boldsymbol{L}_{(q)}\boldsymbol{S}\boldsymbol{L}_{(q)}^t = \left(\begin{smallmatrix} \boldsymbol{A} & \boldsymbol{B} \\ \boldsymbol{C} & \boldsymbol{D} \end{smallmatrix}\right), \tag{43}$$

$$\boldsymbol{\Omega}_{(q)} = \left(\begin{smallmatrix} \boldsymbol{0} & \mathbb{1}_N \\ -\mathbb{1}_N & \boldsymbol{0} \end{smallmatrix}\right), \tag{44}$$

and the symplectic matrix' blocks obey the following relations: $\boldsymbol{B}\boldsymbol{A}^t = \boldsymbol{A}\boldsymbol{B}^t$, $\boldsymbol{D}\boldsymbol{C}^t = \boldsymbol{C}\boldsymbol{D}^t$ and $\boldsymbol{A}\boldsymbol{D}^t - \boldsymbol{B}\boldsymbol{C}^t = \mathbb{1}_N$.

Complex representation

Another representation of interest is the complex representation which can be obtained by taking the new basis vector $\hat{\boldsymbol{Z}} = (\hat{a}_1, \ldots, \hat{a}_N, \hat{a}_1^\dagger, \ldots, \hat{a}_N^\dagger)^{\mathrm{t}} =$

$\boldsymbol{L}_{(c)}\hat{\boldsymbol{Y}}$, with $\boldsymbol{L}_{(c)} = \frac{1}{\sqrt{2}}\begin{pmatrix} \mathbb{1}_N & i\mathbb{1}_N \\ \mathbb{1}_N & -i\mathbb{1}_N \end{pmatrix}$. In this representation, the symplectic matrices and the symplectic form take another block matrix form:

$$\boldsymbol{S}_{(c)} = \boldsymbol{L}_{(c)}\boldsymbol{S}_{(q)}\boldsymbol{L}_{(c)}^{\dagger} = \begin{pmatrix} \boldsymbol{\alpha} & \boldsymbol{\beta} \\ \boldsymbol{\beta}^* & \boldsymbol{\alpha}^* \end{pmatrix}, \tag{45}$$

$$\boldsymbol{\Omega}_{(c)} = -i\boldsymbol{K} = -i\begin{pmatrix} \mathbb{1}_N & \mathbf{0} \\ \mathbf{0} & -\mathbb{1}_N \end{pmatrix}. \tag{46}$$

This representation is very convenient for computations and the symplectic matrices' blocks fulfil some familiar relations: $\boldsymbol{\alpha}\boldsymbol{\alpha}^{\dagger} - \boldsymbol{\beta}\boldsymbol{\beta} = \mathbb{1}_N$ and $\boldsymbol{\alpha}\boldsymbol{\beta}^t = \boldsymbol{\beta}\boldsymbol{\alpha}^t$. These relations have the exact same form as the Bogolyubov identities, the latter can therefore be very naturaly implemented in this formalism by using the complex representation.

3.1.3 *Symplectic transformations from unitary operators*

As we have seen, in the complex representation the symplectic transformations take the form of Bogolyubov transformations, i.e. unitary transformations. This is of course not coincidental, and we will now see how to link a unitary transformation in the usual Hilbert space formalism to its associated symplectic transformation. An arbitrary unitary transformation takes the form $\hat{U} = e^{i\int^t dt' \hat{H}(t')}$, where $\hat{H}$ is the interaction Hamiltonian which is taken to be at most quadratic in the mode operators in order to preserve the gaussianity of the states. One can express this Hamiltonian in terms of its symplectic representation thanks to the relation: $\hat{H} = \hat{\boldsymbol{Z}}^{\dagger} \cdot \mathbf{H} \cdot \hat{\boldsymbol{Z}}$. The symplectic Hamiltonian takes the block form $\mathbf{H} = \begin{pmatrix} \mathbf{A} & \mathbf{B} \\ \mathbf{B}^* & \mathbf{A}^* \end{pmatrix}$, with $\mathbf{A}$ and $\mathbf{B}$ two square blocks of dimension N^2 which verify $\mathbf{A}^{\dagger} = \mathbf{A}$ and $\mathbf{B}^t = \mathbf{B}$, and we therefore have $\mathbf{H}^{\dagger} = \mathbf{H}$. Under a unitary transformation, the state vector evolves as: $\hat{U}^{\dagger}\hat{\boldsymbol{Z}}\hat{U} = \mathbf{S}_{(c)}\hat{\boldsymbol{Z}}$. Applying Hadamard's lemma $e^{-\hat{A}}\hat{Z}e^{\hat{A}} = \hat{Z} - \left[\hat{A}, \hat{Z}\right] + \frac{1}{2!}\left[\hat{A}, \left[\hat{A}, \hat{Z}\right]\right] + \ldots$ to the whole vector $\hat{\boldsymbol{Z}}$, with $\hat{A} = i\int^t dt' \hat{H}(t')$

and using that $\left[\hat{H}, \hat{\boldsymbol{Z}}\right] = \boldsymbol{K}\mathbf{H}\hat{\boldsymbol{Z}}$ (and assuming that the Hamiltonian commutes with itself at different times), we obtain:

$$\begin{aligned}
\hat{U}^\dagger \hat{\boldsymbol{Z}} \hat{U} &= \hat{\boldsymbol{Z}} - \left[i \int^t dt' \hat{H}(t'), \hat{\boldsymbol{Z}} \right] + \frac{1}{2!} \left[i \int^t dt'' \hat{H}(t''), \left[i \int^t dt' \hat{H}(t'), \hat{\boldsymbol{Z}} \right] \right] + \dots \\
&= \hat{\boldsymbol{Z}} - i \int^t dt' \left[\hat{H}(t'), \hat{\boldsymbol{Z}} \right] + \frac{i^2}{2!} \int^t \int^t dt' dt'' \left[\hat{H}(t''), \left[\hat{H}(t'), \hat{\boldsymbol{Z}} \right] \right] + \dots \\
&= \left[\mathbb{1}_{2N} - i\boldsymbol{K} \int^t dt' \mathbf{H}(t') + \frac{1}{2!} \left(-i\boldsymbol{K} \int^t dt' \mathbf{H}(t') \right)^2 + \dots \right] \hat{\boldsymbol{Z}} \\
&= e^{-i\boldsymbol{K} \int^t dt' \mathbf{H}(t')} \hat{\boldsymbol{Z}}.
\end{aligned} \tag{47}$$

We therefore have $\boldsymbol{S} = e^{-i\boldsymbol{K} \int^t dt' \mathbf{H}(t')}$.

3.1.4 *Entanglement*

In order to quantify the entanglement of a quantum state in the covariance matrix formalism, we first need to introduce the Williamson theorem which states that for any square positive-definite matrix $\boldsymbol{\Gamma}$ of dimension $(2N)^2$, there is a unique real symplectic matrix $\boldsymbol{S}$ such that $\boldsymbol{\Gamma}$ takes the Williamson normal form:

$$\boldsymbol{\Gamma} = \boldsymbol{S}^t \tilde{\boldsymbol{\nu}} \boldsymbol{S}, \quad \tilde{\boldsymbol{\nu}} = \bigoplus_{k=1}^{N} \begin{pmatrix} \nu_k & 0 \\ 0 & \nu_k \end{pmatrix}. \tag{48}$$

In the quadrature and complex representations, it reads instead $\boldsymbol{\Gamma}_{(q)} = \boldsymbol{S}_{(q)}^t \left(\begin{smallmatrix} \boldsymbol{\nu} & 0 \\ 0 & \boldsymbol{\nu} \end{smallmatrix}\right) \boldsymbol{S}_{(q)}$ and $\boldsymbol{\Gamma}_{(c)} = \boldsymbol{S}_{(c)}^\dagger \left(\begin{smallmatrix} \boldsymbol{\nu} & 0 \\ 0 & \boldsymbol{\nu} \end{smallmatrix}\right) \boldsymbol{S}_{(c)}$ respectively, where we collected the N symplectic eigenvalues $\nu_k \geq 1$ in the symplectic spectrum matrix $\boldsymbol{\nu} = \mathrm{diag}(\nu_1, \dots, \nu_N)$. One can also obtain these eigenvalues using the more practical formula $\boldsymbol{\nu} = \mathrm{Eig}_+(i\boldsymbol{\Omega}\boldsymbol{\Gamma})$, where Eig_+ stands for the diagonal matrix gathering the positive eigenvalues of $i\boldsymbol{\Omega}\boldsymbol{\Gamma}$. This latter formula works for the three different representations. Now that we have a diagonal expression for the covariance matrix, we can express the purity relation in terms of the symplectic eigenvalues: $\det(\boldsymbol{\Gamma}) = \prod_{k=1}^{N} \nu_k^2 \geq 1$.

We now proceed to define some measures of entanglement for bipartite Gaussian states. Just like it was previously shown in the Hilbert space description, the entanglement of a pure bipartite state can be quantified

thanks to the entropy of entanglement, i.e. the von Neumann entropy of its reduced state. The von Neumann entropy of a Gaussian state is given by:

$$S(\mathbf{\Gamma}) = \sum_{k=1}^{N} \left[\frac{\nu_k + 1}{2} \ln\left(\frac{\nu_k + 1}{2}\right) - \frac{\nu_k - 1}{2} \ln\left(\frac{\nu_k - 1}{2}\right) \right]. \tag{49}$$

The entanglement of a pure bipartite quantum state $\mathbf{\Gamma}_{AB}$ is then measured by the entropy of entanglement $E(\mathbf{\Gamma}_{AB}) = S(\mathbf{\Gamma}_A) = S(\mathbf{\Gamma}_B)$, with $\mathbf{\Gamma}_A = \mathrm{tr}_B \mathbf{\Gamma}_{AB}$ and $\mathbf{\Gamma}_B = \mathrm{tr}_A \mathbf{\Gamma}_{AB}$ the reduced states of $\mathbf{\Gamma}_{AB}$. For mixed bipartite Gaussian states, we can use the negativity as in the Hilbert space picture. The partially transposed state here reads:

$$\mathbf{\Gamma}^{\mathrm{pt}} = \boldsymbol{P}\mathbf{\Gamma}\boldsymbol{P}, \quad \text{with } \boldsymbol{P} = \begin{pmatrix} 1&0&0&0 \\ 0&0&0&1 \\ 0&0&1&0 \\ 0&1&0&0 \end{pmatrix} \tag{50}$$

The partial transposing matrix $\boldsymbol{P}$ was here given in its complex representation. In the real representation it reads $\boldsymbol{P} = \mathbb{1}_2 \oplus \sigma_3$, while in the quadrature representation it has the form $\boldsymbol{P} = \mathbb{1}_2 \oplus \sigma_1$. The negativity is then given by:

$$\mathcal{N}(\mathbf{\Gamma}) = \frac{1}{2} \max\left\{ \frac{1 - \tilde{\nu}}{\tilde{\nu}}, 0 \right\}, \tag{51}$$

with $\tilde{\nu} = \min\left\{ \mathrm{Eig}\left(\mathbf{\Gamma}^{\mathrm{pt}}\right) \right\}$ the smallest symplectic eigenvalue of the partially transposed covariance matrix. Another measure of entanglement related to the negativity is the logarithmic negativity $\mathcal{E}_{\mathcal{N}}(\mathbf{\Gamma}) = \max\{-\ln(\tilde{\nu}), 0\}$.

3.1.5 *Examples of quantum states*

Coherent state

A single coherent state is a Gaussian state that is an eigenvector of the annihilation operator: $\hat{a}_k |\alpha_k\rangle = \alpha_k |\alpha_k\rangle$, with $\alpha_k \in \mathbb{C}$ the coherence parameter. It is a displaced vacuum state: $|\alpha_k\rangle = \hat{D}_k(\alpha_k) |0\rangle$ where $\hat{D}_k(\alpha_k) = e^{\alpha_k \hat{a}_k^\dagger - \alpha_k^* \hat{a}_k}$ is the Weyl displacement operator. Thus, the vacuum state is a coherent state with $\alpha_k = 0$. Another feature of the coherent states is that they minimise the position-momentum Heisenberg uncertainty relation, i.e. $\Delta\hat{x}\Delta\hat{p}_x = \frac{1}{2}$. A single mode coherent state $|\alpha\rangle$ has first and second moments given by:

$\boldsymbol{d} = \sqrt{2}\,(\mathrm{Re}(\alpha), \mathrm{Im}(\alpha))$ and $\boldsymbol{\Gamma} = \mathbb{1}_2$. The covariance matrix is independent of the coherence parameter α, therefore it is the same for any coherent state and equal to the vacuum's.

Two modes squeezed state

Another quantum state of interest is the two modes squeezed state. Such a state is obtained by the squeezing of a two modes coherent state. The two modes squeezing Hamiltonian is $\hat{H} = 2is(\hat{a}_1^\dagger \hat{a}_2^\dagger - \hat{a}_1 \hat{a}_2)$, with $s > 0$. The symplectic representation for this Hamiltonian is then given by: $\mathbf{H} = is\begin{pmatrix} \mathbf{0} & \sigma_1 \\ -\sigma_1 & \mathbf{0} \end{pmatrix}$. We can then obtain the expression for the symplectic transformation:

$$\mathbf{S} = e^{-i\mathbf{KH}} = \begin{pmatrix} \cosh s\, \mathbb{1}_2 & \sinh s\, \sigma_1 \\ \sinh s\, \sigma_1 & \cosh s \mathbb{1}_2 \end{pmatrix}. \tag{52}$$

To obtain two modes squeezed state, we use the symplectic transformation above on a two mode coherent state $|\alpha_1, \alpha_2\rangle = \hat{D}(\alpha_1)\hat{D}(\alpha_2)\,|0\rangle$ which has covariance matrix $\tilde{\boldsymbol{\Gamma}} = \mathbb{1}_4$. We obtain:

$$\boldsymbol{\Gamma}(s) = \begin{pmatrix} \cosh 2s\, \mathbb{1}_2 & \sinh 2s\, \sigma_1 \\ \sinh 2s\, \sigma_1 & \cosh 2s\, \mathbb{1}_2 \end{pmatrix} \tag{53}$$

The two modes squeezed state is a pure bipartite state, we can therefore use the entropy of entanglement to quantify its entanglement. The reduced states of our two modes squeezed state read: $\boldsymbol{\Gamma}_1 = \boldsymbol{\Gamma}_2 = \cosh 2s\, \mathbb{1}_2$. The reduced states therefore have a single eigenvalue $\nu = \cosh 2s$. The entropy of entanglement $E(\boldsymbol{\Gamma}) = S(\boldsymbol{\Gamma}_1) = S(\boldsymbol{\Gamma}_2)$ is thus:

$$\begin{aligned} E(\boldsymbol{\Gamma}) &= \frac{\cosh 2s + 1}{2} \ln\left(\frac{\cosh 2s + 1}{2}\right) - \frac{\cosh 2s - 1}{2} \ln\left(\frac{\cosh 2s - 1}{2}\right) \\ &= 2\cosh^2 s \ln\cosh s - 2\sinh^2 s \ln\sinh s. \end{aligned} \tag{54}$$

The two modes squeezed state's entropy of entanglement vanishes when the squeezing parameter s goes to zero, grows linearly for $0 < s \lesssim 17$, and vanishes again in the $s \to \infty$ limit. Let us now compute the negativity of the two modes squeezed state. The partially transposed covariance matrix for our state is $\boldsymbol{\Gamma}^{\mathrm{pt}} = \begin{pmatrix} \gamma & \mathbf{0} \\ \mathbf{0} & \gamma \end{pmatrix}$ with $\gamma = \begin{pmatrix} \cosh 2s & \sinh 2s \\ \sinh 2s & \cosh 2s \end{pmatrix}$. The eigenvalues are then easily found: $\nu_\pm = e^{\pm 2s}$. Since we took the squeezing parameter s to be

positive, the smallest eigenvalue is ν_- and the negativity of the two modes squeezed states is therefore $\mathcal{N}\left(\mathbf{\Gamma}(s)\right) = \frac{e^{2s}-1}{2}$. We also have the logarithmic negativity: $\mathcal{E}_{\mathcal{N}}\left(\mathbf{\Gamma}(s)\right) = 2s$. Like the entropy of entanglement, the negativity measures vanish in the $s \to 0$ limit. However, contrarily to the former, the negativity measures diverge when $s \to \infty$.

3.2 QUANTUM METROLOGY

Quantum metrology is a theory that provides tools to estimate parameters encoded in quantum states [51]. Any physical transformation can encode parameters in a quantum state, for example time, temperature, or a small perturbation induced by changes in the spacetime curvature [52, 53] can perturb an initialy prepared quantum state. The state then encodes some information about the perturbating parameter, and it can be measured in order to extract some of this information. The precision that can be achieved on such a measurement is bounded by the laws of quantum mechanics, the input state and the chosen measurement [51].

3.2.1 *Quantum fidelity*

A first way to characterise the change in a quantum state due to a perturbation, for example induced by the presence of a curved spacetime background, is the fidelity $\mathcal{F}(\hat{\rho}_0, \hat{\rho}_\epsilon)$ between the altered and unaltered states, $\hat{\rho}_\epsilon$ and $\hat{\rho}_0$ respectively, where ϵ denotes the small perturbation. The fidelity is a quantity measuring the distance between two states in the Hilbert space of states. For two mixed states, the fidelity is given explicitely by $\mathcal{F}(\hat{\rho}_1, \hat{\rho}_2) = \left(\mathrm{tr}\sqrt{\sqrt{\hat{\rho}_1}\hat{\rho}_2\sqrt{\hat{\rho}_1}}\right)^2$. The fidelity has several properties worth mentioning: as one could expect it is symmetric, namely $\mathcal{F}(\hat{\rho}_1, \hat{\rho}_2) = \mathcal{F}(\hat{\rho}_2, \hat{\rho}_1)$. It is bounded: $0 \leq \mathcal{F}(\hat{\rho}_1, \hat{\rho}_2) \leq 1$, and unity is reached when the two states are identical $\mathcal{F}(\hat{\rho}, \hat{\rho}) = 1$. The fidelity tends to zero when the states be-

come increasingly distinguishable. For pure states, the general expression for the fidelity simplifies to the modulus square of the two states' overlap: $\mathcal{F}(|\Psi_1\rangle, |\Psi_2\rangle) = |\langle\Psi_1|\Psi_2\rangle|^2$.

3.2.2 *Quantum fidelity of Gaussian states*

If one works with Gaussian states within the framework of continuous variables described previously, one has explicit formulas for the computation of the fidelity between two states. We recall here that in the continuous variables formalism a Gaussian state $\hat{\rho}$ in the Hilbert space can be represented in the phase space by its first and second moments, the displacement vector $\boldsymbol{d}$ and the covariance matrix σ, respectively. For single mode Gaussian states, the fidelity then explicitely reads [54]:

$$\mathcal{F}(\hat{\rho}_1, \hat{\rho}_2) = \frac{\exp\left(-\frac{1}{2}(\delta\boldsymbol{d})^{\mathrm{t}} \cdot (\boldsymbol{\sigma_1} + \boldsymbol{\sigma_2})^{-1} \cdot \delta\boldsymbol{d}\right)}{\sqrt{\Delta + \Lambda_1} - \sqrt{\Lambda_1}}, \tag{55}$$

$$\Lambda_1 = 4 \det\left(\boldsymbol{\sigma_1} + \frac{i}{2}\boldsymbol{\omega}\right) \det\left(\boldsymbol{\sigma_2} + \frac{i}{2}\boldsymbol{\omega}\right) \geq 0, \tag{56}$$

$$\Delta = \det(\boldsymbol{\sigma_1} + \boldsymbol{\sigma_2}) \geq 1, \tag{57}$$

where $\delta\boldsymbol{d} = \boldsymbol{d_1} - \boldsymbol{d_2}$ and the symplectic form for one mode reduces to $\boldsymbol{\omega} = \left(\begin{smallmatrix} 0 & 1 \\ -1 & 0 \end{smallmatrix}\right)$ in the real representation. For two-mode states, we have [54]:

$$\mathcal{F}(\hat{\rho}_1, \hat{\rho}_2) = \frac{\exp\left(-\frac{1}{2}(\delta\boldsymbol{d})^{\mathrm{t}} \cdot (\boldsymbol{\sigma_1} + \boldsymbol{\sigma_2})^{-1} \cdot \delta\boldsymbol{d}\right)}{\sqrt{\Gamma_2} + \sqrt{\Lambda_2} - \sqrt{(\sqrt{\Lambda_2} + \sqrt{\Lambda_2})^2 - \Delta}}, \tag{58}$$

$$\Lambda_2 = 16 \det\left(\boldsymbol{\sigma_1} + \frac{i}{2}\boldsymbol{\Omega}\right) \det\left(\boldsymbol{\sigma_2} + \frac{i}{2}\boldsymbol{\Omega}\right) \geq 0, \tag{59}$$

$$\Gamma_2 = 16 \det\left((\boldsymbol{\Omega} \cdot \boldsymbol{\sigma_1}) \cdot (\boldsymbol{\Omega} \cdot \boldsymbol{\sigma_2}) - \frac{1}{4}\mathbb{1}_4\right) \geq \Delta, \tag{60}$$

where $\boldsymbol{\Omega} = \boldsymbol{\omega} \oplus \boldsymbol{\omega}$ is the two-mode symplectic form.

3.2.3 *Quantum Fisher information and Cramer-Rào bound*

From the fidelity one can define another quantity related to the distinguishability of quantum states that are perturbed by a common parameter. This quantity is called the Quantum Fisher Information (QFI) and it reads:

$$\mathrm{H}(\epsilon) = \lim_{d\epsilon \to 0} 8 \frac{1 - \sqrt{\mathcal{F}(\hat{\rho}_\epsilon, \hat{\rho}_{\epsilon+d\epsilon})}}{d\epsilon^2}, \tag{61}$$

that is, it is defined with respect to the fidelity between two neighbouring states in the Hilbert space that are parametrised by the same parameter ϵ: $\hat{\rho}_\epsilon$ and $\hat{\rho}_{\epsilon+d\epsilon}$. The QFI quantifies the infinitesimal displacement of the state in the Hilbert space due the infinitesimal change $d\epsilon$. The fidelity between two such states can be expanded perturbatively:

$$\mathcal{F}(\hat{\rho}_\epsilon, \hat{\rho}_{\epsilon+d\epsilon}) = 1 - \frac{1}{2}\mathcal{F}^{(2)} d\epsilon^2 + O(d\epsilon^3), \tag{62}$$

where we used that $\mathcal{F}^{(1)} = \frac{\partial \mathcal{F}(\hat{\rho}_\epsilon, \hat{\rho}_{\epsilon+d\epsilon})}{\partial(d\epsilon)}|_{d\epsilon=0} = 0$, which holds as long as ϵ is the only varying parameter. Then we have

$$\mathrm{H}(\epsilon) = 4\mathcal{F}^{(2)} = 4\frac{\partial^2 \mathcal{F}(\hat{\rho}_\epsilon, \hat{\rho}_{\epsilon+d\epsilon})}{\partial(d\epsilon)^2}|_{d\epsilon=0}. \tag{63}$$

One can see this quantity as the "acceleration" in the change of the quantum state with respect to the change in the parameter encoded by the physical transformation. In other words, it is the state's sensitivity to the perturbation. This quantity bounds the precision $\Delta\epsilon$ on the measurement of the encoded parameter ϵ through the Cramer-Rào bound:

$$|\Delta\epsilon| \geq \frac{1}{\sqrt{N\mathrm{H}(\epsilon)}}, \tag{64}$$

where N is the number of input probes [55]. This inequality provides the bound for the precision of the single parameter estimation of ϵ, for the optimal measurement on the state. It is therefore an ideal measure, in the sense that one will never be able to perform exactly this ideal measurement. However, depending on the choice of the measurement that we make, one can approach very close to this value. The Fisher information can be used to

compute the equivalent measure as the QFI but for a specific measurement process. This was used for example in the study of the thermal noise in a BEC used as a gravitational wave detector [4]. By picking a particular measurement scheme, it was shown that for the choice that was made the Fisher information was very similar to the ideal value given by the QFI [4]. This is however not true in general. Yet, the QFI provides a way to give a first green light for promising schemes when the precision bound that it gives is good enough. More refined computations with the Fisher information for a chosen measurement need to be considered in order to provide a definite experiment proposal.

When the parameter ϵ that we chose to parametrise the changes of the state contains several parameters of interest to be estimated, say ϵ_1 and ϵ_2, then we can use the cascade derivative rule to find a bound for the measurement of each of these parameters: $|\Delta\epsilon_1| \geq 1/\left(\left|\frac{\partial\epsilon}{\partial\epsilon_1}\right|\sqrt{N\mathrm{H}(\epsilon)}\right)$ and $|\Delta\epsilon_2| \geq 1/\left(\left|\frac{\partial\epsilon}{\partial\epsilon_2}\right|\sqrt{N\mathrm{H}(\epsilon)}\right)$. These expressions assume that when we perform the measurement on ϵ_1 (resp. ϵ_2) we know the value of ϵ_2 (resp. ϵ_1) with infinite precision. One can drop this latter assumption and work out a multi-parameter estimation, which we won't detail in this thesis, but for which the theory was given for single modes in [56] and generalised in [57]. Such multi-parameter estimation scheme turns out to be in general beneficial for the estimation, leading to increased precision compared to single parameter estimations [58].

The QFI is a quantity that can be quite involved to compute. A simpler way to obtain a bound for the quantum measurement of a perturbative parameter ϵ is to compute only the zeroth order of the QFI, $\mathrm{H}^{(0)}$. If the latter is non zero, it can be used as a first approximation instead of the full QFI in (64). Of course this only makes sense if ϵ is a small parameter that does not perturb the state too much. The procedure to obtain $\mathrm{H}^{(0)}$ is much simpler than for the complete expression of the QFI since we only need the fidelity between an infinitesimaly altered state and a totally unaltered state. The latter has a similar expression than the former but

with $d\epsilon = 0$. The fidelity between these two quantum states is $\mathcal{F}(\hat{\rho}_0, \hat{\rho}_{d\epsilon})$. We can then obtain the expression for the $\epsilon = 0$ contribution of the QFI: $\mathrm{H}^{(0)} = \lim_{d\epsilon\to 0} 8\,\frac{1-\sqrt{\mathcal{F}_L(|\gamma_0\rangle,|\gamma_{d\epsilon}\rangle)}}{d\epsilon^2} = 4\frac{\partial^2\mathcal{F}(\hat{\rho}_0,\hat{\rho}_{d\epsilon})}{\partial(d\epsilon)^2}|_{d\epsilon=0}$. This is in general easily calculated with the help of a perturbative expansion on the altered quantum state and its fidelity with the unaltered one, up to second order in the infinitesimal change $d\epsilon$.

3.3 LIGHT'S POLARISATION ROTATION AND WIGNER PHASES

In previous sections, the photons were generally taken to be unpolarised in order to have a simple description as excitations of a scalar field, or as Gaussian states in order to be able to work within the framework of the covariance matrix formalism. However, one might be interested in the study of the evolution of the light's polarisation, due to a curved spacetime background and as seen by moving observers. In particular, we look at how quantum states of polarised photons are affected by the curved spacetime background of the Earth in chapter 8, and how they evolve as seen by centrifuged observers in chapter 9. In the present section, we first show how the polarisation is defined with respect to the observer's chosen reference frame, and how it evolves as the light propagates in curved spacetime. From the change of the polarisation we can deduce the change in the photon's quantum state, which comes in the form of a Wigner phase. We also discuss which kind of quantum states would experience an increased effect, and conversely which states are preserved from this alteration.

3.3.1 *Reference frames and tetrads*

An observer defines mathematically its reference frame by a tetrad $\boldsymbol{e}$, with tetrad elements $e_{\hat{a}}{}^{\mu}$ [59]. The tetrad relates physical quantities from their expression in the global coordinates of the spacetime (t, r, θ, ϕ) to the local

Cartesian frame of the observer. In other words, in this local frame the observer sees the spacetime as if it was flat, with the metric of Minkowski spacetime $\boldsymbol{\eta} = \mathrm{diag}(-1, 1, 1, 1)$. The domain of validity of this frame is the portion of spacetime surrounding the observer where the effects of curvature can be neglected. In the observer's local frame, a passing light ray with polarisation 4-vector $\boldsymbol{\psi}$ will be seen with components $\psi^{\hat{a}} = \psi^{\mu} e^{\hat{a}}{}_{\mu} = \psi^{\mu} e_{\hat{b}}{}^{\nu} \eta^{\hat{a}\hat{b}} g_{\mu\nu}$. Hatted indices denote that the quantity is viewed in the observer's local frame, by opposition to quantities with Greek indices which are components of the usual vectors in the global spacetime coordinates. In what follows, we will need to track the evolution of the static observer's frame along the path followed by the light rays. In order to do so, we will define a tetrad field $\boldsymbol{e}(\lambda)$ along the light's null geodesic parametrised by the affine parameter λ.

The tetrad components are defined as follows: first, the timelike component $\boldsymbol{e}_{\hat{0}}$ is set to equal the observer's velocity. Then, the triad of spacelike components $\boldsymbol{e}_{\hat{1}}$, $\boldsymbol{e}_{\hat{2}}$, $\boldsymbol{e}_{\hat{3}}$ of the tetrad are obtained thanks to the orthonormalisation relations $e_{\hat{a}}{}^{\mu} e_{\hat{b}}{}^{\nu} g_{\mu\nu} = \eta_{\hat{a}\hat{b}}$. Each of the three triad components are vectors that have four elements themselves, and these twelve elements are constrained by only nine orthonormalisation relations. There is therefore some gauge freedom in the choice of the triad, and thus of the tetrad. This mathematical gauge represents the observer's freedom of choice of the reference frame. In what follows we will adapt our observer's tetrad to the light's null vector, which will simplify the polarisation rotation computations. To do so we will need to set, say, the third component of the triad $\boldsymbol{e}_{\hat{3}}$ in a particular way that depends on the trajectory of the light ray. This procedure will be explicitly described in the next subsection. After having adapted the tetrad to the light's null vector, there are then only eight tetrad elements $e_{\hat{a}}{}^{\mu}$ left to be determined and seven orthonormalisation equations, therefore all the gauge freedom that is left is encoded in one single tetrad element (and two $\pm$ signs that are due to the second order nature of the two remaining normalisation relations). Extending this procedure to the whole

null geodesic followed by the light ray, we obtain the tetrad field for our static observers.

3.3.2 *Adapted frames and polarisation rotation of light*

Now that we have defined the observers' frames, we will here implement the formalism required to describe the light's polarisation and its rotation due to curved spacetime backgrounds and observers in relativistic motion.

Polarisation vectors and adapted frames

The light's polarisation vector is a spacelike vector orthogonal to the light's null vector, namely $\psi^\mu k_\mu = \psi^{\hat{a}} k_{\hat{a}} = 0$. Because $\boldsymbol{k}$ is null, namely $k^\mu k_\mu = 0$, there exist gauge transformations of the polarisation vector that leave the orthogonality relation invariant:

$$\boldsymbol{\psi} \to \boldsymbol{\psi} + C\,\boldsymbol{k}, \tag{65}$$

where C is an arbitrary real constant. The light's polarisation vector is therefore not uniquely defined by its orthogonality with the light's null vector. This could cause some gauge freedom in our computations, however there is a way to prevent it. We can construct the observer's tetrad in a way such that the polarisation measured in this particular frame will have two of its four components that remain gauge invariant under transformations (65). This procedure amounts to adapting the frame to the null vector of the light ray considered. To do so, we make the simple choice [60]:

$$\boldsymbol{e}_{\hat{3}} = \frac{\boldsymbol{k}}{k^{\hat{0}}} - \boldsymbol{e}_{\hat{0}}, \tag{66}$$

where $k^{\hat{0}} = k^\mu e^{\hat{0}}{}_\mu = -k^\mu v_\mu = \hbar\,\Omega$, with Ω the photon's frequency as measured by the chosen observer. Physically, this choice amounts to aligning the third component $\boldsymbol{e}_{\hat{3}}$ of our observer's tetrad with the light's propagation direction. In mathematical terms, that means that we have $k^{\hat{1}} = k^{\hat{2}} = 0$ and $k^{\hat{3}} = -k^{\hat{0}}$ in the adapted frame. With this choice for the third component of

the triad, the polarisation components in the observer's adapted frame $\psi^{\hat{1}}$ and $\psi^{\hat{2}}$ are gauge invariant under transformations (65).

Polarisation rotation in curved spacetime

In the adapted frames that we have just defined, the polarisation rotation equations take a simple form [60]:

$$\frac{d\psi^{\hat{A}}}{d\lambda} + u^{\mu} w_{\mu\ \hat{B}}^{\ \hat{A}} \psi^{\hat{B}} = 0. \tag{67}$$

Capital letters $A, B \in \{1, 2\}$ denote the indices of the polarisation's gauge free components. We defined the rescaled null vector $\boldsymbol{u} = \boldsymbol{k}/k^{\hat{0}} = \frac{dx}{d\lambda}$, where $x(\lambda)$ is the photon's position at affine parameter λ on the null geodesic. In (67), the quantity we need to compute in order to obtain the polarisation's rotation is the Wigner rotation $u^{\mu} w_{\mu\ \hat{B}}^{\ \hat{A}}$. This Wigner rotation term is expressed thanks to the spin-1 connection:

$$w_{\mu\ \hat{B}}^{\ \hat{A}} = e^{\hat{A}}_{\ \rho} \partial_{\mu} e_{\hat{B}}^{\ \rho} + \Gamma^{\sigma}_{\ \mu\rho} e^{\hat{A}}_{\ \sigma} e_{\hat{B}}^{\ \rho}. \tag{68}$$

In order to compute the Wigner rotation we will thus need to use the expression of the light's null vector, the adapted tetrad field $\boldsymbol{e}(\lambda)$ of static observers along the light's null geodesic, and the Christoffel symbols defined by the metric components and their derivatives, see (9). The explicit expressions for the Christoffel symbols of the Schwarzschild spacetime can be found in [61] for example. We can simplify slightly the equations (67) by noticing that $\boldsymbol{w}_{\hat{A}\hat{B}}$ is an antisymmetric tensor:

$$\frac{d\psi^{\hat{1}}}{d\lambda} + \tilde{\Psi}\psi^{\hat{2}} = 0, \tag{69}$$

$$\frac{d\psi^{\hat{2}}}{d\lambda} - \tilde{\Psi}\psi^{\hat{1}} = 0, \tag{70}$$

with the Wigner rotation:

$$\tilde{\Psi} = u^{\mu} w_{\mu\ \hat{2}}^{\ \hat{1}} = -u^{\mu} w_{\mu\ \hat{1}}^{\ \hat{2}}. \tag{71}$$

In the next subsection, we will describe how the Wigner rotation of the classical polarisation vector described by the coupled equations (69) and

(70) yields a phase in the quantum state of the photons that propagate in curved spacetime and as seen by observers in relativistic motion.

3.3.3 *Photonic wave packets and Wigner phases*

A photonic wave packet is made of a continuous superposition of momentum states weighted by a distribution function. For each of these momentum states, the corresponding helicity state is a superposition of plus and minus helicity eigenstates. If an observer prepares a photon with a balanced distribution of the helicities for all the momentum states (i.e., it is linearly polarised), the quantum state can be written as:

$$|\gamma\rangle = \frac{1}{\sqrt{2}} \sum_{s=\pm 1} \int d\boldsymbol{p}\, \mathrm{F}(\boldsymbol{p})\, |\boldsymbol{p}, s\rangle\,, \tag{72}$$

where $\boldsymbol{p} = (k^{\hat{0}}, k^{\hat{1}}, k^{\hat{2}}, k^{\hat{3}})$ is the photon's null vector as seen by the observer in its chosen reference frame, s is the helicity which can only take values ± 1 for photons, the distribution $\mathrm{F}(\boldsymbol{p}) = F(\vec{\boldsymbol{p}})\, \delta(|\vec{\boldsymbol{p}}|^2 - (k^{\hat{0}})^2)\, \bar{\theta}(k^{\hat{0}})$ with $\bar{\theta}$ the step function and F is the distribution function of the 3-momenta. This distribution function is normalised to unity: $\int d\vec{\boldsymbol{p}}\ |F(\vec{\boldsymbol{p}})|^2 = 1$, i.e. the corresponding annihilation operators $\hat{a}_{\vec{p},s}$ of the photons have the usual commutation relations $[\hat{a}_{\vec{p}_1,s_1}, \hat{a}^\dagger_{\vec{p}_2,s_2}] = \delta(\vec{p}_1 - \vec{p}_2)\delta_{s_1 s_2}$.

Now let's assume that the photon (72) has been prepared by the source of the emitter and $\boldsymbol{p}$ thus represents the photon's momentum as seen by the emitter at the emission event, which is taking place at the affine parameter λ_e on the null geodesic. We are interested in knowing the expression for the quantum state of the photon that will be observed at reception, at affine parameter λ_o. We will give a simple procedure for the computation, but more details can be found in [62]. Let us introduce $\hat{\boldsymbol{U}}$ as the operator that encodes the propagation of the photons from the beginning to the end of a geodesic segment, denoted by affine parameters λ_1 and λ_2 respectively, with here $\lambda_1 = \lambda_e$ and in general $\lambda_e \leq \lambda_1 < \lambda_2 \leq \lambda_o$. The paths we consider for the photons' propagation between emission and observation

might be divided in several of such null geodesic segments, for example due to mirrors or any other quantum optical device that would alter the light's trajectory.

Each momentum-helicity eigenstate that constitutes the photon aquires a different Wigner phase factor because of its dependence on both the photon's propagation direction $\vec{n} = \vec{p}/k^{\hat{0}}$ and helicity s [60]:

$$\hat{U}\,|p, s\rangle = e^{is\Psi(\vec{n})}\,|p', s\rangle\,, \tag{73}$$

where the prime denotes evaluation at the endpoint of the null geodesic considered. Since every momentum-helicity eigenstate picks up a different phase factor, this phase is not global and it does modify the quantum state. In (73) appears the Wigner phase $\Psi(\vec{n})$ that is obtained by integration of the Wigner rotation along the photon's null geodesic:

$$\Psi = \int_{\lambda_1}^{\lambda_2} \tilde{\Psi}\, d\lambda. \tag{74}$$

Applying the propagator $\hat{U}$ to the initial state (72) and using equation (73), we obtain:

$$|\gamma'\rangle = \frac{1}{\sqrt{2}} \sum_{s=\pm 1} \int dp\, e^{is\Psi(\vec{n})} \mathrm{F}(p)\,|p'(p), s\rangle\,. \tag{75}$$

Between the affine parameters λ_1 and λ_2, the photons have followed a single null geodesic. This means that the null vectors p' and p have the same constants of motion and therefore a similar expression but evaluated at different spacetime coordinates. In that sense, p' is a function of the initial momentum p.

Notice that the initial state we chose (72) can be written as a tensor product $|\gamma_p\rangle \otimes |\gamma_s\rangle$ of a momentum state $|\gamma_p\rangle = \int dp\, \mathrm{F}(p)\,|p\rangle$ and helicity state $|\gamma_s\rangle = (|{+1}\rangle + |{-1}\rangle)/\sqrt{2}$, it is therefore a separable state. This is not true anymore for the observed state at reception (75). Because the Wigner phase factor depends both on the photon's propagation direction and helicity, it causes the momentum and helicity states in the wavepacket to appear entangled after propagation in the curved spacetime.

3.3.4 *Helicity states*

We can provide a reference channel where no Wigner phase is acquired by using wavepackets with helicities distributed as a Bell state of the type $(|+_p -_p\rangle \pm |-_p +_p\rangle)/\sqrt{2}$, instead of the simple $|\gamma_s\rangle$ superposition we considered previously. Indeed, in such a Bell state each helicity eigenstate in the tensor products gives a phase opposite to the one given by the other state of the product. The products and therefore the total state remain invariant under the rotation of the polarisation in curved spacetime [63, 64].

On the contrary, one can increase the effect we are looking at by using helicity states distributed as GHZ states $(|+_p\rangle^{\otimes m} \pm |-_p\rangle^{\otimes m})/\sqrt{2}$. In that case, the tensor product of the $+1$ helicity eigenstates acquires m times the Wigner phase Ψ, while the negative helicities tensor product picks up a total phase of $-m\Psi$. The total differential phase of the superposition is therefore $2m\Psi$, in other words we obtain an amplification of the phase by a factor m.

Part II.

Phononic gravitational wave detectors

4

GRAVITATIONAL WAVE INTERACTION WITH A BEC

In this chapter we describe the theory behind the experiment proposal for a compact gravitational wave detector using a Bose-Einstein condensate. Gravitational waves are one of the last predictions of general relativity to have been confirmed by experiment [8]. A first indication of the existence of gravitational waves was given by the measurement of the decay of the Hulse-Taylor binary's orbit [65], that followed precisely the rate given by the emission of gravitational waves predicted by general relativity. Recently, several direct measurements of gravitational waves were achieved by the Laser Interferometer Gravitational-Wave Observatory [8], mostly gravitational waves emitted by colliding black hole pairs, but also by an inspiralling neutron star pair that could be confirmed by optical detection [66]. However such interferometric schemes require huge infrastructure and can only detect gravitational waves received from a specific direction. More refined, compact and versatile detectors will thus be required in order for the field of gravitational waves astronomy to develop substantially in the future, as a new way to observe the Cosmos.

4.1 DESCRIPTION OF THE DETECTOR

Contrarily to the first scheme to have detected gravitational waves, that is LIGO [8], the gravitational wave detector we present here is not an interferometric scheme, but is based on the resonance of a phononic field in a

BEC. This permits a much more compact device than the 4km long interometer used in LIGO. Also, the shape and the orientation of the BEC could be changed rather easily in order to detect gravitational waves coming from different directions, which is not achievable with the current interferometric schemes. In some sense, such a detector would be a quantum version of the Weber experiment where large metal bars were expected to resonate with gravitational waves [67].

Gravitational waves can create particles in cavities, as was found in [68]. In [41] it was shown that a gravitational wave propagating in a trapped BEC creates phonons. When some of the phononic modes in the BEC enter in resonance with the gravitational wave, the mode-mixing and the creation of phonons become large enough to yield a measurable change in the quantum state. The BEC can then be used as a gravitational wave detector. One can tune the parameters of the BEC such as its size, its pressure and density and therefore the speed of sound in the condensate, in order to obtain mode frequencies of phonons that match the resonance condition with the gravitational wave.

4.2 EFFECTIVE BACKGROUND FOR THE PHONONS IN THE CONDENSATE

4.2.1 *Gravitational wave spacetime*

The spacetime of a gravitational wave satisfies the linearised Einstein's equations. This means that the change in the spacetime curvature due to a passing gravitational wave is very small and it can be seen as a perturbation on top of the spacetime background. For a gravitational wave propagating on a flat spacetime background, the metric tensor is given by: $g = \eta + h$, with $\eta = \mathrm{diag}(-1, 1, 1, 1)$ the Minkowski metric and the components of the perturbation are $h_{\mu\nu} \ll 1$. We work in the transverse traceless gauge, namely with $\partial_\mu h^{\mu\nu} = 0$, $h_{0\mu} = 0$ and $h^{\mu}{}_{\mu} = 0$. In this gauge, we can describe a monochromatic gravitational plane wave that is elliptically polarised and

propagating along the z direction. The perturbation $\boldsymbol{h}$ has $h_{xx} = -h_{yy} \equiv h_+$ and $h_{xy} = h_{yx} = h_\times$ as only non-zero components. The h_+ and $h_\times$ perturbations only depend on $(t - z)$ and the $+$ and $\times$ indices refer to the different polarisations of the wave. In this chapter we will work in $1+1$ dimensions, namely the BEC has only one spatial dimension. Such a BEC will only feel the h_+ perturbation, and the spacetime's reduced line element along the 1-dimensional BEC reads $ds^2 = -dt^2 + (1 + h_+)dx^2$.

4.2.2 *Effective metric in the Bose-Einstein condensate*

Now that we have given the mathematical description of the curved spacetime background, we are interested in defining the effective metric on which the phonons propagate. Such a metric is the equivalent for phonons in the BEC to the spacetime's metric for photons. A BEC can be described by a classical mean field Ψ with a small quantum perturbation $\hat{\Pi}$, which is the phononic field propagating on the BEC's surface in a similar way as ripples evolve on a stretch of water. The phononic field verifies a wave equation $\Box\hat{\Pi} = 0$ with the d'Alembert operator $\Box = \frac{1}{\sqrt{-\mathcal{G}}}\partial_\mu(\sqrt{-\mathcal{G}}\mathcal{G}^{\mu\nu}\partial_\nu)$. The metric components of the effective background perceived by the phonons is [69, 70]:

$$\mathcal{G}_{\mu\nu} = \frac{n_0^2\, c_s^{-1}}{\rho_0 + p_0}\left(g_{\mu\nu} + \left(1 - \frac{c_s^2}{c^2}\right)V_\mu V_\nu\right), \tag{76}$$

where we restore the speed of light c for clarity. The metric tensor $\boldsymbol{g}$ is the spacetime's metric as if there was no BEC, the speed of sound is given by $c_s = c\sqrt{\partial p(\rho)/\partial\rho}$ where p and ρ are the pressure and energy density of the BEC respectively, and $\boldsymbol{V}$ is the flows' velocity. The other parameters of the conformal factor, n_0, p_0 and ρ_0 are respectively the density, the pressure and the energy density of the bulk of the BEC, namely of the mean classical background field Ψ. Let us work in the comoving frame of the BEC's flows, i.e. with $V^\mu = c\,\delta^{\mu 0}$. If we further assume a flat spacetime background prior to the gravitational wave's perturbation, we then have an

effective BEC metric of the form $\boldsymbol{\mathcal{G}} = \frac{n_0^2 c_s^{-1}}{\rho_0 + p_0}\text{diag}(-c_s^2, 1, 1, 1)$. The phonons therefore propagate on the BEC with an effective metric that resembles very much the Minkowski spacetime metric where photons propagate, the only differences being the conformal factor and the speed of the field's excitations: the speed of light is here replaced by the speed of sound in the BEC. When the gravitational wave hits the BEC, the BEC's effective metric reads:

$$\boldsymbol{\mathcal{G}} = \frac{n_0^2 c_s^{-1}}{\rho_0 + p_0}\begin{pmatrix} -c_s^2 & 0 & 0 & 0 \\ 0 & 1+h_+ & h_\times & 0 \\ 0 & h_\times & 1+h_+ & 0 \\ 0 & 0 & 0 & 1 \end{pmatrix} \tag{77}$$

For the 1-dimensional BEC that we consider, we have the effective metric:

$$\boldsymbol{\mathcal{G}} = \frac{n_0^2 c_s^{-1}}{\rho_0 + p_0}\text{diag}(-c_s^2, 1 + h_+). \tag{78}$$

The wave equation is conformaly invariant in 1+1 dimensions, in practice we will therefore be able to use the simple metric $\boldsymbol{\mathcal{G}} = \text{diag}(-c_s^2, 1 + h_+)$.

4.3 PHONON CREATION AND MODE-MIXING

In this section we describe how the phonon field evolves due to the presence of the gravitational wave. We first define the phonons as excitations of the quantised massless scalar field of the BEC, which evolve upon the background given in (78). We then compare the phononic field before and during the passing of the gravitational wave thanks to the associated Bogolyubov transformation.

4.3.1 *Quantised phononic field*

Before the passage of the gravitational wave through the BEC, the quantum field of the phonons can be decomposed in the usual way:

$$\hat{\Pi}(t, x) = \sum_{k \in \mathbb{N}^*} \phi_k(t, x)\, \hat{a}_k + \phi_k^*(t, x)\, \hat{a}_k^\dagger, \tag{79}$$

with $\hat{a}_k$ and $\hat{a}_k^\dagger$ respectively the annihilation and creation operators on the flat effective BEC metric. We consider a BEC in a trap of length $L = x_R - x_L$,

with x_L and x_R the positions of the left and right ends of the trap, respectively. Imposing vanishing boundary conditions on the edges of the trap, we obtain the following field modes:

$$\phi_k(t,x) = \frac{1}{\sqrt{k\pi}} \sin\left(k\pi \frac{x - x_L}{L}\right) e^{-i\omega_k t}, \tag{80}$$

with the dispersion relation $\omega_k = k\frac{\pi c_s}{L}$, which is valid as long as $\hbar \mathrm{k}_k \ll m_0\, c_s$, where $\mathrm{k}_k = k\,\pi/L$ and m_0 are respectively the wave number of mode k and the mass of the atoms in the BEC.

4.3.2 *Discrete Bogolyubov transformation*

The passing of the gravitational wave can be seen as a change in the basis of the field modes, i.e. a Bogolyubov transformation. To simplify the computation of such a transformation, we first assume that the change in the spacetime's metric happens in a discrete manner: $h_+ = \epsilon = cst. \ll 1$. The BEC's effective metric then reads $\boldsymbol{\mathcal{G}} = \mathrm{diag}(-c_s^2, 1+\epsilon)$. We work up to first order in ϵ since the amplitude of the gravitational wave is expected to be very small. First, we expand the phonon field in a new basis corresponding to the presence of the wave: $\hat{\Pi}(t,x) = \sum_{k\in\mathbb{N}^*} \Phi_k(t,x)\,\hat{A}_k + \Phi_k^*(t,x)\,\hat{A}_k^\dagger$, where the mode functions and mode operators are denoted in capital letters in the new basis. In order to find the expression of the field modes during the passage of the gravitational wave, we perform a change of coordinates such that the metric becomes conformally flat:

$$ds^2 = -c_s^2 d\eta^2 + (1+\epsilon)dx^2 = (1+\epsilon)(-c_s^2 dt^2 + dx^2), \tag{81}$$

where $dt = d\eta/\sqrt{1+\epsilon}$. The metric we obtain is therefore conformal to the flat metric. The wave equation $\Box\hat{\Pi} = 0$ is conformally invariant in 1+1 dimensions, we thus recover the same expression for the field modes as in the flat case, yet with new coordinates for the boundaries:

$$\Phi_k(t,x) = \frac{1}{\sqrt{k\pi}} \sin\left(k\pi \frac{x - x_L\sqrt{1+\epsilon}}{L\sqrt{1+\epsilon}}\right) e^{-i\frac{\omega_k}{\sqrt{1+\epsilon}}t}. \tag{82}$$

Now that we have the field modes before and after the discrete change due to the gravitational wave, we should be able to compute the discrete Bogolyubov coefficients of the transformation: ${}_0\alpha_{jk}(\epsilon) = (\Phi_j, \phi_k)$ and ${}_0\beta_{jk}(\epsilon) = -(\Phi_j, \phi_k^*)$. We use the inner product (31) and obtain, up to first order in ϵ, the following discrete Bogolyubov coefficients:

$$ {}_0\alpha_{jk}(\epsilon) = -\frac{\left(1+(-1)^{j+k}\right)\sqrt{jk}}{4(j-k)}\,\epsilon \quad (j \neq k), \tag{83} $$

$$ {}_0\beta_{jk}(\epsilon) = \frac{\left(1+(-1)^{j+k}\right)\sqrt{jk}}{4(j+k)}\,\epsilon, \tag{84} $$

and ${}_0\alpha_{jj}(\epsilon) = 1 + O(\epsilon^2)$. Here we made the assumptions of a box that expands and contracts symmetricaly, with center placed at $x = 0$ and therefore boundaries initially at $x_{L/R} = \mp L/2$. Other assumptions, like a box with $x_L = 0$ and $x_R = L$, lead to different Bogolyubov coefficients. This can be easily understood: in the case we are looking at, the center of the cavity is unaffected by the gravitational wave, while in the latter example it is the left boundary of the cavity that remains fixed. These are obviously two different physical situations, that should lead to different changes in the phononic field. Although we will work in the symmetric case, for the sake of generality we provide below the expression of the discrete Bogolyubov coefficients up to first order in ϵ for an arbitrary boundary choice:

$$ {}_0\alpha_{jk}(\epsilon) = \frac{\left(x_L-(-1)^{j+k}(L+x_L)\right)\sqrt{jk}}{2L(j-k)}\,\epsilon \quad (j \neq k), \tag{85} $$

$$ {}_0\beta_{jk}(\epsilon) = -\frac{\left(x_L-(-1)^{j+k}(L+x_L)\right)\sqrt{jk}}{2L(j+k)}\,\epsilon, \tag{86} $$

and ${}_0\alpha_{jj}(\epsilon) = 1 + O(\epsilon^2)$ remains unchanged.

4.3.3 *Validity of the discrete Bogolyubov transformation*

The discrete Bogolyubov coefficients derived in the previous subsection are fulfiling the Bogolyubov identities up to first order in ϵ. This is not an obvious fact: the inner product (31) was constructed for a continuous Bogolyubov transformation, where the spacelike surface of integration is the

same before and after the transformation. For the discrete change in the metric considered here, the spacelike surface at $t = 0^-$ and the one at $t = 0^+$ are different. If we take the case where $\epsilon > 0$ for example, see Figure 1, prior to

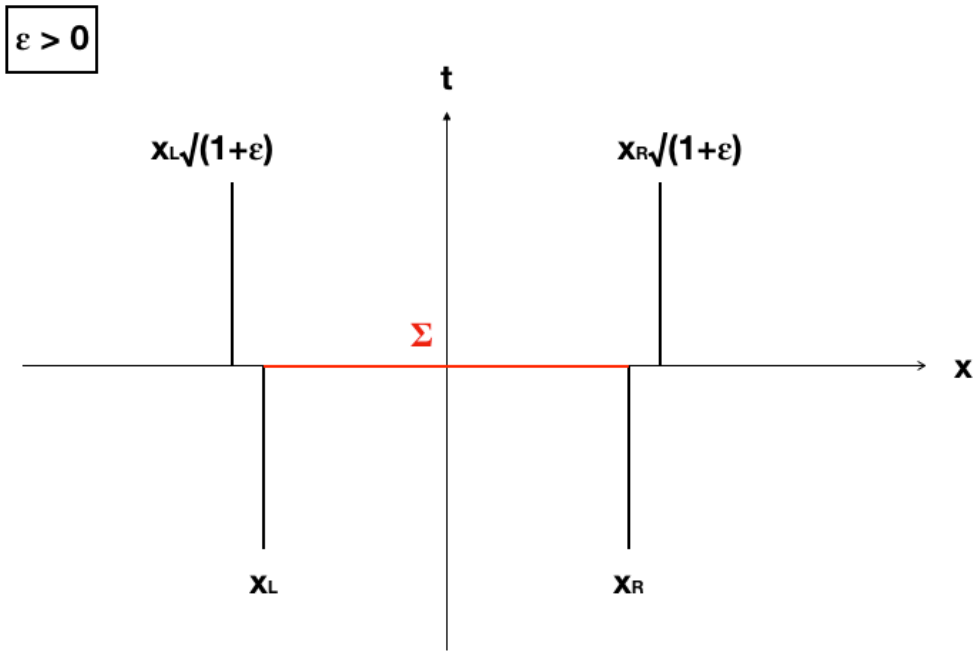

Figure 1.: Discrete cavity expansion

the transformation the field lives on a spacelike hypersurface that is smaller than the one where the field evolves to. This is in principle fine because if we choose the spacelike surface $\Sigma = \{x \in [x_L, x_R]\}$, which corresponds to the spatial extent of the cavity at $t = 0^-$, no portion of the field is lost in the transformation since the future surface is larger than the past one. At $t = 0^+$ the field still lies on Σ, which ensures that the discrete transformation at $t = 0$ is reversible. For $t > 0$ however, some of the field will evolve to the regions $x_L\sqrt{1+\epsilon} < x \leq x_L$ and $x_R \leq x < x_R\sqrt{1+\epsilon}$.

For the contraction case, namely when $\epsilon < 0$, it is in a first place not so clear whether our calculation is fine or not: in that case the hypersurface where the field lives is larger prior to the transformation. Therefore, it seems that some of the field, that at $t < 0$ lived in the regions $x_L < x \leq x_L\sqrt{1+\epsilon}$

and $x_R\sqrt{1+\epsilon} \leq x < x_R$, might leak out of the cavity at $t > 0$, see Figure 2. In order to assert the rightness of our computation, we need to compare

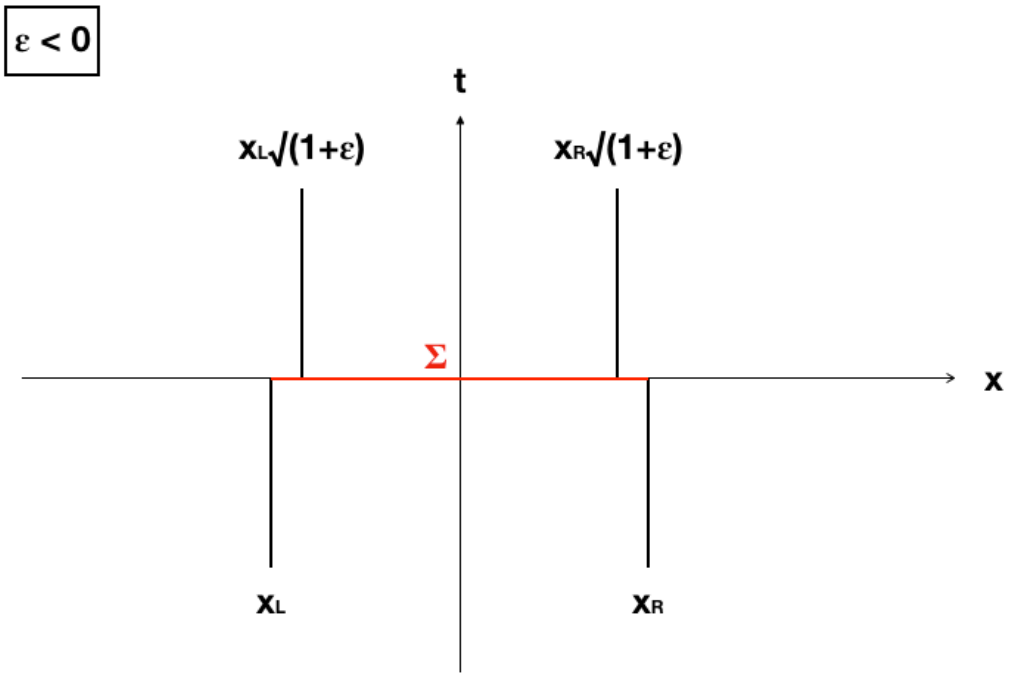

Figure 2.: Discrete cavity contraction

the value for the inner product (31) with integration on the past surface Σ, as we previously did, with an integration on the future hypersurface $\Sigma_\epsilon = \{x \in [x_L\sqrt{1+\epsilon}, x_R\sqrt{1+\epsilon}]\}$. We denote such inner products by $(\Phi_j, \phi_k)_\Sigma$ and $(\Phi_j, \phi_k)_{\Sigma_\epsilon}$ respectively. We do not need to further check for the inner products of the form (Φ_j, ϕ_k^*) since the spatial part of the mode functions, that is relevant for the present inquiry, is real valued. We find:

$$(\Phi_j, \phi_k)_\Sigma - (\Phi_j, \phi_k)_{\Sigma_\epsilon} = O(\epsilon^3), \tag{87}$$

which confirms that the discrete Bogolyubov coefficients we obtain are fine up to second order in the amplitude of the gravitational wave ϵ, and therefore to the order at which we carry out our computations.

4.3.4 *Continuous Bogolyubov transformation*

To obtain the continuous Bogolyubov coefficients for the transformation experienced by the phonons during the whole passing of the gravitational wave, one has to integrate the discrete Bogolyubov coefficients we obtained in (83) and (84). This procedure was introduced in [71] for small accelerations. The same formalism can be applied to small changes in the curved spacetime, e.g. by a gravitational wave. In [41] this was used in order to compute the continuous Bogolyubov transformation induced by the passing gravitational waves on the states of the BEC. However, the formulas in [71] cannot be exactly used in our computation: in order to obtain the first order continuous Bogolyubov coefficients, it is assumed in [71] that the modes' frequencies only change at the second order in the acceleration perturbation. This is however not the case in our calculation since the frequency of the phononic modes change already at first order in ϵ. More general equations thus need to be derived. We follow the same procedure as in [71], but we take into account this change at first order in the modes' frequencies due to the presence of the gravitational wave.

The continuous Bogolyubov coefficients are encoded in the symplectic matrix $\boldsymbol{S} = \begin{pmatrix} \boldsymbol{\alpha} & \boldsymbol{\beta} \\ \boldsymbol{\beta}^* & \boldsymbol{\alpha}^* \end{pmatrix}$. The Bogolyubov identities in matrix form are given by the symplectic relation $\begin{pmatrix} \mathbb{1} & \mathbf{0} \\ \mathbf{0} & -\mathbb{1} \end{pmatrix} = \boldsymbol{S}\begin{pmatrix} \mathbb{1} & \mathbf{0} \\ \mathbf{0} & -\mathbb{1} \end{pmatrix}\boldsymbol{S}^\dagger$. Introducing $\boldsymbol{K} = \begin{pmatrix} {}_0\boldsymbol{\alpha} & {}_0\boldsymbol{\beta} \\ {}_0\boldsymbol{\beta} & {}_0\boldsymbol{\alpha} \end{pmatrix}$, which gathers the discrete Bogolyubov coefficients from inertial motion to perturbed motion, we have:

$$\dot{\boldsymbol{S}} = i\boldsymbol{K}^{-1}\tilde{\boldsymbol{\Omega}}\boldsymbol{K}\boldsymbol{S}, \tag{88}$$

where $\tilde{\boldsymbol{\Omega}} = \mathrm{diag}(\boldsymbol{\Omega}, -\boldsymbol{\Omega})$ and $\boldsymbol{\Omega} = \mathrm{diag}(\Omega_1, \Omega_2, \ldots)$ gathers the perturbed mode frequencies. We will now try to integrate this equation in order to obtain the explicit expression for the Bogolyubov transformation $\boldsymbol{S}$ caused by a real (namely, continuous) gravitational wave.

Gravitational wave

Under the presence of a gravitational wave, up to first order in the amplitude of the gravitational wave ϵ we have:

$$\Omega_n = \omega_n + \Omega_n^{(1)}\,\epsilon = \omega_n - \frac{\omega_n}{2}\,\epsilon, \tag{89}$$

$$_0\boldsymbol{\alpha} = \mathbb{1} + \hat{\boldsymbol{\alpha}}\,\epsilon, \tag{90}$$

$$_0\boldsymbol{\beta} = \hat{\boldsymbol{\beta}}\,\epsilon, \tag{91}$$

$$\boldsymbol{K} = \mathbb{1} + \boldsymbol{K}^{(1)}\,\epsilon. \tag{92}$$

The first order discrete Bogolyubov coefficients $\hat{\boldsymbol{\alpha}}$ and $\hat{\boldsymbol{\beta}}$ are given by (83) and (84). We look for the continuous Bogolyubov coefficients in the form:

$$\boldsymbol{\alpha} = e^{i\boldsymbol{\omega}(\tau_f-\tau_0)}\left(\mathbb{1} + \hat{\boldsymbol{A}}\right), \tag{93}$$

$$\boldsymbol{\beta} = e^{i\boldsymbol{\omega}(\tau_f-\tau_0)}\hat{\boldsymbol{B}}, \tag{94}$$

$$\boldsymbol{S} = e^{i\tilde{\boldsymbol{\omega}}(\tau_f-\tau_0)}\left(\mathbb{1} + \boldsymbol{S}^{(1)}\epsilon(t)\right), \tag{95}$$

where $\tilde{\boldsymbol{\omega}} = \mathrm{diag}(\boldsymbol{\omega}, -\boldsymbol{\omega})$ and $\boldsymbol{\omega} = \mathrm{diag}(\omega_1, \omega_2, ...)$ gathers the unperturbed modes' frequencies, and we introduced the time dependent perturbation $\epsilon(t) = \epsilon f(t)$. The differential equation (88) then reads explicitly

$$i\tilde{\boldsymbol{\omega}}e^{i\tilde{\boldsymbol{\omega}}(t-\tau_0)}\left(\mathbb{1} + \boldsymbol{S}^{(1)}f(t)\,\epsilon\right) + e^{i\tilde{\boldsymbol{\omega}}(t-\tau_0)}\left(\dot{\boldsymbol{S}}^{(1)}f(t) + \boldsymbol{S}^{(1)}\dot{f}(t)\right)\epsilon \tag{96}$$

$$= i\boldsymbol{K}^{-1}\tilde{\boldsymbol{\Omega}}\boldsymbol{K}\boldsymbol{S} \tag{97}$$

$$= i\left(\mathbb{1} - \boldsymbol{K}^{(1)}f(t)\,\epsilon\right)\left(\tilde{\boldsymbol{\omega}} - \frac{\tilde{\boldsymbol{\omega}}}{2}f(t)\,\epsilon\right)\left(\mathbb{1} + \boldsymbol{K}^{(1)}f(t)\,\epsilon\right)e^{i\tilde{\boldsymbol{\omega}}(t-\tau_0)}\left(\mathbb{1} + \boldsymbol{S}^{(1)}f(t)\,\epsilon\right)$$

$$= i\left(\tilde{\boldsymbol{\omega}} + \left(\left[\tilde{\boldsymbol{\omega}}, \boldsymbol{K}^{(1)}\right] - \frac{\tilde{\boldsymbol{\omega}}}{2}\right)f(t)\,\epsilon\right)e^{i\tilde{\boldsymbol{\omega}}(t-\tau_0)}\left(\mathbb{1} + \boldsymbol{S}^{(1)}f(t)\,\epsilon\right) \tag{98}$$

thus

$$e^{i\tilde{\boldsymbol{\omega}}(t-\tau_0)}\left(\dot{\boldsymbol{S}}^{(1)} + \boldsymbol{S}^{(1)}\frac{\dot{f}(t)}{f(t)}\right) = i\left(\left[\tilde{\boldsymbol{\omega}}, \boldsymbol{K}^{(1)}\right] - \frac{\tilde{\boldsymbol{\omega}}}{2}\right)e^{i\tilde{\boldsymbol{\omega}}(t-\tau_0)} \tag{99}$$

and therefore

$$\dot{\boldsymbol{S}}^{(1)} + \boldsymbol{S}^{(1)}\frac{\dot{f}(t)}{f(t)} = i\,e^{-i\tilde{\boldsymbol{\omega}}(t-\tau_0)}\left[\tilde{\boldsymbol{\omega}}, \boldsymbol{K}^{(1)}\right]e^{i\tilde{\boldsymbol{\omega}}(t-\tau_0)} - i\,\frac{\tilde{\boldsymbol{\omega}}}{2}. \tag{100}$$

A solution of (100) is $\boldsymbol{S}^{(1)}(t) = f^{-1}(t)\int^t \boldsymbol{c}(\tau)f(\tau)\,d\tau$, where $\boldsymbol{c}(t)$ is the term in the right hand side of (100). Since $\left[\tilde{\boldsymbol{\omega}}, \boldsymbol{K}^{(1)}\right] = \begin{pmatrix} [\boldsymbol{\omega},\hat{\boldsymbol{\alpha}}] & \{\boldsymbol{\omega},\hat{\boldsymbol{\beta}}\} \\ -\{\boldsymbol{\omega},\hat{\boldsymbol{\beta}}\} & -[\boldsymbol{\omega},\hat{\boldsymbol{\alpha}}] \end{pmatrix}$, we have:

$$\hat{\boldsymbol{A}}(\tau_f,\tau_0) = i\int_{\tau_0}^{\tau_f} e^{-i\boldsymbol{\omega}(t-\tau_0)}\,[\boldsymbol{\omega},\hat{\boldsymbol{\alpha}}]\,e^{i\boldsymbol{\omega}(t-\tau_0)}\,\epsilon(t)\,dt - i\,\frac{\boldsymbol{\omega}}{2}\int_{\tau_0}^{\tau_f}\epsilon(t)\,dt, \quad (101)$$

$$\hat{\boldsymbol{B}}(\tau_f,\tau_0) = i\int_{\tau_0}^{\tau_f} e^{-i\boldsymbol{\omega}(t-\tau_0)}\,\{\boldsymbol{\omega},\hat{\boldsymbol{\beta}}\}\,e^{-i\boldsymbol{\omega}(t-\tau_0)}\,\epsilon(t)\,dt. \quad (102)$$

Using that $\hat{\boldsymbol{\alpha}}^{tp} = -\hat{\boldsymbol{\alpha}}$ and $\hat{\boldsymbol{\beta}}^{\mathrm{tp}} = \hat{\boldsymbol{\beta}}$, which holds for the first order terms of real Bogolyubov coefficients, we find:

$$\hat{A}_{jk}(\tau_f,\tau_0) = i\,(\omega_j-\omega_k)\hat{\alpha}_{jk}\int_{\tau_0}^{\tau_f} e^{-i(\omega_j-\omega_k)(t-\tau_0)}\,\epsilon(t)\,dt - i\,\frac{\omega_k\delta_{jk}}{2}\int_{\tau_0}^{\tau_f}\epsilon(t)\,dt, \quad (103)$$

$$\hat{B}_{jk}(\tau_f,\tau_0) = i\,(\omega_j+\omega_k)\hat{\beta}_{jk}\int_{\tau_0}^{\tau_f} e^{-i(\omega_j+\omega_k)(t-\tau_0)}\,\epsilon(t)\,dt. \quad (104)$$

The contribution due to the change in the frequency up to the first order in the gravitational wave's amplitude ϵ, that is the last term in the right hand side of (103), occurs for diagonal mode mixing coefficients only. This term is the only correction to what was used in [41].

Resonances

In this section we look at the effective Bogolyubov transformations happening to the phononic field when two of the field modes are in resonance with the gravitational wave. In practice, we can tune the parameters of the BEC (size, density, pressure) in order to modify its fundamental frequency $\omega_1 = c_s\,\pi/L$ such that two of the phononic modes resonate with the expected frequency of the gravitational wave to be measured. When such resonance occurs, the relativistic transformation of the phononic field becomes important and measurable. Let us denote the resonating modes by the integers m and n, and the gravitational wave's frequency by Ω_{GW}. Let us assume that the gravitational wave's perturbation takes the form of a simple oscillation $\epsilon(t) = \epsilon\sin\Omega_{\mathrm{GW}}t$. Several resonances can be considered, the most interesting ones being *a priori* $\Omega_+ = \omega_m + \omega_n = \Omega_{\mathrm{GW}}$ and $\Omega_- = \omega_m - \omega_n = \Omega_{\mathrm{GW}}$ with $m > n$. For example, in the initial proposal [41], the choice was made to focus on the particle creation resonance when

$\Omega_+ = \Omega_{\mathrm{GW}}$. In this section we provide a general account for both mode mixing and particle creation resonances, for gravitational waves with frequencies matching Ω_+ and Ω_-. In a first place, we focus on the computation of the integrals $I_{\alpha/\beta} = \int_{\tau_0}^{\tau_f} e^{-i(\omega_j \mp \omega_k)(t-\tau_0)} \sin(\Omega_{\mathrm{GW}} t)\, dt$ from the expressions (103) and (104) respectively. These integrals are where the resonant terms will appear. For simplicity, we set $\tau_f = \tau$ and $\tau_0 = 0$. Let us start with a BEC with Ω_+ matching the gravitational wave's frequency. We find:

$$I_{+,\alpha} = \frac{e^{-i(j-k)\omega_1 \tau}\left((m+n)\cos(\Omega_+\tau) + i(j-k)\sin(\Omega_+\tau)\right) - m - n}{(j-k+m+n)(j-k-m-n)\,\omega_1}, \tag{105}$$

$$I_{+,\beta} = \frac{e^{-i(j+k)\omega_1 \tau}\left((m+n)\cos(\Omega_+\tau) + i(j+k)\sin(\Omega_+\tau)\right) - m - n}{(j+k-m-n)(j+k+m+n)\,\omega_1}. \tag{106}$$

One can notice that we have here two mode mixing resonances but only one particle creation resonance. They occur respectively for $j = k - m - n$ and $j = k + m + n$, and $j = m + n - k$. We recalculate $I_{+,\alpha/\beta}$ assuming such values before integrating in order to obtain the resonant terms. To make these resonant terms apparent, we work in the regime $\omega_1 \tau \gg 1$, that is the resonance regime. This regime is necessary in order to accumulate the effect of the resonance sufficiently and to make the change of the phonons' state measurable, see [41] for more details on the measurability issues and the related metrology computations. In the resonant regime, we have the simplified expressions:

$$I_{+,\alpha} \sim \frac{i}{2}\tau\left(\delta_{j+m+n,k} - \delta_{j,k+m+n}\right), \tag{107}$$

$$I_{+,\beta} \sim -\frac{i}{2}\tau\,\delta_{j+k,m+n}. \tag{108}$$

Let us now consider the case where Ω_- matches the gravitational wave's frequency. We find:

$$I_{-,\alpha} = \frac{e^{-i(j-k)\omega_1 \tau}\left((m-n)\cos(\Omega_-\tau) + i(j-k)\sin(\Omega_-\tau)\right) - m + n}{(j-k+m-n)(j-k-m+n)\,\omega_1}, \tag{109}$$

$$I_{-,\beta} = \frac{e^{-i(j+k)\omega_1 \tau}\left((m-n)\cos(\Omega_-\tau) + i(j+k)\sin(\Omega_-\tau)\right) - m + n}{(j+k+m-n)(j+k-m+n)\,\omega_1}. \tag{110}$$

Here we have two mode mixing resonances and two particle creation resonances: respectively for $j = k - m + n$ and $j = k + m - n$, and for $j = n - m - k$ and $j = m - n - k$. In the resonance regime $\omega_1 \tau \gg 1$, we have:

$$I_{-,\alpha} \sim \frac{i}{2}\tau\,(\delta_{j,k-m+n} - \delta_{j,k+m-n}), \tag{111}$$

$$I_{-,\beta} \sim \frac{i}{2}\tau\,(\delta_{j+k,n-m} - \delta_{j+k,m-n}). \tag{112}$$

The extra term from the first order change in the modes' frequencies, which we derived in (83), turns out to be negligible: it is a simple oscillation term which does not resonate. In the resonant regime it is therefore neglected along with all the other oscillatory terms that we already neglected. Now that we know the resonant terms, we can write the relevant Bogolyubov coefficients in the resonant regime, depending on which resonance we are interested in.

Explicit Bogolyubov coefficients

In order to obtain the explicit expression of the transformation experienced by the phonon field when a gravitational wave passes during a time τ, we now combine the results obtained above together with the discrete Bogolyubov coefficients (83) and (84) in the expression for the continuous Bogolyubov coefficients (103) and (104). We recall that we have defined the Bogolyubov matrices as $\boldsymbol{\alpha} = e^{i\omega\tau}\left(\mathbb{1} + \hat{\boldsymbol{A}}\right)$ and $\boldsymbol{\beta} = e^{i\omega\tau}\hat{\boldsymbol{B}}$. When $\Omega_+ = \Omega_{\mathrm{GW}}$, we have in the resonant regime $\omega_1 \tau \gg 1$:

$$\hat{A}_{jk}(\tau) \sim \omega_1 \tau \frac{1 + (-1)^{j+k}}{8} \sqrt{jk}\,(\delta_{j+m+n,k} - \delta_{j,k+m+n})\,\epsilon \tag{113}$$

$$\hat{B}_{jk}(\tau) \sim \omega_1 \tau \frac{1 + (-1)^{j+k}}{8} \sqrt{jk}\,\delta_{j+k,m+n}\,\epsilon. \tag{114}$$

When $\Omega_- = \Omega_{\mathrm{GW}}$ instead, we obtain:

$$\hat{A}_{jk}(\tau) \sim \omega_1 \tau \frac{1 + (-1)^{j+k}}{8} \sqrt{jk}\,(\delta_{j,k-m+n} - \delta_{j,k+m-n})\,\epsilon \tag{115}$$

$$\hat{B}_{jk}(\tau) \sim \omega_1 \tau \frac{1 + (-1)^{j+k}}{8} \sqrt{jk}\,(\delta_{j+k,m-n} - \delta_{j+k,n-m})\,\epsilon. \tag{116}$$

The Bogolyubov coefficients that we have obtained all have the same amplitude, the only differences in the Bogolyubov matrices being which coefficients resonate with the gravitational wave. For example, when $\Omega_+ = \Omega_{GW}$, the only mode mixing coefficients that resonate are given by the (j,k) that fulfil either $j = k + m + n$ or $k = j + m + n$, while the particle creation resonance occurs for the $j = m + n - k$ for all positive $k < m + n$. When $\Omega_- = \Omega_{GW}$, the non vanishing coefficients appear for other couples of (j,k). One can note however that all the coefficients for which $j + k$ is an odd number vanish. This is due to the choice of the symmetric cavity, and it would not happen for another choice of boundary condition. This can be seen by comparing the discrete Bogolyubov coefficients (83) and (84) we have used with the general ones in (85) and (86). Also notice that for both resonances $\Omega_+ = \Omega_{GW}$ and $\Omega_- = \Omega_{GW}$ there is no couple of non zero integers (j,k) such that we have both a mode mixing resonance and a particle creation resonance occuring at the same time.

4.4 CONCLUSION

In this chapter we have introduced the theory of the resonance of phononic modes in a Bose-Einstein condensate interacting with a gravitational wave. In a first place, we successfully derived the expression for the Bogolyubov transformation associated to a discrete change in the spacetime metric background of the BEC, up to first order in the perturbation. Then we derived the continuous Bogolyubov coefficients for a realistic, continuous gravitational wave. We then looked at different resonance scenarios and gave the explicit expression for the appropriate Bogolyubov transformations of the phononic field.

Based on the results obtained in this chapter, we will be able to look at the noise induced by the shaking of the cavity in the next chapter, along with other noise studies e.g. thermality.

5

NOISE IN THE PHONONIC GRAVITATIONAL WAVE DETECTOR

In this chapter, we review some noise sources for the proposed BEC gravitational wave detector described in the previous chapter. Possible sources of noise include in particular sismic noise, i.e. shaking of the cavity where the BEC and its phonons are trapped, and the noise due to the temperature of the BEC, i.e. cause by the thermal agitation of the atoms.

5.1 NOISE DUE TO THE SHAKING OF THE CAVITY

Here we study the influence of small displacements in the position of the cavity, which could lead to some changes in the field. In general we denote such displacements by the dimensionless parameter η, that we will keep up to order η^2 in our computations. The perturbation η will displace the cavity by a distance $\eta L \ll L$, where L is the length of the cavity. In the first subsection we look at how such a displacement transforms the phononic field within a cavity at rest. In the following subsection, this transformation is combined with the one induced by the gravitational wave in order to estimate how the shaking noise could affect the gravitational wave detection. We perform all these computations using discrete Bogolyubov transformations. Not only the computation is simpler so, but also one can expect that noise displacements actually happen almost discretely, as sudden hops, which justifies the approximation.

5.1.1 *Shaking cavity*

Following a similar procedure as in 4.3.2, we here compute the discrete Bogolyubov transformation experienced by the field modes when the cavity is slightly displaced in a Minkowski spacetime background (see Figure 3).

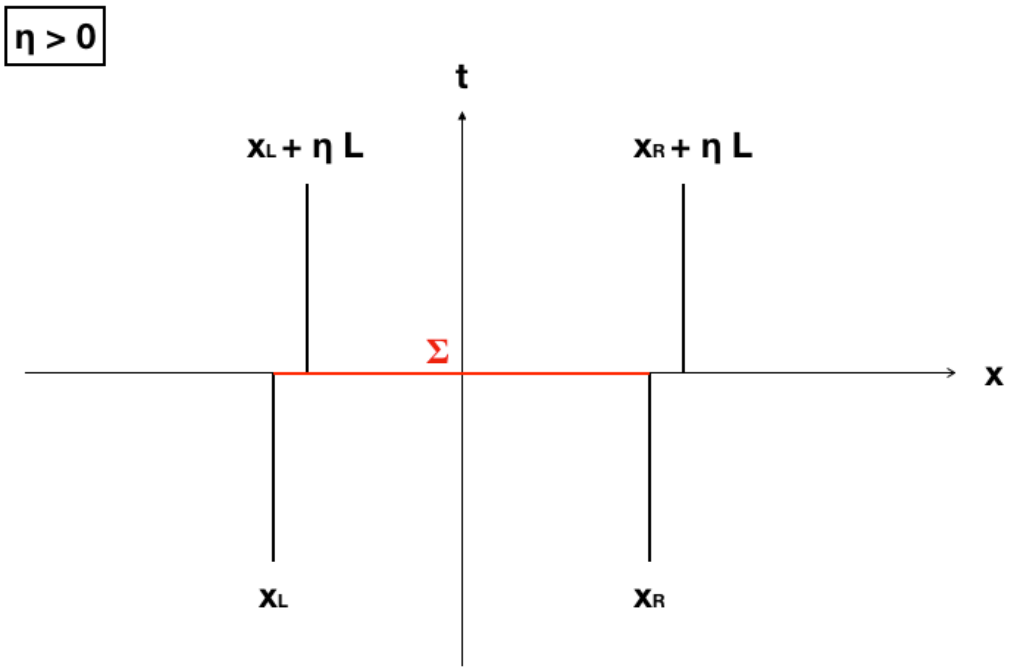

Figure 3.: Discrete cavity displacement. Here η is taken to be positive, the $\eta < 0$ case is obtained easily by shifting the boundaries x_L and x_R after transformation to the left instead.

The modes in the cavity are initially again given by (80) and the ones in the displaced cavity are:

$$\Phi_k(t,x) = \frac{1}{\sqrt{k\pi}} \sin\left(k\pi \frac{x - x_L}{L} - \eta\right) e^{-i\omega_k t}. \tag{117}$$

We then obtain the discrete Bogolyubov coefficients for the displacement:

$$\alpha_{jk}(\eta) = \sqrt{jk}\frac{1-(-1)^{j+k}}{j-k}\,\eta + O(\eta^3) \quad (j \neq k), \tag{118}$$

$$\beta_{jk}(\eta) = -\sqrt{jk}\frac{1-(-1)^{j+k}}{j+k}\,\eta + O(\eta^3), \tag{119}$$

and when $j = k$ we have $\alpha_{jj}(\eta) = 1 - \frac{\pi^2}{2}\,j^2\,\eta^2 + O(\eta^3)$. Note that β_{jj} vanishes identically, and not only perturbatively. This is a consequence of the invariance of the modes' frequencies under the displacement of the cavity. Notice that we find several Bogolyubov coefficients already up to first order in η only. This means that the effect of displacements up to the same amplitude as the stretching (resp. contracting) of the distances due to the gravitational wave are relevant and should be taken into account. Note that in a continuous picture the noise terms shouldn't resonate and therefore should be erased by the increased signal.

Here, as in subsection 4.3.3, we are also concerned by the validity of the discrete approximation we are using: there are possible leaks of the field due to the mismatch between the spacelike hypersurfaces delimited by the cavity before and after the displacement. Following the same procedure as before, we find:

$$(\Phi_j, \phi_k)_\Sigma - (\Phi_j, \phi_k)_{\Sigma_\eta} = O(\eta^3), \tag{120}$$

where $\Sigma_\eta = \{x \in [x_L + \eta L, x_R + \eta L]\}$. Namely, there is no leak of the field up to the order of our computation and we can therefore safely use these discrete Bogolyubov coefficients.

Here the frequencies of the modes do not change after the transformation, one can directly apply the techniques developed in [71] in order to obtain the continuous Bogolyubov coefficients. Up to first order in η, these read:

$$\boldsymbol{A}(t) = e^{i\boldsymbol{\omega}(t-t_0)}\left(\mathbb{1} + \tilde{\boldsymbol{A}} + O(\eta^2)\right), \tag{121}$$

$$\boldsymbol{B}(t) = e^{i\boldsymbol{\omega}(t-t_0)}\tilde{\boldsymbol{B}} + O(\eta^2), \tag{122}$$

where $\omega = \mathrm{diag}(\omega_1, \omega_2, ...)$ gathers the modes' frequencies and:

$$\tilde{A}_{jk} = i(\omega_j - \omega_k)\alpha^{(1)}_{jk} \int_{t_0}^{t} e^{-i(\omega_j - \omega_k)(\tau - t_0)} \eta(\tau)\, d\tau, \tag{123}$$

$$\tilde{B}_{jk} = i(\omega_j + \omega_k)\beta^{(1)}_{jk} \int_{t_0}^{t} e^{-i(\omega_j + \omega_k)(\tau - t_0)} \eta(\tau)\, d\tau, \tag{124}$$

where $\alpha^{(1)}_{jk}$ and $\beta^{(1)}_{jk}$ denote the first order discrete Bogolyubov coefficients found in (118) and (119), respectively. The noise function η is a random function of time, which frequency spectrum can be obtained by experimental characterisation. Knowing the frequency spectrum of the noise, one would then be able to model it through $\eta(\tau)$ in order to assert how it affects the probe states that are to be used in the gravitational wave detector.

5.1.2 *Shaking cavity with gravitational wave*

We now repeat the computation but including the effects of both the gravitational wave and the shaking of the cavity. We again work up to first order in ϵ, up to second order in η and we keep cross terms $O(\epsilon\,\eta)$ only. The mode functions of the phonon field experiencing both effects read:

$$\Phi_k(t, x) = \frac{1}{\sqrt{k\pi}} \sin\left(k\pi \frac{x - x_L\sqrt{1+\epsilon}}{L\sqrt{1+\epsilon}} - \eta\right) e^{-i\frac{\omega_k}{\sqrt{1+\epsilon}}t}. \tag{125}$$

We can now obtain the Bogolyubov coefficients for the transformation:

$$\alpha_{jk}(\epsilon, \eta) = -\sqrt{jk}\frac{1 + (-1)^{j+k}}{4(j-k)}\,\epsilon + \sqrt{jk}\frac{1 - (-1)^{j+k}}{j-k}\,\eta + j\sqrt{jk}\frac{1 - (-1)^{j+k}}{2(j-k)^2}\,\epsilon\,\eta, \tag{126}$$

$$\beta_{jk}(\epsilon, \eta) = \sqrt{jk}\frac{1 + (-1)^{j+k}}{4(j+k)}\,\epsilon - \sqrt{jk}\frac{1 - (-1)^{j+k}}{j+k}\,\eta - j\sqrt{jk}\frac{1 - (-1)^{j+k}}{2(j+k)^2}\,\epsilon\,\eta, \tag{127}$$

for $j \neq k$. When $j = k$, we have $\alpha_{jj}(\epsilon, \eta) = 1 - \frac{\pi^2}{2} j^2 \eta^2$ and the particle creation coefficients simplify $\beta_{jj}(\epsilon, \eta) = \frac{1}{4}\epsilon$. We will now enquire into possible leaks of the field during this discrete transformation. See Figures 4 and 5 for the eight different configurations that can occur when both effects happen jointly.

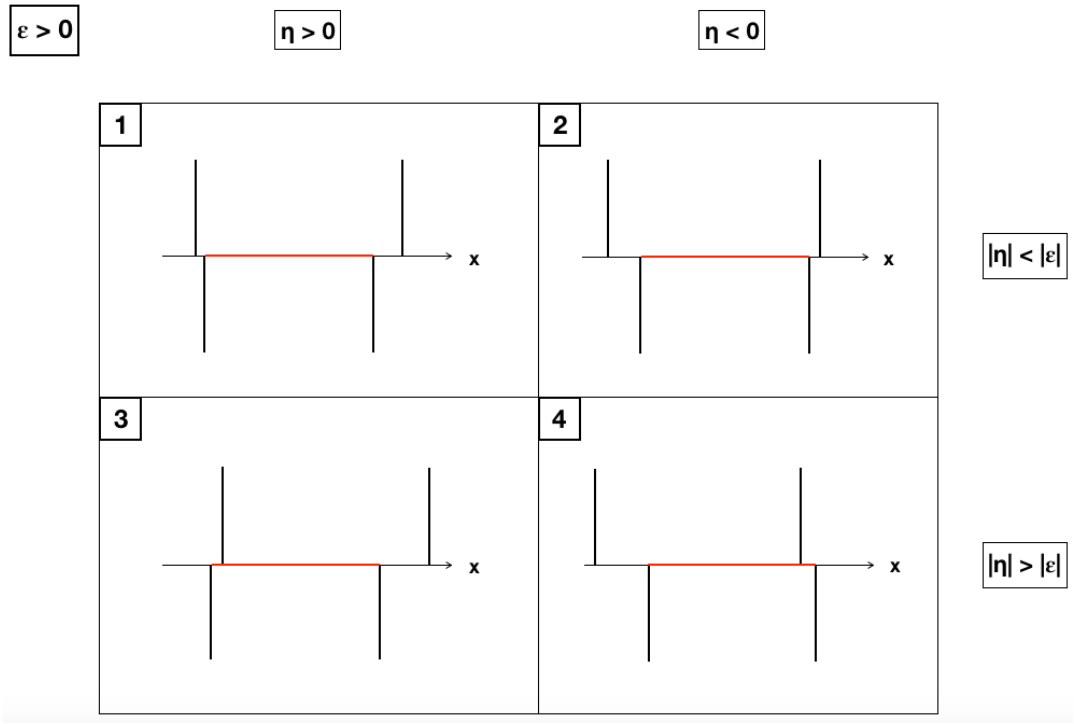

Figure 4.: Discrete cavity expansion including noise. Transformations 3 and 4 could possibly lead to leaks of the field.

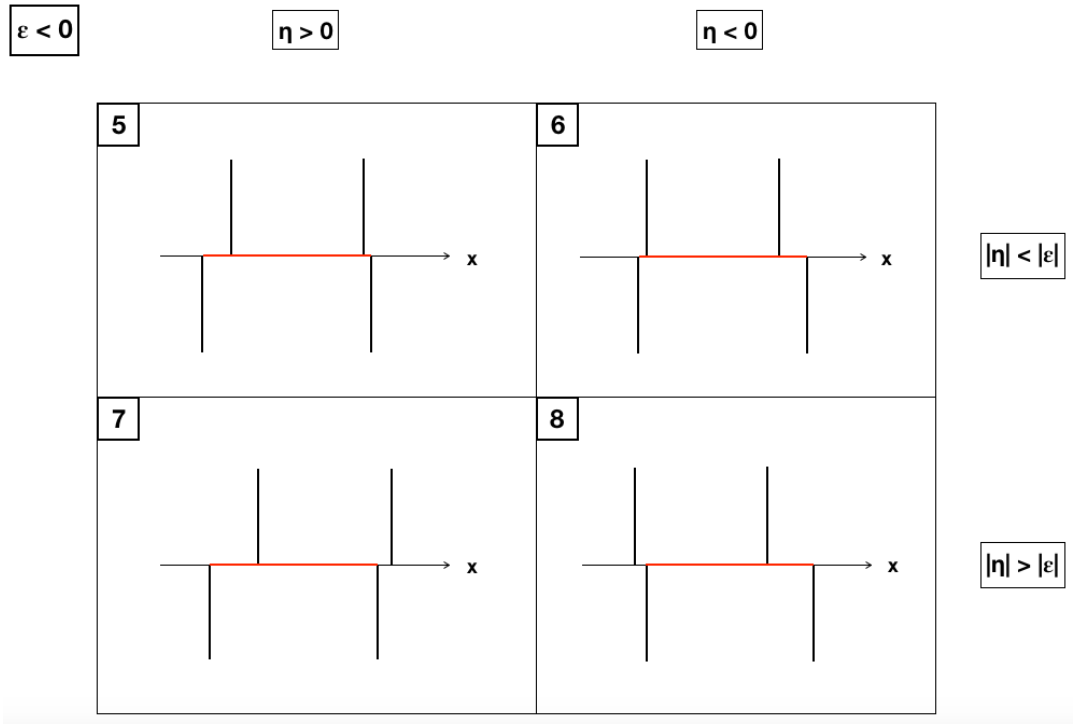

Figure 5.: Discrete cavity contraction including noise. The four transformations could possibly lead to leaks of the field.

One can see that among these eight cases, six of them are potentially pathologic (from case 3 to 8). In the contracting cavity cases (5 to 8), this had to be expected as it was already the case even without the shaking of the cavity. However, the expanding cavity transformation which was leak free before including the noise can in principle have leaks of the field when the amplitude of the noise $|\eta|$ is larger than the amplitude of the gravitational wave ϵ. Yet, following again the same procedure as in the previous computations, we find that:

$$(\Phi_j, \phi_k)_\Sigma - (\Phi_j, \phi_k)_{\Sigma'} = O\left(\epsilon^2, \eta^3, \epsilon\,\eta^2\right), \tag{128}$$

with the spacelike hypersurface of the cavity immediately after the transformation $\Sigma' = \{x \in [(x_L + \eta L)\sqrt{1+\epsilon}, (x_R + \eta L)\sqrt{1+\epsilon}]\}$. Therefore, up to the order we decided to work we can safely use the discrete Bogolyubov computation for the eight cases displayed above. These results however hold only when the noise considered has an amplitude at most of the square-root of the gravitational wave's amplitude, i.e. for $|\eta| \lesssim 10^{-11}$. Stronger sources of sismic noise would need a more systematic treatment.

5.2 NOISE DUE TO THE CONDENSATE'S THERMALITY

We now would like to find out which is the influence of the BEC's thermality on the state of the phonons used to detect the gravitational wave. This question was addressed in a different way in [4], where the effect of the states' thermality on the quantum metrology results was characterised. In this section, we give a simple analysis in order to obtain analytical insights on the effect of temperature on the quantum state of the phonons. For simplicity, we consider the phononic field to be constituted by only two modes: $m = 2$ and $n = 1$. In reality the phononic field is constituted by many more, but this approximation will simplify considerably the computations and won't change the result to the perturbative order at which we consider the temperature. The two modes are considered to be the ones resonating

with the gravitational wave. We thus have either $\Omega_+ = 3\omega_1 = \Omega_{GW}$ or $\Omega_- = \omega_1 = \Omega_{GW}$. The initial thermal state in the BEC reads:

$$\boldsymbol{\sigma}_{\text{th}} = \text{diag}(\nu_2 \mathbb{1}_{\mathbf{2}}, \nu_1 \mathbb{1}_{\mathbf{2}}), \tag{129}$$

where $\nu_j = \coth(j\beta/2)$ and $\beta = \hbar\omega_1/k_B T$. In the limit of small temperatures, namely when $\beta \to \infty$, we have $\nu_j \sim 1 + e^{-j\beta} + O(e^{-2j\beta})$. We thus have:

$$\boldsymbol{\sigma}_{\text{th}} = \mathbb{1}_{\mathbf{4}} + \text{diag}(\mathbf{0}, e^{-\beta}\, \mathbb{1}_{\mathbf{2}}) + O(e^{-2\beta}). \tag{130}$$

If the temperature is negligible in the condensate, the initial state is simply a vacuum state $\boldsymbol{\sigma}_{\text{vac}} = \mathbb{1}_{\mathbf{4}}$, as it was considered to be in the initial proposal [41]. Therefore, the difference in the initial state compared to the ideal case is $\Delta\boldsymbol{\sigma} = \boldsymbol{\sigma}_{\text{th}} - \boldsymbol{\sigma}_{\text{vac}} = \text{diag}(\mathbf{0}, e^{-\beta}\, \mathbb{1}_{\mathbf{2}})$, up to lowest order in the temperature.

One of the key features of the BEC gravitational wave detector is the squeezing of the two modes resonating with the wave. The resulting squeezed state is indeed much more sensitive to the perturbation caused by the passing gravitational wave. Let's now apply the squeezing operation to the thermal perturbation:

$$\boldsymbol{S}_{\text{sq}}{}^{\dagger} \Delta\boldsymbol{\sigma} \boldsymbol{S}_{\text{sq}} = e^{-\beta} \begin{pmatrix} \sinh^2 r\, \mathbb{1}_2 & -\sinh r \cosh r\, \sigma_x \\ -\sinh r \cosh r\, \sigma_x & \cosh^2 r\, \mathbb{1}_2 \end{pmatrix}. \tag{131}$$

The squeezed initial state of the phononic field inside the BEC before the passage of the gravitational wave therefore reads

$$\boldsymbol{\sigma}_{\mathbf{0}} = \begin{pmatrix} (\cosh^2 r + \sinh^2 r)\, \mathbb{1}_2 & -\sinh 2r\, \sigma_x \\ -\sinh 2r\, \sigma_x & (\cosh^2 r + \sinh^2 r)\, \mathbb{1}_2 \end{pmatrix} + e^{-\beta} \begin{pmatrix} \sinh^2 r\, \mathbb{1}_2 & -\frac{\sinh 2r}{2}\, \sigma_x \\ -\frac{\sinh 2r}{2}\, \sigma_x & \cosh^2 r\, \mathbb{1}_2 \end{pmatrix}. \tag{132}$$

To keep analytical insights, we investigate the effect of the transformation due to a sudden change in the metric, a 'discrete gravitational wave' as we previously saw. One can obtain the exact result by carrying the same computation but with the continuous gravitational wave transformation derived in the previous chapter, at the expense of the result's compactness. Using (83) and (84) (and the expression of ${}_0\alpha_{jj}$ below these), we find the symplectic matrix associated to the discrete Bogolyubov transformation:

$$\boldsymbol{S}_{\epsilon} = \begin{pmatrix} \mathbb{1}_2 & \frac{\epsilon}{4}\, \mathbb{1}_2 \\ \frac{\epsilon}{4}\, \mathbb{1}_2 & \mathbb{1}_2 \end{pmatrix}. \tag{133}$$

The state during the passage of the wave $\sigma_\epsilon = {S_\epsilon}^\dagger \sigma_0 S_\epsilon$ therefore reads

$$\sigma_\epsilon = \begin{pmatrix} (1+2\sinh^2 r)\,\mathbb{1}_2 - \frac{\epsilon}{2}\sinh 2r\,\sigma_x & \frac{\epsilon}{2}(1+2\sinh^2 r)\,\mathbb{1}_2 - \sinh 2r\,\sigma_x \\ \frac{\epsilon}{2}(1+2\sinh^2 r)\,\mathbb{1}_2 - \sinh 2r\,\sigma_x & (2\cosh^2 r - 1)\,\mathbb{1}_2 - \frac{\epsilon}{2}\sinh 2r\,\sigma_x \end{pmatrix} + \Delta\sigma_\epsilon, \tag{134}$$

with the thermal perturbation

$$\Delta\sigma_\epsilon = e^{-\beta}\begin{pmatrix} \sinh^2 r\,\mathbb{1}_2 - \frac{\epsilon}{4}\sinh 2r\,\sigma_x & \frac{\epsilon}{4}(1+2\sinh^2 r)\,\mathbb{1}_2 - \frac{\sinh 2r}{2}\,\sigma_x \\ \frac{\epsilon}{4}(1+2\sinh^2 r)\,\mathbb{1}_2 - \frac{\sinh 2r}{2}\,\sigma_x & \cosh^2 r\,\mathbb{1}_2 - \frac{\epsilon}{4}\sinh 2r\,\sigma_x \end{pmatrix}. \tag{135}$$

We can also rewritte the state as

$$\sigma_\epsilon = \begin{pmatrix} \mathbb{1}_2 & 0_2 \\ 0_2 & -\mathbb{1}_2 \end{pmatrix} + \left(1 + \frac{e^{-\beta}}{2}\right)\begin{pmatrix} 2\sinh^2 r\,\mathbb{1}_2 - \frac{\epsilon}{2}\sinh 2r\,\sigma_x & \frac{\epsilon}{2}(1+2\sinh^2 r)\,\mathbb{1}_2 - \sinh 2r\,\sigma_x \\ \frac{\epsilon}{2}(1+2\sinh^2 r)\,\mathbb{1}_2 - \sinh 2r\,\sigma_x & 2\cosh^2 r\,\mathbb{1}_2 - \frac{\epsilon}{2}\sinh 2r\,\sigma_x \end{pmatrix}. \tag{136}$$

In this latter expression the contribution from the condensate's thermality appears as a simple perturbation of the state transformed by the gravitational wave. One could use this expression to expand perturbatively quantities of interest, such as for quantum metrology calculations, in order to obtain analytical expressions for the thermal deviations from the known results [41].

5.3 OUTLOOK AND FURTHER NOISE STUDIES

In this chapter we provided a theory for the evaluation of the effects from the shaking of the gravitational wave detector's cavity where the BEC is trapped. We derived the Bogolyubov transformation for a discrete displacement of the cavity occuring during the passing of the gravitational wave. Provided with the noise spectrum obtained experimentaly, we would be able to integrate these discrete Bogolyubov coefficients in order to characterise the complete transformation on the BEC's states. The combined effect of the shaking noise and of the gravitational wave was also characterised.

We then considered the thermal agitation of the atoms, which was neglected in a first place in the initial proposal [41], where the atoms where considered to have zero temperature. The influence of thermality was already approached differently in references [4, 5]. In the previous section we

provided another different approach yielding an explicit analytic expression for the quantum state of the two resonant thermal modes of the phononic field during the passage of a gravitational wave.

It is worth mentionning that other sources of noise have been investigated recently in the litterature, like phonon decoherence due to phonon-phonon interactions [72], and three different damping mechanisms in the BEC have been discussed in [73]: Landau damping, Beliaev damping and atomic evaporation. These correspond respectively to: absorbtion of energy from the perturbations of the bulk by the thermal bath of excitations, decay of single phonons to two phonons of lower energies, and interatomic interactions and thermal fluctuations of the condensate leading to atomic losses.

An analogue gravity approach was also developed in [73]. There the problem is reversed, the parameters of the BEC are tuned such that the effective metric for the phonons mimics the spacetime background of a gravitational wave, although the actual spacetime background metric is the one of Minkowski. This would enable to test the features of the BEC gravitational wave detector in the absence of the wave, and therefore to improve it and prepare it for actual detections.

Part III.

Quantum communication and metrology in space

6

RADIAL QUANTUM COMMUNICATION AND METROLOGY IN KERR SPACETIME

The field of quantum communications promises several technical improvements to current classical communications. One example is the use of quantum cryptography which would make communications more secure, thanks to more robust protocols than the classical ones [74]. More fundamental aspects can also be studied using quantum communications. For example, the interplay between quantum physics and relativity can be probed through quantum communications between moving observers and within schemes in a curved spacetime background [34]. The results of the measurements can then be compared with the predictions obtained by theories that were developed in the overlap of quantum physics and relativity, the most understood of these being quantum field theory in curved spacetime [40].

Knowing quantitatively how quantum communications are affected by the curved spacetime background would enable to compensate undesirable relativistic effects in future quantum technologies. Precise values of the necessary corrections in such quantum communication setups can only be obtained with an accurate knowledge of the spacetime parameters. We thus need to employ techniques from the field of quantum metrology, which aims at exploiting quantum resources, such as entanglement, to estimate physical parameters [51]. Within a standard estimation protocol, an input quantum state undergoes a transformation that encodes the parameter to be estimated. The resulting state of this transformation is then compared,

by means of the fidelity, to a neighbouring state which is infinitesimally close in terms of the parameter. One can define a distance between these two states that is directly related to the Quantum Fisher Information (QFI), which in turn is directly related to the maximum precision one can obtain in an estimation scheme. A final measurement provides an estimation of the value of the parameter in a single-shot run [51].

Typical applications of quantum metrology range from phase estimation in quantum optics to estimating the gravitational potential with Bose Einstein Condensates (BECs) [41, 37]. However, when estimating relativistic parameters, gravity usually appears as an external potential, or a phase modification, which does not overcome the inherent inconsistency between quantum physics and relativity [75]. Recently, this gap has been bridged and quantum field theory in curved spacetime has been employed as the core framework to compute the ultimate bounds on ultra-precise measurements of relativistic parameters. In particular, it was shown that it is possible to use the shifting induced on the frequency distribution of single photons ascending the gravitational potential of a static planet to estimate with great precision the distance between a user based on Earth and one on a satellite [34, 35]. In this case, gravity isn't affecting the quantum state as the simple addition of a phase. The effects due to curved spacetime can therefore not be explained by a simple *ad hoc* implementation of proper time in a classical quantum mechanics scheme. Furthermore, it was shown that these effects can have potentially high impact on specific types of quantum key distribution (QKD) protocols [34]. This direction has the potential of leading towards the development of new relativistic and quantum technologies aimed at testing the predictions of quantum field theory in curved spacetime in space-based experiments with satellites.

In this work we extend the analysis carried out in previous works which investigated quantum estimation techniques in scenarios where photons are exchanged between Earth and a satellite [35]. There, the Earth was assumed as static and the effects on the propagation of the photons depend only on

the Schwarzschild radius of the Earth. Here we consider a rotating planet, and we model the metric outside the mass distribution by the well known Kerr metric [47]. The transformation induced by the curvature on the traveling photon reduces to a beam-splitter, a well known linear transformation in quantum optics [76]. We can therefore restrict ourselves to Gaussian states and employ the powerful covariance matrix formalism that allows to achieve analytical insight in scenarios that involve Gaussian states and linear unitary transformations [54, 50]. In particular, we seek out the effects of rotation on previously employed entanglement-swapping protocols [34, 35].

We find the error bound on the equatorial angular velocity of the Earth and compare it with that achieved with cutting edge technology. The rate of improvement of quantum optical technologies and the rapid increase of the control over quantum systems suggest that in the near future our scheme might provide a reliable way to outperform current technologies based on classical means.

The chapter is organised as follows. In Section 6.1, we present the process of exchanging photons between Earth and a satellite, we characterise and model the system, and we give the mathematical formalism that is going to be relevant for the general relativistic calculations that will follow. In Section 6.2, we derive the expression of the frequency shift for the photon travelling through the Kerr spacetime. Section 6.3 consists of the relativistic quantum metrology calculations. It introduces the relevant perturbative quantities that are affecting the states, and derives the Quantum Fisher Information (QFI) for the system studied, and hence the estimated error bounds for the spacetime parameters. Section 6.4 introduces the satellite to satellite scheme and the related precision estimations are computed in the same fashion as in the Earth to satellite case. Finally, Section 6.5 briefly discusses how the effects computed in this work can affect a simple QKD protocol, specifically comparing the magnitude of the effect with what has been found in [34].

6.1 DESCRIPTION OF THE SCHEME

6.1.1 *Description of the experiment*

A photon is sent radially, namely with $\theta = cst.$ and $\phi = cst.$, by Alice from a laboratory on Earth's equator to Bob who is in a satellite circularly orbiting at radius r_B in the equatorial plane of the Kerr spacetime. A schematic representation of the setup can be found in Fig. 6.

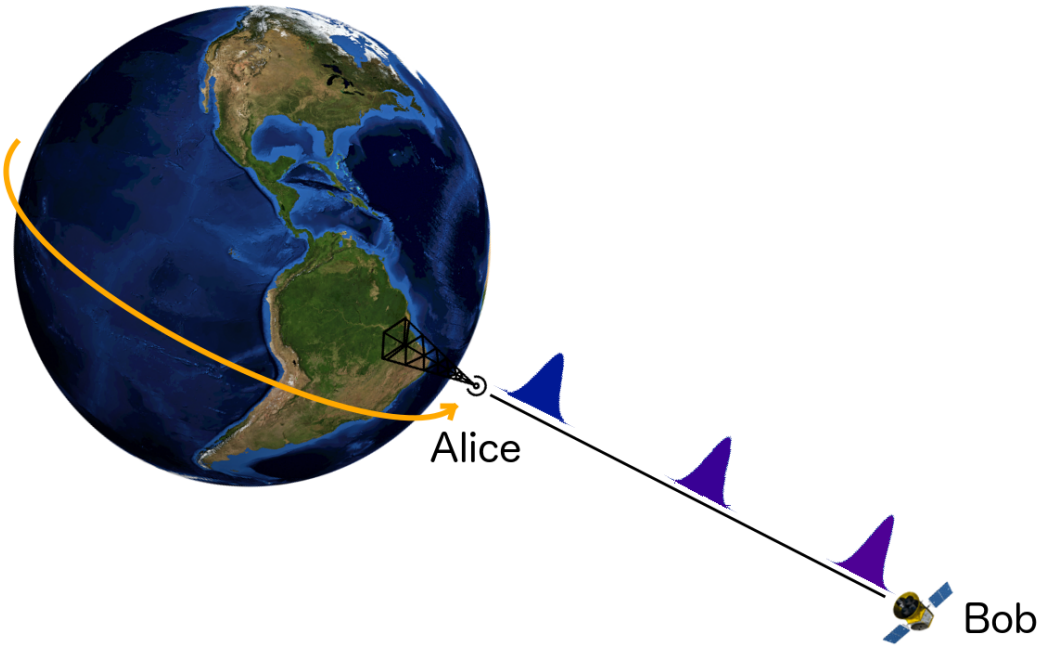

Figure 6.: Alice on Earth sends a photon (localised around the straight line) to Bob in the satellite. The photon experiences the effects of the curvature of spacetime along the whole path while propagating, which can be seen in the picture by the progressive tightening and redshifting of the Gaussian wavepacket. The final effect is a nonlocal and cumulative effect due to travel along the whole path.

6.1.2 *Wave packet characterisation*

In this work we employ photons which are geometrically radial, namely with vanishing angular velocities $\dot{\phi}_\gamma = 0 = \dot{\theta}_\gamma$. We will see that in Kerr space-time such photons have a non trivial angular momentum constant of motion, contrarily to the Schwarzschild case. The evolution of the quantum field is thus a 1+1 dimensional problem. Such a photon can be modelled by a wave packet of frequency distribution $F_{\omega_0}(\omega)$ of monochromatic plane waves with frequency ω and peaked at ω_0. The annihilation operator associated to this photon by an observer (infinitely) far from Earth is:

$$\hat{a}_{\omega_0}(t) = \int_0^{+\infty} d\omega \, e^{-i\omega t} F_{\omega_0}(\omega) \, \hat{a}_\omega. \tag{137}$$

The canonical bosonic commutation relations $[\hat{a}_{\omega_0}(t), \hat{a}^\dagger_{\omega_0}(t)] = 1$ for the bosonic operator (137) at any instant of time follow directly from those for the sharp frequency operators $[\hat{a}_\omega, \hat{a}^\dagger_{\omega'}] = \delta(\omega - \omega')$ and from the normalisation of the frequency distribution function $F_{\omega_0}(\omega)$ i.e., $\int_0^\infty d\omega |F_{\omega_0}(\omega)|^2 = 1$.

It is possible to rewrite the annihilation operator (137) of the same photon as described by Alice or Bob. We then follow [34] and we have:

$$\hat{a}_{\Omega_{K,0}}(\tau_K) = \int_0^{+\infty} d\Omega_K \, e^{-i\Omega_K \tau_K} F^{(K)}_{\Omega_{K,0}}(\Omega_K) \, \hat{a}_{\Omega_K}, \tag{138}$$

where the index $K = A, B$ refers to observer Alice or Bob respectively. The quantity Ω_K is the frequency of the photon as measured locally by the observer K with proper time τ_K. We have introduced the peak frequency $\Omega_{K,0}$ of the frequency distribution $F^{(K)}_{\Omega_{K,0}}$, and the bosonic canonical commutation relations for each observer read $[\hat{a}_{\Omega_K}, \hat{a}^\dagger_{\Omega_K}] = 1$.

Alice now prepares and sends a wave packet $F^{(A)}_{\Omega_{A,0}}$ at radius r_A which is received by Bob on the satellite as a wave packet $F^{(B)}_{\Omega_{B,0}}$ at radius r_B. Throughout its journey, the wave packet has changed due to the spacetime being curved. The relation between the two frequency distributions has been already found in [34]. We define the frequency shift f through the relation

$\Omega_B = f\Omega_A$, which will be made explicit later (notice that we are not using the same definition for f as in [34, 35]). Then one finds:

$$F^{(B)}_{\Omega_{B,0}}(\Omega_B) = \sqrt{\frac{1}{f}}\, F^{(A)}_{\Omega_{A,0}}\left(\frac{1}{f}\,\Omega_B\right). \tag{139}$$

Bob knows that the photon Alice has sent was characterised by $F^{(A)}_{\Omega_{A,0}}$. One way to quantify the change in the state of the photon is to use the fidelity between the initial state prepared with wave packet $F^{(A)}_{\Omega_{A,0}}$ and the final state received with wave packet $F^{(B)}_{\Omega_{B,0}}$. The fidelity $\mathcal{F} = |\Theta|^2$ for a single photon in a pure state is simply defined through the overlap function between the two frequency distributions:

$$\Theta = \int_0^{+\infty} d\Omega_B\, F^{(B)\star}_{\Omega_{B,0}}(\Omega_B) F^{(A)}_{\Omega_{A,0}}(\Omega_B). \tag{140}$$

The fidelity tends to zero for photons traversing regions of spacetime with sufficiently strong curvature, while it would reach unity in flat spacetime.

A convenient choice of wave packet is a normalised Gaussian wave packet of width σ_K and with a frequency distribution of the form:

$$F^{(K)}_{\Omega_{K,0}}(\Omega_K) = \frac{1}{\sqrt[4]{2\pi\sigma_K^2}} e^{-\frac{(\Omega_K-\Omega_{K,0})^2}{4\sigma_K^2}}. \tag{141}$$

We therefore employ (140) and (141) (also see [34]) to find:

$$\Theta = \sqrt{\frac{2(1+\delta)}{1+(1+\delta)^2}}\, e^{-\frac{\delta^2\Omega^2_{B,0}}{4(1+(1+\delta)^2)\sigma_B^2}}, \tag{142}$$

the amount of shifting being quantified by the new parameter δ defined by[1]:

$$\delta = f - 1. \tag{143}$$

In the following, we will derive the explicit formula for f in terms of the spacetime parameters.

1 Here we adopt the same convention for the parameter δ as in [35] for consistency with this previous work.

6.2 FREQUENCY SHIFT IN KERR SPACETIME

6.2.1 *Preliminaries*

The general frequency shift formula for a photon emitted from Alice on Earth and received by Bob in the satellite reads [44, 77]:

$$f = \frac{\Omega_B}{\Omega_A} = \frac{\Big[\boldsymbol{k}.\dot{\boldsymbol{X}}_B\Big]_{|X=X_B}}{\Big[\boldsymbol{k}.\dot{\boldsymbol{X}}_A\Big]_{|X=X_A}}, \tag{144}$$

where $\dot{\boldsymbol{X}}_A$ and $\dot{\boldsymbol{X}}_B$ are the four-velocities of Alice and Bob respectively, while $\boldsymbol{k}$ is the tangent vector to the affinely parametrised null geodesic that the photon follows. For simplicity of the computations, we restrain our study to a satellite that follows a geodesic circular orbit, i.e. $\dot{r}_B = 0$, and which is constrained to the equatorial plane of the Kerr spacetime, thus $\dot{\theta}_B = 0$. Alice on the rotating Earth also has $\dot{r}_A = \dot{\theta}_A = 0$. And our photon is geometrically radial, namely $k^\theta = k^\phi = 0$. We thus have:

$$k^\mu(\dot{X}_K)_\mu = k^t(\dot{t}_K\, g_{tt} + \dot{\phi}_K\, g_{t\phi}), \tag{145}$$

where again $K = A, B$. The velocity of our observers are [49, 78]:

$$\dot{\boldsymbol{X}}_A = \gamma_A\big(\partial_t + \omega_A\,\partial_\phi\big), \tag{146}$$

$$\dot{\boldsymbol{X}}_B = \gamma_B\big((1 + \epsilon\, a\,\omega_B)\,\partial_t + \epsilon\,\omega_B\,\partial_\phi\big), \tag{147}$$

where $\epsilon = +1$ for direct orbits (i.e., when the satellite co-rotates with the Earth), and $\epsilon = -1$ for retrogade ones (i.e., the opposite way). The parameter $\omega_A = d\phi_A/dt_A$ denotes Earth's angular coordinate velocity at the equator, while $\omega_B = \sqrt{M/r_B^3}$ is Bob's orbit frequency. The factors γ_K are obtained through the normalisation relations $(\dot{X}_K)^\mu(\dot{X}_K)^\nu g_{\mu\nu} = -1$ and read:

$$\gamma_A = \Big(1 - \omega_A^2\big(r_A^2 + a^2\big) - \frac{2M}{r_A}\big(1 - a\,\omega_A\big)^2\Big)^{-\frac{1}{2}}, \tag{148}$$

$$\gamma_B = \Big(1 - \frac{3M}{r_B} + 2\,\epsilon\, a\,\omega_B\Big)^{-\frac{1}{2}}. \tag{149}$$

The tangent vector to the photon's worldline reads:

$$\boldsymbol{k} = E_p \left(\frac{1}{1 - \frac{2M}{r}} \partial_t + \sqrt{\kappa}\, \partial_r \right), \tag{150}$$

$$\kappa = 1 + \frac{a^2}{r^2}\left(1 + \frac{2M}{r}\right) + \frac{4}{1 - \frac{2M}{r}} \frac{M^2\, a^2}{r^4}, \tag{151}$$

where it has been used that for such a geometrically radial photon we have:

$$L_\phi = -a \frac{E_\gamma}{1 - \frac{2M}{r}} \frac{2M}{r}. \tag{152}$$

The constants of motion E_p and L_ϕ are respectively the energy and longitudinal angular momentum of the photon as would be measured by an inertial observer at space infinity. These quantities are conserved along geodesics thanks to the presence of the Killing fields ∂_t and ∂_ϕ, respectively. After evaluation at $\boldsymbol{X}_B$, the explicit form of the numerator in (144) thus reads:

$$[k^\mu (\dot{X}_B)_\mu]_{|\boldsymbol{X}_B} = -E_p\, \gamma_B \left(1 + \epsilon \frac{a\, \omega_B}{1 - \frac{2M}{r_B}} \right). \tag{153}$$

The denominator of (144), after evaluation at $\boldsymbol{X}_A$, reads:

$$[k^\mu (\dot{X}_A)_\mu]_{|\boldsymbol{X}_A} = -E_p\, \gamma_A \left(1 + \frac{2M}{r_A} \frac{a\, \omega_A}{1 - \frac{2M}{r_A}} \right). \tag{154}$$

The A and B subscripts on the quantities Δ and κ denote evaluation at r_A and r_B respectively. We now have all the ingredients to compute explicitly the frequency shift of the photon (144).

6.2.2 *Frequency shift formula*

Plugging (153) and (154) in (144), we obtain the explicit expression of the frequency shift for the photon exchanged between Alice on Earth and Bob in the circularly orbiting satellite. We find:

$$f = \frac{1 + \epsilon \frac{a\, \omega_B}{1 - \frac{2M}{r_B}}}{1 + \frac{2M}{r_A} \frac{a\, \omega_A}{1 - \frac{2M}{r_A}}} \sqrt{\frac{1 - \frac{2M}{r_A}(1 - a\, \omega_A)^2 - (a^2 + r_A^2)\omega_A}{1 - \frac{3M}{r_B} + 2\, \epsilon\, a\, \omega_B}}. \tag{155}$$

In the Schwarzschild limit $a, \omega_A \to 0$, it simplifies to:

$$f_S = \sqrt{\frac{1 - \frac{2M}{r_A}}{1 - \frac{3M}{r_B}}}. \tag{156}$$

Therefore, equation (155) reduces to the known result for a radial photon in a static planet spacetime that has been used in [34, 35]. As expected by the symmetry of the problem in the case of a radial photon propagating in Schwarzschild spacetime, the result does not depend on the direction of rotation of the satellite, namely on ϵ. One can also notice that, in this limit, photons received on satellites orbiting at radius $r_B = \frac{3}{2} r_A$ will not experience any frequency shift. In the Schwarzschild picture, this is the altitude at which the gravitational effect of the Earth and the special relativistic effect due to the motion of the satellite compensate each other, and Bob's clock rate becomes equal to the clock rate of Alice. Indeed, the satellite's motion around the Earth slows down Bob's proper time, but the higher altitude of Bob introduces a lower redshift which therefore has also a lower effect on Bob's clock rate, as compared to Alice. Special relativistic effects thus dominate the frequency shift of photons received at altitudes below $r_B = \frac{3}{2} r_A$, where photons will actually be received blue-shifted, while the photons will be received red-shifted at $r_B > \frac{3}{2} r_A$ where the gravitational frequency shift dominates. A last relevant check is to verify the absence of frequency shift in flat spacetime. Unsurprisingly, taking the flat limit of (155), namely $M, a, \omega_A \to 0$, we find that in Minkowski spacetime $f_{\mathcal{M}} = 1$.

6.3 QUANTUM ESTIMATION OF ROTATION PARAMETERS OF THE EARTH

In this section, we apply quantum estimation techniques to find the ultimate bounds on the precision of measurements of parameters of the Earth.

6.3.1 *Summary of spacetime parameters*

In our result (155) for the frequency shift of a radial photon traveling from Earth to space, there are five dimensionless perturbative parameters of interest, for which we give numerical values in the table 2.

Quantity (N. Units)	Quantity (S.I.)	Value	Orbit
M/r_A	GM/r_Ac^2	6.95×10^{-10}	/
M/r_B	GM/r_Bc^2	1.05×10^{-10}	GEO
		5.29×10^{-10}	LEO
a/r_A	a/r_A	5.11×10^{-7}	/
a/r_B	a/r_B	7.73×10^{-8}	GEO
		3.89×10^{-7}	LEO
$r_A\,\omega_A$	$r_A\,\omega_A/c$	1.55×10^{-6}	/

Table 2.: Dimensionless perturbative parameters of the frequency shift.

We consider two orbits for satellites, low Earth orbits at $r_B(\text{LEO}) = r_A +$ 2000km and geostationary ones $r_B(\text{GEO}) = r_A + 35784\text{km}$.

6.3.2 *Quantification of the frequency shift*

The amount of change in the photon's frequency distribution is quantified by the shift parameter δ:

$$\delta = \frac{\Omega_B}{\Omega_A} - 1, \tag{157}$$

where Ω_B/Ω_A has an explicit expression in (155). We proceed by expanding this expression perturbatively in the parameters from table 2. We obtain:

$$\delta = \delta_S + \delta_{rot} + \delta_c, \tag{158}$$

where δ_S is a first order Schwarzschild term, δ_{rot} is the lowest order rotation term, and we gather all higher order corrections in δ_c. We give explicit values of the first two:

$$\delta_S = \frac{1}{4}\frac{r_S}{r_A}\frac{1-2\frac{L}{r_A}}{1+\frac{L}{r_A}}, \tag{159}$$

$$\delta_{rot} = -\frac{(r_A\,\omega_A)^2}{2} \sim -10^{-12}, \tag{160}$$

where we have introduced Earth's Schwarzschild radius $r_S = 2M$ and the distance between Alice and Bob, $L = r_B - r_A$. Notice that δ_S in (159) is different to the δ displayed in the Schwarzschild scenario papers [34, 35]. It comes from the fact that we are expanding the *total* frequency shift (155) taking into account both special and general relativistic effects, while in [34, 35] the parameter δ has been obtained by expanding only the gravitational frequency shift. With the values used in table 2, we have $\delta_S \sim 10^{-10}$ for LEO orbits and $\delta_S \sim -10^{-10}$ for GEO orbits. Lowest order terms from δ_c are of order 10^{-21}, we can therefore safely neglect them from now on.

If one assumes that the positions of Alice and Bob are known with sufficient (in principle, infinite) precision, one can employ (158) to express the precision $\Delta\delta$ on measurements on δ in terms of the precision Δr_S on the Schwarzschild radius of the Earth:

$$\Delta\delta = \delta_S \frac{\Delta r_S}{r_S}. \tag{161}$$

We have used that for the orbits we consider $|\delta_S| \gg |\delta_c|$ to neglect terms coming from δ_c. Yet, as noticed in (156), there is no frequency shift in Schwarzschild spacetime for orbits at altitude $L = r_A/2$, and consequently δ_S vanishes for these orbits. Hence, for orbits with $L \sim r_A/2$ we would need to take higher order corrections from δ_c into account, and (161) will have a more involved expression.

We are also interested in the precision one can achieve for the measurement of Earth's equatorial angular velocity. The relation between $\Delta\delta$ and $\Delta\omega_A$ is simply:

$$\Delta\delta = 2\delta_{rot}\frac{\Delta\omega_A}{\omega_A}. \tag{162}$$

We will now proceed to employ the quantum estimation techniques necessary to find the ultimate bounds on the measurement errors we have explicitly found above. In order to achieve this goal, we need to compute the Quantum Fisher Information $\mathrm{H}(\delta)$ which will allow us to employ the Cramér-Rao theorem.

6.3.3 *Quantum Fisher information and parameter estimation*

Following [35], we employ an initial two mode squeezed state and compute the fidelity $\mathcal{F}$ in order to obtain the QFI. For the regime we are interested in, $\delta \ll \frac{\Omega^2}{8\sigma^2}\delta^2 \ll 1$, the fidelity reads:

$$\mathcal{F} = 1 - \frac{\Omega_1^2 + \Omega_2^2}{4\sigma^2}\sinh^2(s)\, d\delta^2, \tag{163}$$

where s denotes the squeezing parameter, σ the spread of the frequency distribution of the photon, and Ω_i denote the peak frequencies of the distribution of each mode, i.e., $i = 1, 2$. From this we compute the QFI as:

$$\mathrm{H} = \frac{\Omega_1^2 + \Omega_2^2}{\sigma^2}\sinh^2(s). \tag{164}$$

Finally, we find our desired result using the Cramér-Rao bound:

$$|\Delta\delta| \geq \frac{\sigma}{\sqrt{N(\Omega_1^2 + \Omega_2^2)}\sinh(s)}. \tag{165}$$

In the following we specialise equation (165) to different estimations of physical parameters of the Earth, such as estimation of the Schwarzschild radius or the equatorial angular velocity of the Earth.

6.3.4 *Optimal bounds for the error on spacetime parameters*

In this section we will focus on applying the previous techniques to estimate the ultimate error bounds on the Schwarzschild radius r_S and on the equatorial angular velocity ω_A of the Earth. We assume absence of losses and use typical values for the parameters of the setup such as the bandwith $\sigma = 10^6$Hz, the peak frequencies $\Omega_1 = \Omega_2 = \Omega = 7 \times 10^{14}$Hz and the allowed number of measurements $N = 10^{10}$. In practice, these numbers imply a measurement time of $N\sigma^{-1} \sim$ 3hours. Furthermore, we present results for squeezing $s = 2$, which is achievable with state-of-the-art technology [35, 79]. The optimal bound for the error on the measurement of Earth's Schwarzschild radius is given by:

$$\frac{|\Delta r_S|}{r_S} \geq \frac{1}{\sqrt{2N}\sinh(s)} \frac{\sigma}{\Omega} \left|\delta_S\right|^{-1}. \tag{166}$$

The rotation terms being negligible, the result is essentially the same bound as in [35] for measurements of the Schwarzschild radius, namely we obtain a relative precision of $|\Delta r_S / r_S| \sim 10^{-5}$ for LEO orbits and $|\Delta r_S / r_S| \sim 10^{-6}$ for GEO orbits. Yet, these values now take into account special relativistic effects due to Alice's and Bob's motion, which were neglected in [35].

For orbits at altitude around $L \sim \frac{r_A}{2}$ however, the Schwarzschild term δ_S in (166) vanishes, we then need to add the lowest order terms from δ_c. These are several orders of magnitude smaller than δ_S, therefore satellites orbiting at these altitudes are not recommended for the experiments proposed here since the precision they would provide for the measurement of the Schwarzschild radius is significantly lower. This result is new compared to the study carried in [35], since it comes from taking into account special relativistic effects due to the satellite's motion.

We shift our attention to estimating the bound for the equatorial angular velocity of the Earth. We get:

$$\frac{|\Delta \omega_A|}{\omega_A} \geq \frac{1}{2\sqrt{2N}\sinh(s)} \frac{\sigma}{\Omega} \left|\delta_{rot}\right|^{-1}, \tag{167}$$

which gives bounds of order $|\Delta\omega_A|/\omega_A \sim 10^{-3}$. We are five orders of magnitude below the IERS Numerical Standards that give a relative uncertainty of order 10^{-8} [80], as well as the per billion precision of a recent direct measurement involving large ring laser gyroscopes [81] and of old interferometer experiments [82]. However, given the current rate of improvement in quantum technologies, it is reasonable to assume that, in the near future, we will be able to employ higher squeezing values and photons of higher energy. Finally, larger number of measurement probes would also contribute to enabling us to exceed the state-of-the-art precision.

6.4 SATELLITE TO SATELLITE COMMUNICATION

Another possible experimental setup would see two parties, Bob and Charlie, both following geodesic circular orbits in the equatorial plane of the Earth, at altitudes r_B and r_C respectively, with $r_B > r_C$ (see Figure 7).

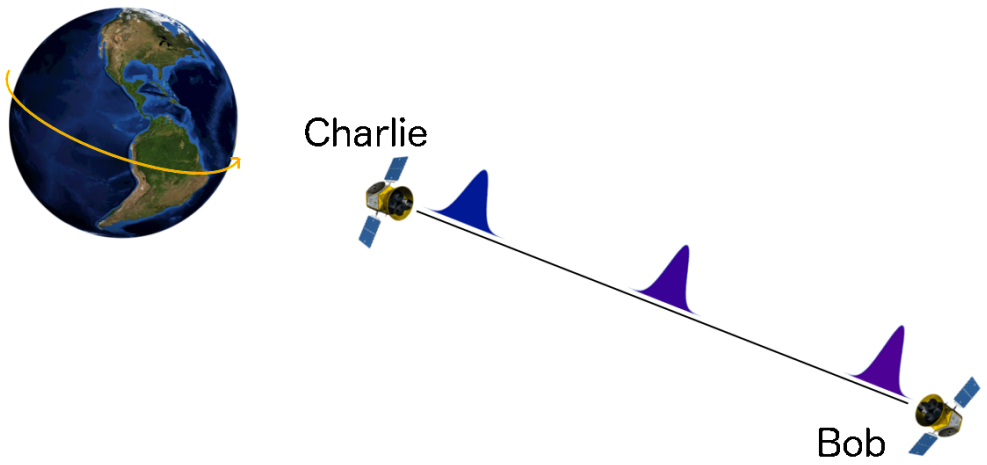

Figure 7.: Charlie in a LEO satellite exchanges photons with Bob in GEO. The wave packets experience a similar distortion as in the Earth-satellite scheme.

The advantage of this setup is that the channel (i.e., the free space between the two parties) is free from the noise introduced for example by the presence of the atmosphere in the case of Alice sending photons from Earth to Bob's satellite [29, 22]. Using (144) with Charlie instead of Alice and (153) for Bob and Charlie, the frequency shift formula for a photon emitted from Charlie's device and received later by Bob on a higher satellite reads:

$$\frac{\Omega_B}{\Omega_C} = \frac{1+\epsilon\frac{a\,\omega_B}{1-\frac{2M}{r_B}}}{1+\eta\frac{a\,\omega_C}{1-\frac{2M}{r_C}}}\sqrt{\frac{1-\frac{3M}{r_C}+2\,\eta\,a\,\omega_C}{1-\frac{3M}{r_B}+2\,\epsilon\,a\,\omega_B}}, \tag{168}$$

where all the quantities with a C subscript are the same as Bob's but substituting r_B with r_C and ϵ with η. Similarly to Bob's ϵ, $\eta = \pm 1$ depending on which way Charlie's satellite revolves around the Earth. In this expression there are four perturbative parameters of interest: the Schwarzschild parameters M/r_B, M/r_C, and the Kerr parameters a/r_B, a/r_C. In order to obtain the shift quantity $\delta_s = (\Omega_B/\Omega_C) - 1$ that quantifies the shift in the frequency distribution of the photon, we need to expand perturbatively (168) with respect to these four parameters. We find:

$$\delta_s = \delta_{s,S} + \delta_{s,rot} + \delta_{s,c}, \tag{169}$$

with:

$$\delta_{s,S} = -\frac{3}{4}\frac{L\,r_S}{r_C^2}\frac{1}{1+\frac{L}{r_C}} \sim -10^{-10}, \tag{170}$$

$$\delta_{s,rot} = \frac{1}{4}\frac{r_S\,a^2}{r_C^3}\left(\left(1+\frac{L}{r_C}\right)^{-3}-1\right) \sim -10^{-23}, \tag{171}$$

where now $L = r_B - r_C > 0$. The terms $\delta_{s,c}$ are higher order contributions that are negligible, and we gave numerical values for $\delta_{s,S}$ and $\delta_{s,rot}$ for Charlie following a LEO and Bob a GEO. Notice that in this scheme where both observers are geodesic, contrary to the Earth-satellite setup where Alice is accelerated, there are here no orbits for which the Schwarzschild term $\delta_{s,S}$

vanishes. We can now express the error $\Delta\delta_s$ on our shift parameter δ_s in terms of the error on the spacetime parameters. We find:

$$\Delta\delta_s = (\delta_{s,S} + \delta_{s,rot})\frac{\Delta r_S}{r_S} \approx \delta_{s,S}\frac{\Delta r_S}{r_S}, \tag{172}$$

$$\Delta\delta_s = 2\delta_{s,rot}\frac{\Delta a}{a} = 2\delta_{s,rot}\frac{\Delta\omega_A}{\omega_A}, \tag{173}$$

where we have used for the last equality that $a = 2I\omega_A/r_S$, where I is Earth's moment of inertia. For a photon sent from Charlie on a low Earth orbit ($r_C \sim 8000$km) to Bob on a geostationary one ($r_B \sim 42000$km), we find the order of magnitude for the precision on the Schwarzschild radius to be $|\Delta r_S|/r_S \sim 10^{-6}$ and on the rotation parameters $|\Delta a|/a \sim |\Delta\omega_A|/\omega_A \gg 1$. Therefore, in this satellite to satellite scheme, the rotation parameters measurements are losing several orders of magnitude of precision compared to the Earth to satellite setup. This is understandable by looking at the nature of the observer. On Earth, Alice is strongly dragged by Earth's rotation while the satellites experience only a slight dragging due to the weak rotation of the spacetime. It is then not surprising that the satellite to satellite setup, which is made of two geodesic orbiting observers, is less sensitive to the rotation parameters of the Kerr spacetime. However, the value for the precision on the measurement of the Schwarzschild radius is similar to the Earth to satellite scheme, making both setups equally good in theory. Yet, one has to keep in mind that a satellite to satellite scheme will provide channels free from any atmospheric noise and should therefore eventually yield more precise measurements.

6.5 QUANTUM KEY DISTRIBUTION PROTOCOL IN KERR SPACETIME

In order to complete our analysis of the possible means of detecting these effects, we can compute the Quantum Bit Error Rate (QBER) for a simple QKD protocol, following closely what has been done in [34]. The protocol goes as follows (see also Figure 8 for the diagram of the protocol): Alice and Bob both have single photon sources, and two memories each: $A1, A2$

for Alice and $B1, B2$ for Bob. Each source sends an optical mode towards a beamsplitter, and each of the reflected beams is saved in a memory. The transmitted beams of one user (e.g. Alice's) are propagated to the other user (Bob, in this case). The transmitted optical modes from memories $A1$ and $B1$ are then entangled at the receiver's lab through a beamsplitter, and similarly for $A2$ and $B2$. Alice then beam splits $A1$ and $A2$ and each output branch of the beamsplitter is measured by a detector. Bob performs the same operation with $B1$ and $B2$. If each user has one detector clicking, the protocol has been working successfully. The probability for Alice and Bob to share the same bit, i.e., the probability for memories $A1, B1$ and $A2, B2$ to have the same state is denoted by p. The QBER is the rate of bits that were not shared between Alice and Bob, i.e. QBER $= 1 - p$.

We employ the same protocol between Alice and Bob and adapt it to our new results, which take into account Earth's rotation and special relativistic effects. From [34] we have:

$$\text{QBER} \sim \frac{\delta^2}{8}\frac{\Omega^2}{\sigma^2}, \tag{174}$$

in the regime $\delta \ll \frac{\Omega^2}{8\sigma^2}\delta^2 \ll 1$. In the Earth to satellite setup, the contribution of the rotation to δ in (158) is negligible for most orbits. We obtain a QBER of order 10^{-4} for communications to LEO orbits and 10^{-2} to GEO orbits. For orbits at radii $r_B \sim \frac{3}{2}r_A$ however, the rotation term becomes dominant and the QBER shrinks to $\sim 10^{-8}$. Hence, these orbits are recommended to reduce the QBER in Earth to satellite quantum communications.

In the satellite to satellite case, the Schwarzschild part of the shift is always dominant. The value of the shift between a LEO and a GEO satellite is similar to the GEO orbits case in the Earth to satellite scheme, hence the value for the QBER for quantum communications between a LEO and a GEO satellite is of order 10^{-2}. However, taking into account atmospheric effects in the ground to satellite case would make the satellite to satellite scheme more accurate than a Earth to GEO QKD protocol.

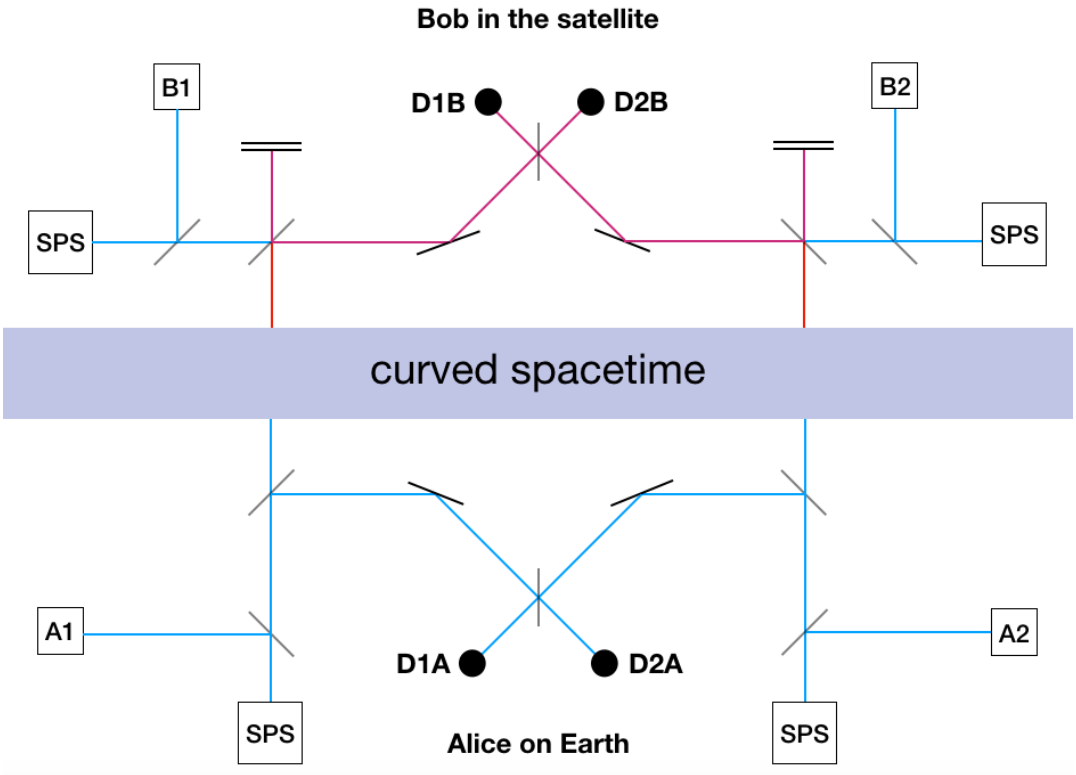

Figure 8.: Diagram of the QKD protocol between Alice and Bob. SPS boxes denote single photon sources, while boxes A1, A2, B1 and B2 represent the quantum memories. Beamsplitters are drawn in gray and mirrors in black. The photons emitted by Alice on Earth towards Bob are redshifted: the initial light beam (in blue) results after propagation through curved spacetime (indigo rectangle) in a redshifted beam (in red). This latter beam is then entangled at a beamsplitter with a mode prepared by Bob. This entangled state (purple lines) is then mixed with the other mode before detections. Detectors are displayed as thick black dots.

The errors we have quantified here occur because the wavepackets corresponding to the optical modes $A1$ and $A2$ have changed during their propagation towards Bob. The reduced overlap between sent and emitted states translates into errors in the QKD protocol. A significant share of these

errors can be corrected by perfoming a linear shift in frequencies on the received wavepackets in order to align their peak frequency with the emitted ones, before measurement. However, due to the change in the shape of the propagated wavepackets, this operation will not completely cancel the errors induced on the QKD protocol by the relativistic effects.

6.6 ENTANGLEMENT DEGRADATION DUE TO CURVED SPACETIME

After having looked at the errors caused by the curved spacetime background on a QKD protocol, we here describe how the entanglement of prepared quantum states of photons can be altered by the light's propagation in curved spacetime. We take the simple example of a two mode squeezed state, for which the continuous variables representation alongside with several measures of entanglement were given in section 3.1.5. This is an entagled state with negativity $\mathcal{N}(\sigma_{\text{ini}}) = \frac{e^{2s}-1}{2}$. To compute the transformation due to the spacetime, we again need to introduce a fiducial mode for each of the emitted modes. The initial two-mode squeezed state composed by modes a and b will be beamsplitted by the curved spacetime background to modes c and d, respectively. Modes c and d are initially in the vacuum state. The whole state of the initial system consisting of the two prepared modes together with the two fiducial modes reads:

$$\boldsymbol{\sigma}_{\text{tot}} = \begin{pmatrix} \cosh 2s\, \mathbb{1}_2 & \mathbf{0} & \sinh 2s\, \sigma_x & \mathbf{0} \\ \mathbf{0} & \mathbb{1}_2 & \mathbf{0} & \mathbf{0} \\ \sinh 2s\, \sigma_x & \mathbf{0} & \cosh 2s\, \mathbb{1}_2 & \mathbf{0} \\ \mathbf{0} & \mathbf{0} & \mathbf{0} & \mathbb{1}_2 \end{pmatrix}, \tag{175}$$

and the symplectic transformation associated with the effect of the curved spacetime background is given by $\boldsymbol{S} = \boldsymbol{\alpha} \oplus \boldsymbol{\alpha}$, with:

$$\boldsymbol{\alpha} = \begin{pmatrix} \cos\theta_a & 0 & \sin\theta_a & 0 \\ 0 & \cos\theta_b & 0 & \sin\theta_b \\ -\sin\theta_a & 0 & \cos\theta_a & 0 \\ 0 & -\sin\theta_b & 0 & \cos\theta_b \end{pmatrix}. \tag{176}$$

The beamsplitting angles $\theta_{a,b} = \arccos\Theta_{a,b}$ encode the changes due to the curved spacetime, where $\Theta_{a,b} \approx 1 - \frac{\delta^2\Omega_{a,b}^2}{8\sigma^2}$ is the overlap between emitted and received modes which was given in (142) for mode a and b respectively.

The received state after propagation in the curved spacetime background of the Earth $\sigma = \mathrm{tr}_{c,d}(S\sigma_{\mathrm{tot}}S^{\dagger})$ explicitly reads

$$\sigma = \begin{pmatrix} 1+2\Theta_a^2 \sinh s^2 & 0 & 0 & \Theta_a\Theta_b \sinh 2s \\ 0 & 1+2\Theta_b^2 \sinh s^2 & \Theta_a\Theta_b \sinh 2s & 0 \\ 0 & \Theta_a\Theta_b \sinh 2s & 1+2\Theta_a^2 \sinh s^2 & 0 \\ \Theta_a\Theta_b \sinh 2s & 0 & 0 & 1+2\Theta_b^2 \sinh s^2 \end{pmatrix}. \tag{177}$$

Following the procedure described in 3.1.4 and assuming for simplicity that both modes have the same frequency distribution, i.e. $\Omega_a = \Omega_b \doteq \Omega$, we find the smallest symplectic eigenvalue of the partial transpose of our received state σ to be $\tilde{\nu} = 1 - \Theta^2(1 - e^{-2s})$ and therefore the negativity of the received state is $\mathcal{N}(\sigma) = \frac{\Theta^2 \sinh s}{\cosh s + \sinh s(1-2\Theta^2)}$. Note that if we work with vacuum states, i.e. with $s = 0$, the received state remains a vacuum state under relativistic transformations (i.e. (177) is the identity matrix in this case and the null displacement vector remains null), and therefore $\tilde{\nu} = 1$ and $\mathcal{N}(\sigma) = 0$. Recall that $0 \leq \Theta \leq 1$, the latter limit value occuring in the case where no relativistic effect comes into play (e.g. for an exchange of photons between inertial observers with the same velocity in a flat spacetime). When such effects do kick in, in general $\Theta \lesssim 1$ and the overlap would tend to 0 only for extreme curvature backgrounds or huge relative velocities between the observers. Notice that when there is no relativistic effects we recover $\mathcal{N}(\sigma) = \mathcal{N}(\sigma_{\mathrm{ini}})$. We can now compute the relative loss of entanglement due to the relativistic effects arising from the curved spacetime background and due to the observers' motion:

$$\Delta\mathcal{N} \doteq \frac{\mathcal{N}(\sigma_{\mathrm{ini}}) - \mathcal{N}(\sigma)}{\mathcal{N}(\sigma_{\mathrm{ini}})} = \frac{e^s(1-\Theta^2)}{\cosh s + \sinh s(1-2\Theta^2)}. \tag{178}$$

In terms of the shift parameter δ, we have $\Theta \approx 1 - \delta^2 \frac{\Omega^2}{8\sigma^2}$ and therefore:

$$\Delta\mathcal{N} \approx e^{2s}\delta^2 \frac{\Omega^2}{4\sigma^2}, \tag{179}$$

which for the values we have used previously gives a loss of negativity of about 6% for both LEO and GEO orbits. Here again, if the satellite orbits at altitude $L \sim r_A/2$, the negativity of the entangled state is preserved and $\Delta\mathcal{N} \to 0$. Note that both the exact and the approximate expressions of $\Delta\mathcal{N}$

above are valid only for $s > 0$. The non zero value of $\Delta\mathcal{N}$ in the case $s = 0$ is only an artefact of a limit of the form $0/0$.

6.7 CONCLUSION

In this chapter we have derived an expression for the general relativistic frequency shift of a photon travelling through Earth's rotating surrounding spacetime. We have specialised to photons travelling with vanishing angular velocities from an equatorial laboratory on Earth towards a satellite revolving in the equatorial plane of the Kerr spacetime. This study provides analytical insight and successfully extends previous results obtained for Schwarzschild spacetime [34, 35]. We have found that including the rotation of the Earth does not change previous estimates obtained for the Schwarzschild radius in a quantum metrology scheme. However, we were able to estimate the precision for the quantum measurement of the equatorial angular velocity of the Earth. We find that the error bound predicted for the equatorial angular velocity of the Earth can exceed the precision obtained with the state of the art when high values of squeezing and a large number of probe systems (or measurements) are employed. Suitably chosen signals, such as frequency comb, instead of Gaussian-shaped frequency distributions, could also improve precision [83, 84]. Taking into account special relativistic effects, we have also found a specific class of circular orbits where the frequency of the received photons remains almost unchanged. For quantum metrology purposes these orbits have to be avoided since the quantum state of the photons is less perturbed, yet they are very useful for minimal curved spacetime disturbance channels for quantum communication. To complete our analysis, we have added a study of the error bounds for the same parameters when communication occurs between two satellites, which has relevance for practical implementations of many quantum information schemes, such as proposed implementations of QKD through satellite nodes [30, 33]. We conclude that recent advances in quantum technologies, which

include the ability to create larger values of squeezing, show the promising opportunities of improving the state of the art for measurements of physical parameters of the Earth.

7

QUANTUM COMMUNICATION AND METROLOGY IN SCHWARZSCHILD SPACETIME

Quantum experiments measuring relativistic effects are now becoming increasingly frequent, whether performed in the lab [20] or using schemes involving satellites [21]. In the present work, we are especially interested in the latter. In fact, we aim at completing the work started in [34] where a theoretical framework for the study of relativistic effects on quantum states exchanged between Earth and satellites was established. Frequency modes of light were considered and their evolution in the Schwarzschild spacetime background was studied in quantum communication and cryptography schemes. This work has been extended in [35] where quantum metrology techniques were used to estimate the precision for quantum measurements of physical parameters of the Earth. Finally, the effects of the rotation of the Earth and communications between satellites were looked at in the previous chapter and these results were published in [1].

The present chapter aims at further extending these studies, that were only considering radial communications. We use different schemes here, the link scheme between Earth and satellites that was described in the previous chapter, but also a reflecting scheme where the photons sent from Earth are reflected back by the passing satellite. In the latter scheme, the received photon states measured on Earth have thus not experienced any gravitational or Doppler shift. The change in their quantum state is mostly due to the energy kick delivered by the reflection on the moving satellite's

mirror. In both schemes, the angularity of the beam gives an effect which turns out to be larger than the shift in energy experienced by photons in the schemes considered in previous works [34, 35, 1]. This enables us to obtain improved metrology results without even using squeezed states.

The structure of the chapter is as follows: in section 7.1, we provide the mathematical formalism to describe the light beam and its photons' states. In 7.2, we detail both the link and reflecting satellite schemes. We then work out in 7.3 the expression for the energy shifts altering the quantum states of light. In section 7.4.1, we perform the quantum metrology computations in order to estimate the precision bounds one can obtain for a quantum measurement on physical parameters encoded in the perturbed photons' states. Numerical values of these parameters are then used in 7.4.2 to obtain the optimal bounds for the measurements of the Earth's Schwarzschild and mean radii, and also for the satellite's height. In 7.5 we compute the quantum bit error rate for a simple quantum key distribution protocol in the case where the relativistic effects are not compensated for. Finally, we conclude and discuss our results in the last section 7.6.

7.1 LIGHT RAYS AND PHOTONIC STATES

In this section we describe the optical pulses and their propagation in curved spacetime. Their trajectory in the curved background is given in 7.1.1, where we consider light rays with a small azimuthal angular momentum but arbitrary polar angular momentum. In 7.1.2, we give the description of the quantum state and show how it is affected by its propagation in the Schwarzschild spacetime surrounding the Earth.

7.1.1 *Light ray with small azimuthal angular momentum*

We consider light rays with a small azimuthal angular momentum, i.e. $|l_\phi| \ll \sqrt{\kappa}$. In practice, this means that the azimuthal coordinate ϕ of the photon varies very slowly during the light's propagation. This is just a matter of calculational convenience as with the Schwarzschild spacetime's spherical symmetry any plane containing the center of the Earth is equivalent to work with than any other. For such light rays, the null vector (15) simplifies to:

$$\boldsymbol{k} = E_p\left(\frac{1}{f(r)}\,\partial_t + \epsilon_r\sqrt{1-f(r)\frac{\kappa}{r^2}}\,\partial_r + \frac{\epsilon_\theta}{r}\sqrt{\frac{\kappa}{r^2}}\,\partial_\theta + \frac{l_\phi}{r^2\sin^2\theta}\,\partial_\phi\right) + O\left(l_\phi^2\right), \quad (180)$$

where we denoted $f(r) = 1 - \frac{2M}{r}$ to compactify the expression. The constraint (18) can now be easily integrated:

$$\Delta\phi = \epsilon_\theta\frac{l_\phi}{\sqrt{\kappa}}\int_{\theta_1}^{\theta_2}\frac{d\theta}{\sin^2\theta} + O\left(l_\phi^3\right) = \epsilon_\theta\frac{l_\phi}{\sqrt{\kappa}}(\cot\theta_1 - \cot\theta_2) + O\left(l_\phi^3\right). \quad (181)$$

We therefore have:

$$l_\phi \approx \sqrt{\kappa}\frac{\Delta\phi}{|\cot\theta_2 - \cot\theta_1|}. \quad (182)$$

This expression is valid for $|\Delta\phi| \ll |\cot\theta_2 - \cot\theta_1|$ only. Taking now a look at the other constraint (17), it simplifies to:

$$\epsilon_r\int_{r_1}^{r_2}\frac{dr}{r^2\sqrt{1-\left(1-\frac{2M}{r}\right)\frac{\kappa}{r^2}}} = \frac{|\Delta\theta|}{\sqrt{\kappa}} + O\left(l_\phi^2\right), \quad (183)$$

with $\Delta\theta \equiv \theta_2 - \theta_1$. Note that the constraint doesn't depend on l_ϕ anymore. Unfortunately, the radial integral is still not easily integrable, and we will need to solve it numerically to obtain the values of κ.

7.1.2 *Wave packets of photons*

A photon can be modeled by a wavepacket in superposition of momentum-helicity states. We prepare our initial quantum state in a balanced distribution of $|+1\rangle$ and $|-1\rangle$ helicity states (i.e., a linearly polarised state):

$$|\gamma\rangle = \frac{1}{\sqrt{2}}\sum_{s=\pm1}\int d\boldsymbol{p}\,\mathrm{F}(\boldsymbol{p})\,|\boldsymbol{p}, s\rangle\,, \quad (184)$$

with the helicity $s = \pm 1$, the photon's 4-momenta as measured in the observer's local reference frame $\boldsymbol{p} = (k^{\hat{0}}, k^{\hat{1}}, k^{\hat{2}}, k^{\hat{3}})$, the 4-momenta distribution function $\mathrm{F}(\boldsymbol{p}) = F(\vec{\boldsymbol{p}})\,\delta(|\vec{\boldsymbol{p}}|^2 - (k^{\hat{0}})^2)\,\bar{\theta}(k^{\hat{0}})$ with $\bar{\theta}$ the step function and the distribution of the 3-momenta F. The distribution F is normalised in the following way: $\int d\vec{\boldsymbol{p}}\ |F(\vec{\boldsymbol{p}})|^2 = 1$, which also implies the normalisation of F. As a consequence, the annihilation operators $\hat{a}_{\vec{p},s}$ for the photons have the usual bosonic commutation relations $[\hat{a}_{\vec{p}_1,s_1}, \hat{a}^\dagger_{\vec{p}_2,s_2}] = \delta(\vec{p}_1 - \vec{p}_2)\,\delta_{s_1 s_2}$.

To simplify the calculations we assume that the observers pick a reference frame, implemented mathematically by a tetrad with components $e_{\hat{a}}{}^{\mu}$, which is adapted to the prepared/received photons such that the local momenta are $\boldsymbol{p} = (k^{\hat{0}}, 0, 0, -k^{\hat{0}})$. This is easily achieved and the details of the procedure can be found in the dedicated section 3.3.2. The photon's energy as seen in this local adapted frame is $k^{\hat{0}} = k^\mu e^{\hat{0}}{}_\mu = -k^\mu v^{\ \nu} g_{\mu\nu} = \hbar\Omega$, where v is the observer's velocity and Ω is the photon's frequency as measured by the observer. In the emitter's frame, the wavepackets have therefore the following expression:

$$|\gamma\rangle = \frac{1}{\sqrt{2}} \sum_{s=\pm 1} \int d\Omega\, F(\Omega)\, |\Omega, s\rangle\,. \tag{185}$$

In the following section, we will consider schemes where the photons are exchanged between Earth and a satellite. We are thus interested in knowing how such propagation of the light would alter the quantum state. When momentum-helicity states of photons propagate in a curved spacetime, they pick up the so called Wigner phase Ψ. If we denote by $\hat{\boldsymbol{U}}$ the propagator that encodes such propagation in the curved spacetime, we have [60]:

$$\hat{\boldsymbol{U}}\, |\Omega, s\rangle = e^{is\Psi(\vec{\boldsymbol{n}})}\, |\Omega', s\rangle\,, \tag{186}$$

where the frequency of the propagated state $\Omega' \neq \Omega$ in general in curved spacetime. We can relate these frequencies by the frequency shift f: $\Omega' = f\Omega$. In the link scenario, the frequency shift f will be caused by both the Doppler and gravitational shifts. In the reflection scheme, since the photons are prepared and measured by static observers at the same altitude, there

will be no gravitational or Doppler shift. The frequency shift f is in this case only due to the change in energy at the satellite's reflection event.

The Wigner phase Ψ does not depend on the frequency of the photons, however it depends on their direction $\vec{n} = \vec{p}/|\vec{p}|$, as seen in the observer's local frame. After propagation, the expression for the photon's wavepacket as seen in the receiver's adapted frame is:

$$|\gamma'\rangle = \int d\Omega\, F(\Omega)\, |f\Omega\rangle \otimes \sum_{s=\pm 1} \frac{e^{is\Psi(\vec{n})}}{\sqrt{2}}\, |s\rangle\,. \tag{187}$$

In this expression we made explicit that the initial photon state (185) which is separable remains a separable state after propagation as seen in the chosen adapted frames. Note that this is not true in general and this is solely due to our convenient choice of reference frame. In another reference frame, one would not be able to model the wavepacket of momenta by a frequency distribution only, therefore we would not have been able to pull the Wigner phase factor out of the integral in (187). This means that the momentum and the helicity states would have appeared entangled due to the propagation in the curved spacetime. Although the measured state remains separable in our chosen frame, note that the Wigner phase is not a global phase: it has a different sign for each of the two helicity states of the superposition.

7.2 EARTH-SATELLITE SCHEMES

We now propose several schemes where photons are sent to a satellite, which either reflects them back to Earth or measures them aboard.

7.2.1 *The reflection scheme*

The setup of our first proposed scheme is the following and can be seen in Figure 9. A station on Earth emits photons towards a satellite equipped with a mirror, which is judiciously oriented in order to reflect the photons back to Earth to the same station or to another laboratory (see for example [22, 23]

for a practical implementation). For the sake of simplicity, we assume that in the case there are two laboratories on Earth, they are located almost at the same longitude ϕ, although they can be arbitrarily far in terms of latitude θ. Since the photons are prepared and measured by static observers at the

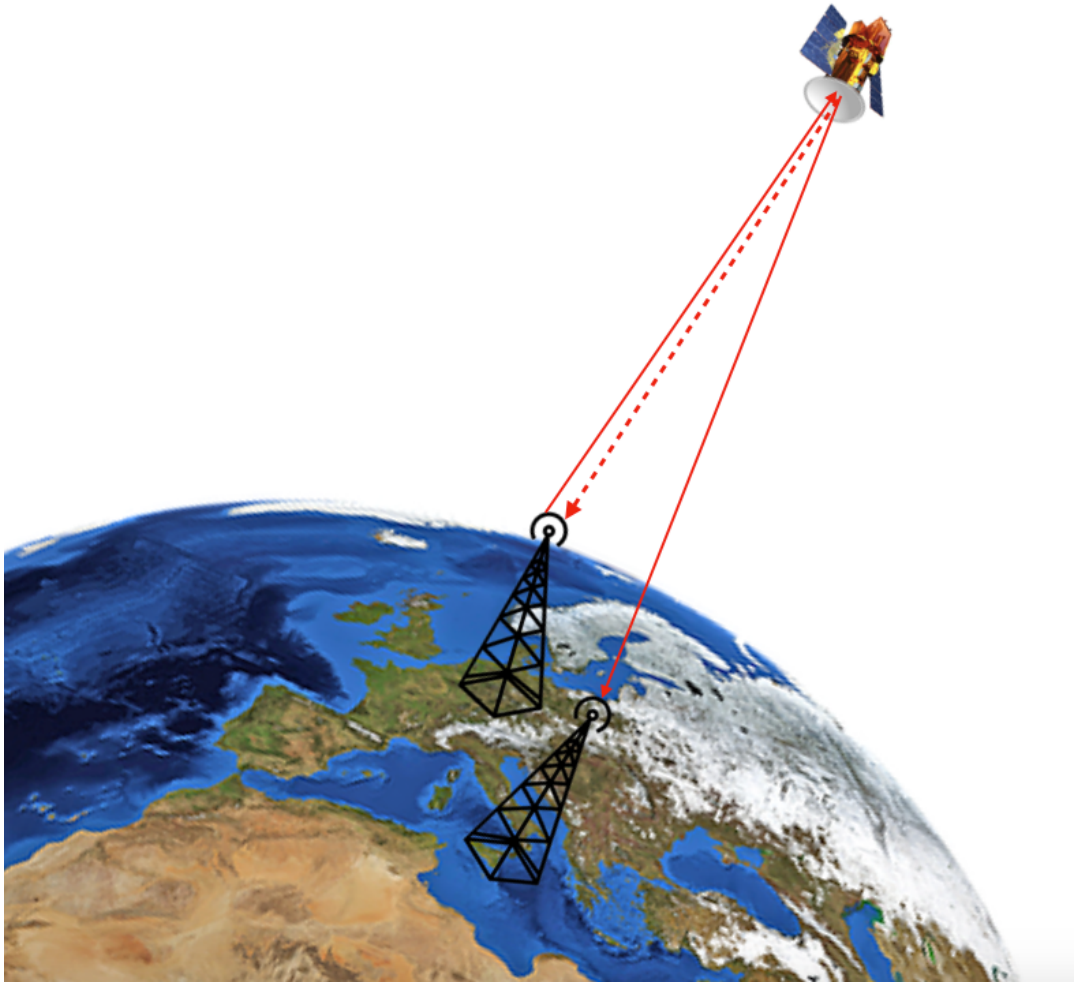

Figure 9.: Schematic representation of the proposed experiment. Photonic signals are sent from a station on Earth towards a satellite equiped with a mirror (in grey) and follow null geodesics (red line). They are reflected by the passing satellite (here placed at LEO) and they are then received at the same station (dotted line) or at another laboratory on Earth (thick line).

same altitude, there will be no gravitational or Doppler shift. The frequency

shift f_r in this scheme is therefore only due to the change in energy that occurs at each reflection event on the satellites.

This scheme is interesting in particular because the satellite is here only a passive object, which doesn't need to have any quantum source or measuring device on board.

7.2.2 *The link scheme*

The second proposed scheme is similar to the schemes considered in the previous chapter and in earlier works [34, 35, 1]. It consists in a station on Earth exchanging photons with a satellite (see Figure 10). However, here we do not restrain ourselves to radial light rays, and the photons can be sent from either the station or the satellite. This scheme can therefore be deployed in either uplink or downlink, and with angular light beams. In this second scheme there is no reflection, therefore the frequency shift f_l for this setup is made of the gravitational and Doppler shifts only.

The main advantage of this scheme is that the photons need to cross the atmosphere only once. The atmosphere is a significant source of noise, the second scheme is therefore more resilient to such noise than the first one.

7.2.3 *Orbit configuration*

There are many possible orbit configurations for such schemes.

Orb1 The satellite can be in geostationary orbit (GEO), which implies that its orbit lies in the Earth's equatorial plane, with inclination $\alpha = \theta_s = 90^\circ$.

Orb2 We can also choose a satellite to be located in a low Earth orbit (LEO), which is an orbit at altitude $h \leq 2000$km.

Orb3 The last family of orbits which we will consider are the very low Earth orbits (VLEO). They have an altitude $h \lesssim 300$km, i.e., low in

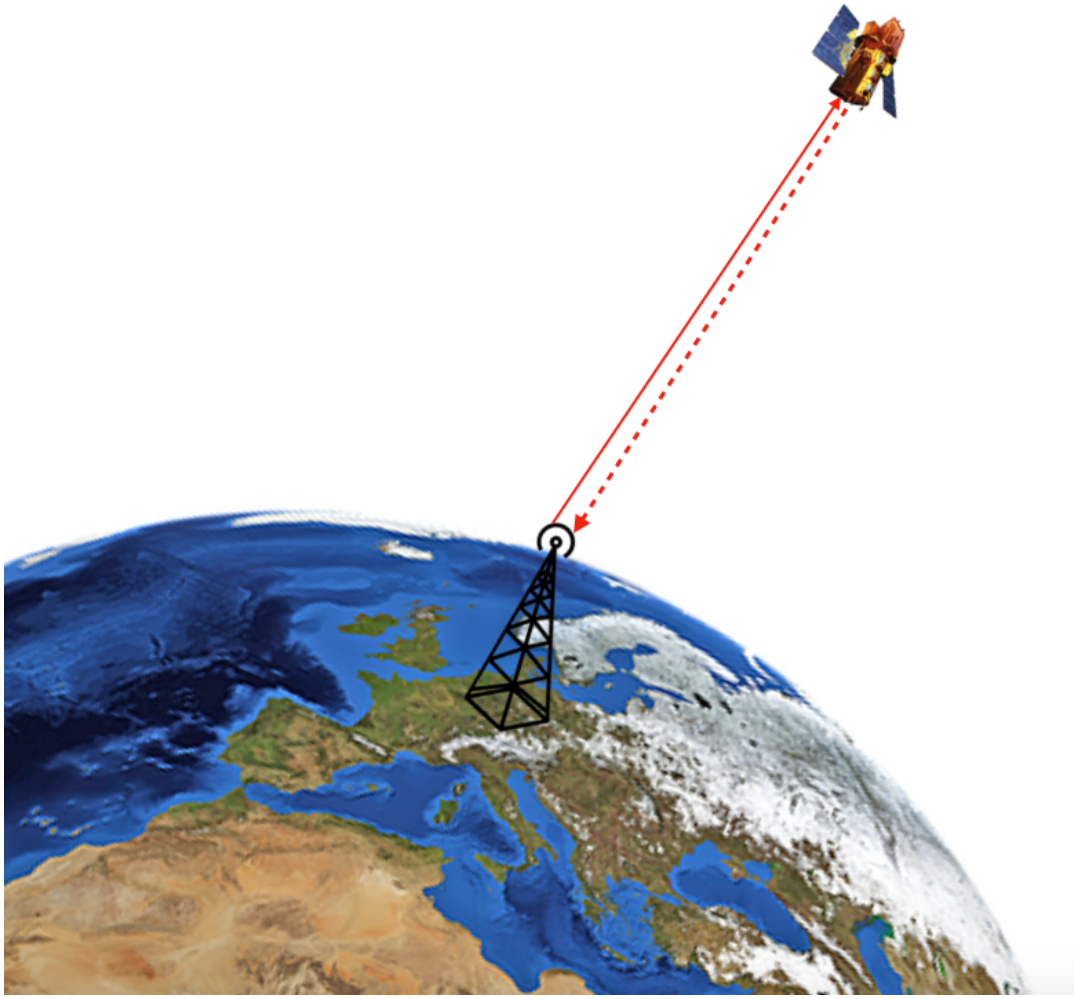

Figure 10.: Schematic representation of the proposed experiment. Photonic signals are sent from a station on Earth towards a satellite and follow null geodesics (red line). Alternatively, a downlink can also be considered (dotted line).

the thermosphere. Such satellites may experience significant atmospheric dragging due to the low altitude. However, the Gravity field and steady-state Ocean Circulation Explorer (GOCE) satellite orbited the Earth at 255km for more than four years thanks to its aerodynamic shape and ion propulsion [85]. Therefore, using satellites at these altitudes is not impossible.

7.3 FREQUENCY SHIFTS

In this section we describe how the frequencies of the photons are affected by the curved spacetime in each of the two schemes studied. In the reflection scheme, a change of energy is experienced by the photons at the reflection event. In the link scenario, gravitational redshift occurs gradually, all along the light's trajectory, until the detection where an extra Doppler shift contribution adds up due to the observer's motion.

7.3.1 *Reflection on satellite mirrors*

We first describe the change induced at the reflection event occuring in the scheme described in 7.2.1. Both the null vector and the polarisation vector of a light ray change when it is reflected by the satellite. The change in polarisation may induce an extra Wigner phase contribution to the one acquired during propagation in (187). Also, the momentum vector changes both in energy and direction: at the reflection event, some of the kinetic energy of the satellite is transferred to the photon and the light ray is deviated. We will see that the change in energy itself depends on how the light ray is deviated, since it depends on the satellite's motion and the ray's incident angle on the surface of the mirror.

The light ray with an arbitrary incident null vector $\boldsymbol{k}$ of the form (15) reflected by a moving satellite with velocity $\boldsymbol{v_s}$ given in (13) will have a null vector $\boldsymbol{k'}$ of the form (15) as well, but with a different energy constant E'_p and with new directional parameters ϵ'_r, ϵ'_θ, l'_ϕ and κ'. The expression for the new energy constant E'_p can be obtained by employing the constraint $\boldsymbol{k}\cdot\boldsymbol{v_s} = \boldsymbol{k'}\cdot\boldsymbol{v_s}$ at the reflection event. We find the reflection shift $f_r = E'_p/E_p$ in energy to have the expression

$$f_r = \frac{1-\sqrt{\frac{M}{R_s}}\delta_{\text{ang}}\left(\epsilon_\theta,\kappa,l_\phi\right)}{1-\sqrt{\frac{M}{R_s}}\delta_{\text{ang}}\left(\epsilon'_\theta,\kappa',l'_\phi\right)}, \tag{188}$$

where

$$\delta_{\text{ang}}\left(\epsilon_\theta, \kappa, l_\phi\right) = \epsilon_\zeta \frac{l_\phi}{R_s} \frac{\sin\alpha}{\sin^2\theta_s} + \epsilon_\omega \epsilon_\theta \frac{\sqrt{\kappa - l_\phi^2 \cot^2\theta_s}}{R_s} \sqrt{1 - \frac{\sin^2\alpha}{\sin^2\theta_s}}. \quad (189)$$

We introduced δ_{ang} a function encoding the angular parameters ϵ_θ, κ and l_ϕ of the light ray. Notice that the change in energy (188) clearly encodes the change in the direction of the ray, apart from the sign of the radial direction ϵ_r. If the photon's constants of propagation ϵ_θ, κ and l_ϕ have the same value before and after the reflection, then $f_r = 1$ and there is thus no effect. This occurs when the mirror's orientation is parallel to the satellite's 3-velocity at the reflection event. This could be used to provide a reference channel defined as the channel with no effect, which could be used to account for any noise in the signal in scenarios where there is an effect. Also note that, as long as the incident light ray is not radial, the effect does not vanish when the light is reflected back to the initial laboratory. In this case, $\kappa' = \kappa$ but $\epsilon'_\theta = -\epsilon_\theta$ and $l'_\phi = -l_\phi$. Let us now review how different satellite configurations affect the energy of the reflected photons.

GEO. For a reflection by a geostationary satellite, i.e. at polar angle $\theta_s = \alpha = \pi/2$, the energy kick (188) reduces to:

$$f_r = \frac{1 - \epsilon_\zeta \frac{l_\phi}{R_s}\sqrt{\frac{M}{R_s}}}{1 - \epsilon_\zeta \frac{l'_\phi}{R_s}\sqrt{\frac{M}{R_s}}}. \quad (190)$$

This class of satellites only has an azimuthal velocity, which is the reason why the energy it can impart to the photons is only a function of the azimuthal part of the light's angular momentum. Since we will assume l_ϕ to be small, the change in energy due to the reflection by a GEO satellite can be expected to be small as well in the setup we chose.

LEO. Another interesting class of satellites is those with polar orbits. These satellites pass above both poles during each revolution. Therefore,

they are characterised by an inclination $\alpha = 0$ and are typically found in LEO. The energy shift for this case is

$$f_r = \frac{1 + \epsilon_\omega \, \epsilon_\theta \sqrt{\frac{\kappa M}{R_s^3}}}{1 + \epsilon_\omega \, \epsilon'_\theta \sqrt{\frac{\kappa' M}{R_s^3}}} + O\left(\frac{l_\phi^2}{\kappa}\right). \tag{191}$$

Here we considered the approximation of small azimuthal angular momentum for the photons, that lead to expression (182), namely $\kappa - l_\phi^2 \cot^2 \theta_s \approx \kappa$, and therefore $\epsilon_\theta \sqrt{\kappa}$ represents the polar angular momentum constant of the photon. One can then notice the similarity of (191) with (190). Yet, the effect here can be expected to be significantly higher than for GEO since we consider non perturbative changes in the polar coordinate θ of the photons.

7.3.2 *Gravitational and Doppler shifts*

In the scenario described in 7.2.2, the photons with null vector $\boldsymbol{k}$ (15) emitted from Earth by the static observer with 4-velocity v_E (12) to a satellite with velocity v_s (13) experience a frequency shift f_l of the form:

$$f_l = \left(1 - \delta_{\text{ang}}\left(\epsilon_\theta, \kappa, l_\phi\right) \sqrt{\frac{M}{R_s}}\right) \sqrt{\frac{1 - \frac{2M}{R_E}}{1 - \frac{3M}{R_s}}}. \tag{192}$$

For a radial photon, namely when δ_{ang} vanishes, we recover the expression of the frequency shift from the previous works in Schwarzschild spacetime [34, 35]. Notice that the angular contribution to the shift comes in $\sqrt{M/R_s} \sim 10^{-5}$, while the radial contribution comes in $M/R_s \sim 10^{-10}$. That is, when the photons have sufficient angular momentum and thus non negligible δ_{ang}, the main contribution to the shift comes from this angular term. An interesting fact is that we can relate the frequency shift of the link scenario to the reflection shift of a light beam reflected radially:

$$f_l = f_r\left(l'_\phi = \kappa' = 0\right) \sqrt{\frac{1 - \frac{2M}{R_E}}{1 - \frac{3M}{R_s}}}. \tag{193}$$

Let us now study the frequency shifts experienced by photons for specific classes of satellites orbits.

GEO. For satellites orbiting in the Earth's equatorial plane, the frequency shift reduces to

$$f_l = \left(1 - \epsilon_\zeta \frac{l_\phi}{R_s}\sqrt{\frac{M}{R_s}}\right)\sqrt{\frac{1-\frac{2M}{R_E}}{1-\frac{3M}{R_s}}}. \tag{194}$$

Here again, as we consider photons with small azimuthal angular momenta, this shift is likely to be small.

LEO. For low altitude satellites that we consider to follow polar orbits:

$$f_l = \left(1 - \epsilon_\theta\, \epsilon_\omega \sqrt{\frac{\kappa\, M}{R_s^3}}\right)\sqrt{\frac{1-\frac{2M}{R_E}}{1-\frac{3M}{R_s}}} + O\left(\frac{l_\phi^2}{\kappa}\right). \tag{195}$$

This frequency shift is expected to be larger than in the GEO case, and than radial ones considered in the previous chapter and earlier works [34, 35, 1].

7.4 QUANTUM METROLOGY OF PHYSICAL PARAMETERS OF THE EARTH

In this section we use quantum metrology techniques to derive the optimal bounds on precision measurements of spacetime parameters of the Earth encoded in the states (187) received after propagation in one of the schemes shown above. We first compute a theoretical bound and we then provide numerical values in order to compare the magnitude with the state of the art.

7.4.1 *Quantum metrology of spacetime parameters*

Here we derive the formula for the overlap between the states that have propagated through one of the paths described in the previous section and the fiducial emitted states. We then compute the related fidelity and quantum Fisher information. Using the latter, we derive the Cramér-Rao bound for the estimation of the precision of quantum measurement on physical parameters of the schemes.

Overlap between emitted and measured states

In our study, the initial state of the photons is (185), while the received state (187) picked up a Wigner phase Ψ and an energy shift f. The overlap $\Theta = \langle \gamma | \gamma' \rangle$ between the emitted and received states can be easily computed:

$$\Theta = \cos(\Psi) \int d\Omega \, F^*(f\Omega) \, F(\Omega), \tag{196}$$

which has required us to use the orthonormalisation relations $\langle \tilde{s} | s \rangle = \delta_{\tilde{s}s}$ and $\langle \tilde{\Omega} | f\Omega \rangle = \delta(\tilde{\Omega} - f\Omega)$. We consider, as in previous studies [34, 35, 1], a real Gaussian distribution F of the form

$$F(\Omega) = \frac{1}{(2\pi\sigma^2)^{\frac{1}{4}}} \exp\left(-\frac{(\Omega - \Omega_0)^2}{4\sigma^2} \right). \tag{197}$$

We are interested in obtaining an explicit expression for the momentum contribution $I = \int d\Omega \, F^*(f\Omega) \, F(\Omega)$ of the overlap (196). Using (197) together with (188), we obtain

$$I \approx \exp\left[-\left(\delta_{\text{ang}}(\epsilon_\theta, \kappa, l_\phi) - \delta_{\text{ang}}\left(\epsilon'_\theta, \kappa', l'_\phi \right) \right)^2 \frac{\Omega_0^2}{8\sigma^2} \epsilon^2 \right]. \tag{198}$$

In the above expression we have introduced the dimensionless perturbative parameter $\epsilon = \sqrt{M/R_s}$, and we have assumed that we work in a regime where $10^{-5} \sim \epsilon \ll \epsilon^2(\Omega_0^2/\sigma^2)$. In this regime the Wigner phase is small (see the next chapter or [3] for values of such phases) and the effects computed here are significantly larger. Therefore, from now on we will ignore the contribution from the effects of gravity on the helicity of the photons. Note that (198) was derived for the reflecting scheme 7.2.1, using (188). However, the expression of the overlap for the link scheme described in 7.2.2 is

$$I \approx \exp\left[-\delta_{\text{ang}}^2(\epsilon_\theta, \kappa, l_\phi) \frac{\Omega_0^2}{8\sigma^2} \epsilon^2 \right]. \tag{199}$$

Namely, we can actualy use (198) for both schemes provided that we set $\delta_{\text{ang}}\left(\epsilon'_\theta, \kappa', l'_\phi \right) = 0$ for the link scheme.

Fidelity of quantum states and quantum Fisher information

We start by computing the fidelity between the received state that encodes the spacetime's parameter $\epsilon = \sqrt{M/R_s}$ and the fiducial emitted one. The latter has a similar expression than the former but with $\epsilon = 0$. The fidelity between these two quantum states is simply $\mathcal{F}(|\gamma_0\rangle, |\gamma_\epsilon\rangle) = |\Theta|^2 \approx I^2$. Let's now consider two states that have both gone through the path of one of the schemes described in 7.2, but that have experienced an energy shift with an infinitesimal difference $d\epsilon$ in the parameter $\epsilon = \sqrt{M/R_s}$. We use the fidelity between these two states to define the quantum Fisher information $\mathrm{H}(\epsilon)$ as

$$\mathrm{H}(\epsilon) = \lim_{d\epsilon \to 0} 8 \frac{1 - \sqrt{\mathcal{F}(|\gamma_\epsilon\rangle, |\gamma_{\epsilon + d\epsilon}\rangle)}}{d\epsilon^2}. \tag{200}$$

We can then obtain the expression for the $\epsilon = 0$ contribution of the QFI, $\mathrm{H}^{(0)} = \lim_{d\epsilon \to 0} 8 \frac{1 - \sqrt{\mathcal{F}_L(|\gamma_0\rangle, |\gamma_{d\epsilon}\rangle)}}{d\epsilon^2}$, which reads

$$\mathrm{H}^{(0)} \approx \left[\delta_{\mathrm{ang}}\left(\epsilon_\theta, \kappa, l_\phi\right) - \delta_{\mathrm{ang}}\left(\epsilon'_\theta, \kappa', l'_\phi\right)\right]^2 \frac{\Omega_0^2}{\sigma^2}. \tag{201}$$

To obtain (201), we used the expression of (198) for an infinitesimal value $d\epsilon$ of our parameter ϵ. We could then expand the expression up to lowest order in $d\epsilon \frac{\Omega_0}{\sigma} \ll 1$. Inserting this expression into (200) together with $\epsilon = 0$, and finally taking the limit $d\epsilon \to 0$, we obtain the result above. We are now able to use the Cramér-Rao inequality [55]

$$|\Delta\epsilon| \geq \frac{1}{\sqrt{N\mathrm{H}(\epsilon)}} \approx \frac{1}{\sqrt{N\mathrm{H}^{(0)}}}, \tag{202}$$

where N is the number of probes used in the experiment. We now have all the tools required to give the bound on precision of physical measurement of spacetime parameters of the Earth.

Estimation of physical parameters of the Earth

Our main control parameter $\epsilon = \sqrt{M/R_s}$ is a function of physically relevant parameters. For example, we can use it to estimate the bound for the pre-

cision on the Schwarzschild radius of the Earth $r_S = 2M$, using our input photon states (187). First we note that $|\Delta\epsilon| = \frac{|\Delta M|}{2\sqrt{MR_s}} = \frac{|\Delta r_S|}{2\sqrt{2r_S R_s}}$, therefore

$$\frac{|\Delta r_S|}{r_S} \geq \frac{2\sqrt{2}}{\sqrt{N\mathrm{H}^{(0)}}}\sqrt{\frac{R_s}{r_S}}. \tag{203}$$

The other parameter encoded in ϵ is the satellite's radius $R_s = R_E + h$. We find $|\Delta\epsilon| = \frac{|\Delta R_E|}{2(R_E+h)}\sqrt{\frac{M}{R_E+h}}$ and $|\Delta\epsilon| = \frac{|\Delta h|}{2(R_E+h)}\sqrt{\frac{M}{R_E+h}}$, which give us

$$\frac{|\Delta R_E|}{R_E} \geq \frac{2}{\sqrt{N\mathrm{H}^{(0)}}}\frac{R_s}{R_E}\sqrt{\frac{R_s}{M}}, \tag{204}$$

$$\frac{|\Delta h|}{h} \geq \frac{2}{\sqrt{N\mathrm{H}^{(0)}}}\frac{R_s}{h}\sqrt{\frac{R_s}{M}}. \tag{205}$$

We have just derived the theoretical bounds for the precision of quantum measurements on the Schwarzschild and average local radius of the Earth, and on the satellite's altitude h. In what follows, we use experimental values in order to obtain numerical estimates for these bounds.

7.4.2 *Numerical values*

We first review which values of the parameters we are able to use, and we then provide numerical precision bounds for thequantum measurement of physical parameters of the satellite schemes considered.

Numerical values of the parameters

In the expressions of the energy shifts (188) and (192), there are physical parameters of the Earth, of the light's trajectory and of the satellite's orbit. The satellite orbits are located at altitude $h = R_s - R_E$. For LEO orbits, we choose a polar orbit with inclination parameter $\alpha = 0°$, and with $h =$ 2000km, namely the highest altitude to be considered as LEO. For the VLEO ones, we take the parameters of the GOCE satellite, i.e., altitude of $h =$ 255km and inclination of $\alpha = 6.7°$. In the table 3, we give the values for the parameters appearing in the expression of the energy shift (188).

Quantity (natural u.)	Quantity (S.I. u.)	Position	Light ray trajectory	Value
M/R_s	GM/R_sc^2	LEO	/	5.29×10^{-10}
		VLEO	/	6.69×10^{-10}
l_ϕ/R_s	l_ϕ/R_s	LEO	$\rightarrow$ Lab1	1.01×10^{-4}
			$\rightarrow$ Lab2	-8.99×10^{-5}
		VLEO	$\rightarrow$ Lab1	7.64×10^{-4}
			$\rightarrow$ Lab2	/
κ/R_s^2	κ/R_s^2	LEO	$\rightarrow$ Lab1	0.49
			$\rightarrow$ Lab2	0.58
		VLEO	$\rightarrow$ Lab1	0.88
			$\rightarrow$ Lab2	/

Table 3.: Dimensionless physical parameters in the energy shifts.

The numerical values for the rescaled angular constants l_ϕ and κ are obtained through the approximate analytical expression (182) and by numerical integration of the constraint equation (183), respectively. Notice that in table 3 we give the values of l_ϕ/R_s and κ/R_s^2 only for downlinks. For an uplink with the same trajectory, the value of l_ϕ only changes sign while κ has exactly the same value. The following numerical values were used for the parameters appearing in these expressions: we considered two stations on Earth with angular coordinates $(\theta_1, \phi_1) = (37.48^\circ, 13.40^\circ)$ and $(\theta_2, \phi_2) = (51.88^\circ, 13.36^\circ)$, namely in Berlin (Germany) and Palermo (Italy) respectively. We denote these stations by Lab1 and Lab2, respectively. The reflection or the measurement aboard the satellite occur at $(\theta_s, \phi_s) = (15^\circ, 13.38^\circ)$ for LEO orbits or $(\theta_s, \phi_s) = (30^\circ, 13.38^\circ)$ for VLEO orbits, depending on the orbit considered. Such coordinates guarantee the validity of the approximate expression (182) for the azimuthal angular momentum constant l_ϕ. Notice that in the case of VLEO orbits, there is no null

geodesic for the photons that connects the satellite to Lab2. For a scheme using a VLEO orbit, we will thus only consider communications with Lab1.

Precision bounds results

We are finally able to employ (203) and (201) to give numerical values for the highest sensitivity attainable for the measurements discussed above. We use the numerical values given in 7.4.2 together with the number of probes of $N = 10^{10}$, the bandwidth in frequencies of $\sigma = 10^6$Hz and the peak frequency of $\Omega_0 = 7 \times 10^{14}$Hz. Table 4 contains our final estimates.

Satellite orbit	Light trajectory	$\Delta r_S / r_S$	$\Delta R_E / R_E$	$\Delta h / h$
VLEO	Lab1 $\rightarrow$ Lab1	6.06×10^{-10}	6.30×10^{-10}	1.57×10^{-8}
	Sat $\rightarrow$ Lab 1	1.21×10^{-9}	1.26×10^{-9}	3.15×10^{-8}
LEO	Lab1 $\leftrightarrows$ Lab2	8.50×10^{-10}	1.12×10^{-9}	3.56×10^{-9}
	Lab1 $\rightarrow$ Lab1	8.87×10^{-10}	1.17×10^{-9}	3.71×10^{-9}
	Lab2 $\rightarrow$ Lab2	8.15×10^{-10}	1.07×10^{-9}	3.41×10^{-9}
	Sat $\rightarrow$ Lab1	1.77×10^{-9}	2.33×10^{-9}	7.43×10^{-9}
	Sat $\rightarrow$ Lab2	1.63×10^{-9}	2.14×10^{-9}	6.83×10^{-9}

Table 4.: Precision bounds obtained through the quantum metrology scheme described above, for the different possible configurations of the reflecting and downlink schemes. Results for uplinks are very similar to those of the downlinks.

In the case of reflecting schemes 7.2.1, irrespectively of the orbit and configuration considered, we obtain a bound for the relative error on the measurement of the Schwarzschild radius of the order $\Delta r_S / r_S \sim 10^{-10}$. The state of the art in classical experiments give a value of 2×10^{-9} for the precision of the measurement of the Earth's Schwarzschild radius [80]. Our result is therefore one order of magnitude better than the state of the art using classical measurements. The results obtained for the link scheme 7.2.2

is a great improvement from previous works considering squeezed states of photons sent radially from Earth and measured by a satellite, looked at in the previous chapter and [35, 1]. The precision obtained is now of the order of magnitude of the state-of-the-art measurement, namely $\sim 10^{-9}$. Note that we could have used squeezed states in order to improve the result further. We leave analysis in this direction to future work.

We also find bounds on relative errors for the Earth's mean radius (over the area on Earth spanned by the light ray's propagation above it), which are of the order $\Delta R_E/R_E \sim 10^{-9} - 10^{-10}$ for different configurations involving the LEO polar satellite and VLEO respectively. For a measurement of the altitude of the satellite, the result is better for the LEO set ups with a precision bound of $\Delta h/h \sim 10^{-9}$, while we have $\Delta h/h \sim 10^{-8}$ with a VLEO.

Note that for all the configurations considered here in the reflecting scheme, we have $\epsilon'_\theta = -\epsilon_\theta$. It is particularly interesting to work with such kind of configurations since, in this case, the leading terms in the overlap (198) add up instead of competing. The effect is therefore significantly larger for such configurations than for set ups with $\epsilon'_\theta = \epsilon_\theta$. Also note that despite the better results of the reflecting scheme, the link schemes provide a channel that crosses the atmosphere only once, while in the reflecting scheme the light needs to cross it twice. Therefore, one should expect much less atmospheric noise in the link schemes 7.2.2.

Finally we notice that here, contrarily to the scheme studied in the previous chapter, the result obtained is far better for LEO satellites than for GEO satellites. There are two reasons for this. The first one is that we considered schemes where most of the angular momentum of the photon is polar and not azimuthal, while a GEO satellite only has an azimuthal velocity. This means that the reflection by a GEO satellite cannot transfer much energy to the photons in the reflecting scheme. In the link scheme, the change in energy due to the angular nature of the beam appears through the Doppler shift occuring because of the satellite's motion. Because the light's angular momentum is mostly polar, and because the GEO satellite only has an

azimuthal velocity which is also quite slow compared to satellites in LEO, the resulting Doppler shift is very small when using GEO. Instead, the polar satellites in LEO and almost polar VLEO that we considered see much larger Doppler shifts, also because of their greater velocities. This happens only because we decided to set up the scheme in a plane corresponding to a nearly constant azimuthal angle ϕ value all along the light's trajectory. Thanks to the spacetime's spherical symmetry, one could have chosen any other plane, and this argument could even be reversed to the advantage of the GEO by deciding to work in a nearly constant polar angle θ scheme. The second reason is due to the very nature of the effect: in the scheme described in the previous chapter, both gravitational shift and Doppler shift of frequencies are measured, and the latter effect dominates for a LEO orbit, but it is reduced in part by the competing gravitational redshift. Furthermore, for photons sent to a GEO satellite, the gravitational redshift largely dominates, which explains the stronger result than for a LEO orbit in the radial link scenarios [1]. However, in the schemes we study here, the effect comes either from the satellite directly communicating its kinetic energy to the reflected photons in the scheme 7.2.1, or mostly from the angularity of the beam through Doppler shifts in the link schemes 7.2.2. Both effects directly increase in amplitude with the satellite's velocity, which is larger for lower orbiting satellites. Therefore, this is the very reason why LEO satellites are better for the schemes studied here than GEO.

7.5 QKD PROTOCOL IN SCHWARZSCHILD SPACETIME

In this section we briefly compute the QBER for the simple QKD protocol described in 6.5, here implemented in the reflecting and link schemes we previously introduced in 7.2. We find the following QBER:

$$\text{QBER} = 1 - \mathcal{F}(|\gamma_0\rangle, |\gamma_\epsilon\rangle) \tag{206}$$

$$\approx 1 - \exp\left[-\left(\delta_{\text{ang}}\left(\epsilon_\theta, \kappa, l_\phi\right) - \delta_{\text{ang}}\left(\epsilon'_\theta, \kappa', l'_\phi\right)\right)^2 \frac{\Omega_0^2}{4\sigma^2}\epsilon^2\right], \tag{207}$$

for the reflecting schemes 7.2.1. For the link schemes 7.2.2, equation (207) holds but with $\delta_{\text{ang}}\left(\epsilon'_\theta, \kappa', l'_\phi\right) = 0$. Using the parameters given in 7.4.2, we can compute the QBER for all the configurations for which we obtained metrology results in table 4. We find that the QBER reaches unity for all of these. Namely, the relativistic effects are so important that without properly correcting for them one wouldn't be able to use such configurations for establishing a working QKD protocol. This happens because the frequency shifts we have obtained in this study are large enough to severely reduce the overlap between the emitted and received frequency distributions: the change in the peak frequency is larger than the bandwidth of the wavepackets. In practice, similar reflecting scenarios do not display such high error rates [22]. The reason behind this is that the correctable frequency shift was properly compensated for in the experiment [22]. This is done by performing a linear shift in frequencies in the received signal until an optimal overlap is obtained with the emitted wavepackets. Such compensation reduces drastically the effects described above. However, it does not completely cancel them since the shape of the received wavepacket also changed compared to the emitted one, which prevents the two frequency distributions from overlaping perfectly.

7.6 CONCLUSION

We performed a quantum metrology procedure on quantum superpositions of momentum-helicity states of photons in a scheme involving a reflecting satellite. In the regimes we are working in, we find that the effect from the Wigner phases acquired by the helicity states are negligible compared to the changes experienced by the momentum states.

The results we obtain then depend on the scheme considered and on the orbit of the satellite. In the reflecting scheme, for a reflecting satellite in geostationary orbit, the photons we considered are almost not affected by the reflection. On the contrary, with a satellite in low Earth orbit, the effect due to the kinetic energy of the reflecting satellite is important. In the link scheme, lower orbits are also to be favoured: the lower the satellite is, the larger is its velocity and therefore the measured Doppler shift. The quantum states of the photons are perturbed by the change in energy, and we find significantly improved quantum metrology results in both schemes: using such low orbits, we find a precision for the quantum measurement of the Schwarzschild radius of the Earth that is one order of magnitude better than the state of the art, which has been obtained thus far by classical means. We also find good precisions attainable for the quantum measurement of the Earth's radius and of the satellite's altitude. We can imagine improved schemes that could further enhance the effect, for example by considering configurations with several reflecting satellites, or by creating a path loop where the received photons are sent again multiple times. Combining the link and reflecting schemes could also be interesting, for example sending a light pulse from Earth to a satellite reflecting it to another satellite. In this latter case, the three effects would come into play: the Doppler, the gravitational and the reflection shifts would cumulate.

In this chapter we have provided the theory for a realistic Earth-satellite scheme that should lead to novel quantum measurements of spacetime parameters such as the Schwarzschild radius of the Earth. The increased preci-

sion obtained from the measurement would have an immediate implication on the development of quantum technologies as measuring devices. A better accuracy for the values of the Earth's physical parameters and of technical parameters like the altitude of the satellite would have a direct effect on Global Navigation Satellite Systems (GNSS). Our study shows that the use of quantum states together with quantum metrology techniques opens the possibility of improving the current technology. This improvement could also be taken advantage of in a wide range of other classical experiments utilising relativistic effects: for example the recent Aeolus experiment [86] that measures Earth's winds by analysing the Doppler shift of light pulses reflected on the atmosphere back to the satellite. This experiment is the symmetric reverse version of the reflecting scheme we considered here, and it could obtain improved precisions by using quantum states of light such as squeezed states.

Part IV.

Helicity states of photons in relativistic quantum communication

8

HELICITY STATES OF PHOTONS IN SCHWARZSCHILD SPACETIME

The polarisation rotation of light seen by observers in motion in Minkowski spacetime and its effect on the quantum state of photons has been widely investigated: photons' helicity states and the structure of Wigner's little group was studied in [87, 88, 64], the influence of the detector's motion on entangled helicity states of light has been worked out in [89, 90] and a QFT formalism for the Einstein-Podolsky-Rosen (EPR) correlations of polarised photons was established in [91]. Finally, the theory was applied to quantum communications in [92] and to quantum information in [93, 63].

In this chapter we look at the effect induced on quantum states of photons by the rotation of the light's polarisation during propagation in a Schwarzschild spacetime background. The first inquiry on the rotation of the light's polarisation plane due to the presence of a (spinning) massive body was carried out by Skrotskii [94]. A thorough treatment of the light's polarisation rotation can be found in [95, 96], where explicit formulas are given for scattering scenarios in the Kerr spacetime, and in [97] where the rotation is derived for perturbations due to a massive object both spinning and in translational motion. Many physical cases of polarisation rotation are considered in the literature, the main ones being: rotation of polarisation induced by astrophysical [98] and cosmological gravitational waves [99], for example for cosmic microwave background [100] and quasars' [101] photons experiencing vector perturbations in the metric,

gravitational lensing by massive objects passing through the light's trajectory [102, 97] with relativistic velocities [103, 104], or with spinning angular momentum [105, 106, 107, 108], and finally in optical interferometry in a near-Earth environment [109]. In [109], the polarisation vectors of two light rays are compared when they recombine after having travelled through two paths at different altitudes and therefore under different gravitational potentials.

This latter scheme is the closest to what we want to achieve in the sense that it is a controllable near-Earth experiment. However, here we study instead the evolution of the photons' helicity quantum states sent to satellites and reflected back to Earth. The present work is intended to extend previous computations focusing on frequency modes of photons that were developed in the earlier work [34] to the light's polarisation degree of freedom. In this chapter, we mostly work with the general formalism that has been derived in [60, 62], which provides the description for the rotation of the light's polarisation in curved spacetime together with the link between this effect and the Wigner phase acquired by the quantum state of the photons.

The structure of the chapter is as follows: in section 8.1, we provide the mathematical description for the light's propagation in the curved spacetime surrounding the Earth. Section 8.2 proceeds to compute explicitly the Wigner rotation for the considered light rays, observers and reference frames, which then enable us to compute the Wigner phase acquired by helicity states along the null geodesics. In section 8.3, we present the two operational schemes that we consider, where the light rays travel through a closed path consisting in several null geodesic segments between Earth and the satellite(s). We then give the total Wigner phase picked up by the photons' helicity states along the closed path. We then use numerical values in section 8.4 to give the amplitude of the acquired Wigner phases for each of the configurations that we have considered. Finally, we conclude and discuss our results in section 8.5.

8.1 NULL VECTOR WITH CONSTANT AZIMUTHAL COORDINATE ϕ

In order to simplify the computation and to provide simple analytical formulas for the Wigner phases, we will assume that the light rays can be sent with a constant azimuthal angle ϕ, namely that $l_\phi = 0$ in (15). For $l_\phi = 0$, the null vector takes the following simplified expression:

$$\boldsymbol{k} = E_p \left(\frac{1}{1 - \frac{2M}{r}} \partial_t + \epsilon_r \sqrt{1 - \left(1 - \frac{2M}{r}\right) \frac{\kappa}{r^2}}\, \partial_r + \frac{\epsilon_\theta}{r} \sqrt{\frac{\kappa}{r^2}}\, \partial_\theta \right). \tag{208}$$

Because the light rays are confined to $\phi = cst.$ planes, κ now plays the role of the square of the polar (i.e. related to the θ angle) angular momentum as seen by an inertial observer at space infinity. Mathematically, the constant $\epsilon_\theta \sqrt{\kappa}$ is here equivalent to the l_ϕ constant of motion of a null vector (15) confined to the equatorial plane $\theta = \pi/2$. Note that due to the spacetime's spherical symmetry, we could have worked equivalently in any other plane containing the center of the Earth. We chose to work in a $\phi = cst.$ plane for simplicity, but also because the calculations for this configuration would be easier to extend to the case of the rotating Earth, since most of the rotation effects would be orthogonal to this plane. Yet, we still need to use the general procedure to obtain the value of κ, which means to integrate and solve the relation $dr/k^r = d\theta/k^\theta$. Employing (208), we obtain:

$$\epsilon_r \int_{r_1}^{r_2} \frac{dr}{r^2 \sqrt{1 - \left(1 - \frac{2M}{r}\right) \frac{\kappa}{r^2}}} = \epsilon_\theta \frac{\Delta\theta}{\sqrt{\kappa}}, \tag{209}$$

where $\Delta\theta = \theta_2 - \theta_1$, and the indices 1 and 2 denote evaluation at initial and ending points of the null geodesic respectively. Now, even in this special case where $l_\phi = 0$ it is not easy to obtain a simple analytical formula for κ unless we make some approximation. In general it will be required to solve this equation numerically if we require the value of κ for an arbitrary propagation of the ray. To get physical insights on the behaviour of κ, we can use an expansion up to first order in κ/r^2 in order to solve (209). We always at least have $\kappa < r_{\text{min}}^2$, with $r_{\text{min}} = \min\{r_1, r_2\}$, which can be seen

from the expression of the radial component of the null vector in (15). In the constrained case $\kappa \ll r_{\text{min}}^2$, we obtain:

$$\kappa \approx \frac{r_1^2 r_2^2}{(r_1 - r_2)^2} \Delta\theta^2. \tag{210}$$

This approximate expression is valid provided that $|\Delta\theta| \ll \frac{|r_1 - r_2|}{r_{\text{max}}} = \Delta\theta_c$, with $r_{\text{max}} = \max\{r_1, r_2\}$. The critical angular difference $\Delta\theta_c$ is quite small in most realistic cases, which is why in general one has to solve (209) numerically instead of using the simple expression given in (210). However one can use (210) in some cases, for example when a light ray is exchanged between a lab close to the equator towards a geostationary satellite.

8.2 LIGHT'S POLARISATION ROTATION AND WIGNER PHASES

We here compute the Wigner rotation experienced by the light's polarisation vector between two static observers at different events. We are then able to calculate the associated Wigner phase that will affect the quantum states of the photons propagating in the curved spacetime around the Earth.

8.2.1 *Polarisation rotation for static observers*

The tetrad field associated to the family of static observers along the light's null geodesic has zeroth component $\boldsymbol{e}_{\hat{\mathbf{0}}}(\lambda) = \boldsymbol{v}_{\boldsymbol{E}}(r(\lambda))$, where $r(\lambda)$ stands for the radial coordinate of the photon at affine parameter λ, and $\boldsymbol{v}_{\boldsymbol{E}}$ was given in (12). We then follow the adaptation procedure (66), in a first place by considering the expression of a general null vector (15). We have $k^{\hat{0}} = \boldsymbol{k} \cdot \boldsymbol{e}_{\hat{\mathbf{0}}}\, \eta^{\hat{0}\hat{0}} = -\boldsymbol{k} \cdot \boldsymbol{v}_{\boldsymbol{E}} = E_p / \sqrt{1 - 2M/r}$, and we obtain the expression of the third triad component:

$$\boldsymbol{e}_{\hat{\mathbf{3}}} = \sqrt{f(r)} \left(\epsilon_r \sqrt{1 - f(r) \frac{l_\phi^2 + \kappa}{r^2}}\, \partial_r + \frac{\epsilon_\theta}{r} \sqrt{\frac{\kappa - l_\phi^2 \cot^2\theta}{r^2}}\, \partial_\theta + \frac{l_\phi}{r^2 \sin^2\theta}\, \partial_\phi \right), \tag{211}$$

where we again defined $f(r) = 1 - \frac{2M}{r}$ for compactness. The remaining first and second triad components $\boldsymbol{e}_{\hat{\mathbf{1}}}$ and $\boldsymbol{e}_{\hat{\mathbf{2}}}$ are then obtained using the or-

thonormalisation relations of the tetrad, as explained in 3.3.1. We give their cumbersome expressions in appendix B.1. The computation of the Wigner rotation $\tilde{\Psi}$ for the general null vector (15) and for the general adapted frame is very involved.

In order to simplify the computation, let us now consider light rays constrained to a $\phi = cst.$ plane, with null vector (208). To obtain a convenient result we also make a simplifying choice for the reference frame: we take the value $e^{\theta}_{\hat{2}} \doteq B = \frac{1}{r}\sqrt{1-\frac{\kappa}{r^2}}$ for the free component of the tetrad displayed in appendix B.1. Making this choice, the expression of the Wigner rotation vanishes in the flat spacetime limit $M \to 0$. To finish fixing the reference frame, we set the signs $\eta_1 = \eta_2 = +1$. The triad associated to this choice of reference frame is displayed in appendix B.2. We now proceed to calculate the Wigner rotation using (68), (245) and (208). Expanding up to lowest order in the small dimensionless parameter $\epsilon = \sqrt{M/R_E}$, where M and R_E are again the Earth's mass and average radius respectively, we find:

$$\tilde{\Psi} = -\frac{\epsilon_r}{r}\frac{3r^2-\kappa}{r^2-\kappa}\sqrt{\frac{\kappa}{2r^2}\frac{R_E}{r}}\,\epsilon + O\left(\epsilon^3\right), \tag{212}$$

For a null geodesic with a vanishing constant κ, there is no Wigner rotation as seen in the chosen frame. Here, since we already have $l_\phi = 0$, such trajectories would correspond to radial light rays where both angles θ and ϕ remain constant along the null geodesic. Notice that the Wigner rotation (212) is independent on the energy of the photons which is encoded in E_p, as it should be [87]. This will remain of course true for the Wigner phase that will be computed in the next subsection.

8.2.2 *Wigner phase between static observers*

Using (74) and (212), we compute the Wigner phase acquired by the momentum-helicity states of photons travelling in the Schwarzschild spacetime from $r(\lambda_1) = R_1$ to $r(\lambda_2) = R_2$. We obtain:

$$\begin{aligned}\Psi &= \int_{R_1}^{R_2} \tilde{\Psi}\, \frac{dr}{u^r} \\ &= \epsilon \sqrt{\frac{R_E\, \kappa}{2}} \int_{R_1}^{R_2} -\frac{3\, r^2 - \kappa}{(r^3 - \kappa\, r)^{\frac{3}{2}}}\, dr + O\left(\epsilon^3\right) \\ &= \sqrt{2} \left(\sqrt{\frac{R_E}{R_2}} \sqrt{\frac{\kappa}{R_2^2 - \kappa}} - \sqrt{\frac{R_E}{R_1}} \sqrt{\frac{\kappa}{R_1^2 - \kappa}} \right) \epsilon + O\left(\epsilon^3\right). \end{aligned} \tag{213}$$

We can notice here again that for static observers and for the frame choice we have made, there is no Wigner phase for a light ray with a purely radial trajectory, namely with $l_\phi = \kappa = 0$.

In the next section we apply the result obtained in (213) to schemes where quantum optical signals are exchanged between laboratories on Earth through reflecting satellites nodes.

8.3 POLARISED PHOTONIC SIGNALS IN EARTH-SATELLITE SCHEMES

The schemes described in this section consist in a station on Earth emitting polarised photonic signals to a satellite, which in turn reflects these signals either to another satellite or to another laboratory on Earth. The signal is then communicated back to the emitter's lab to form a closed path. We are interested in schemes where light travels closed paths (thanks to judiciously positioned mirrors) because we can compare polarisation states in a natural way only when the associated light rays have parallel null vectors [60]. This is because the polarisation vector is always defined by its orthogonality to the light's null vector: $\boldsymbol{k} \cdot \boldsymbol{\psi} = 0$. Therefore, to talk about polarisation without specifying the corresponding null vector (or momentum) is meaningless. One can thus only compare polarisations associated to parallel null vectors.

In curved spacetime this is not easily achieved in general, unless in the case of a stationary spacetime background (like in the present study) when the light ray comes back to the same space location it was emitted from and with the same initial propagation direction. To align the received light ray with the emitted one, it suffices to have a mirror at the reception location, oriented in such a way that the light ray would take the same propagation direction that it had when it was emitted. Placing the detection device very close to the emitting source after this last reflection would thus enable to measure photons which null vectors are parallel to the emitted ones.

8.3.1 *Earth-satellite schemes*

We consider schemes where the light rays have trajectories with a constant azimuthal angle ϕ, for which we have obtained the explicit expression of the Wigner phase (213). We therefore need to choose a configuration where the labs on Earth and the satellite reflection events are all at the same azimuthal angle ϕ. The satellites themselves are not constrained to orbit in the $\phi = cst.$ plane and can have an arbitrary motion as long as they are at the azimuthal coordinate ϕ when they reflect the light rays. Note that in practice, due to the Earth's rotation the signals reflected by the satellites would need to be received at a slightly different azimuthal coordinate to be at the same longitude on Earth's surface. However, this is ignored in our calculation since we assume the Earth to be static by using the Schwarzschild metric for the spacetime around the Earth. Because of the short time the light takes to propagate in the loop, it is a fair assumption to make.

One reflecting satellite

The first scheme (see Fig. 11) consists in two neighbouring laboratories on Earth at the same longitude, but at different latitudes. The optical signals are emitted from one station to a passing satellite that reflects them (in the

same fashion as in the satellite experiments [22, 23]) to the other lab, which in turn sends them back to the emitter's laboratory. We cannot simply reflect the light rays back from the satellite to the emitter's lab, because this would yield no effect. In this scheme we will consider different satellite orbits, from very low Earth orbits (VLEO) to geostationary ones (GEO).

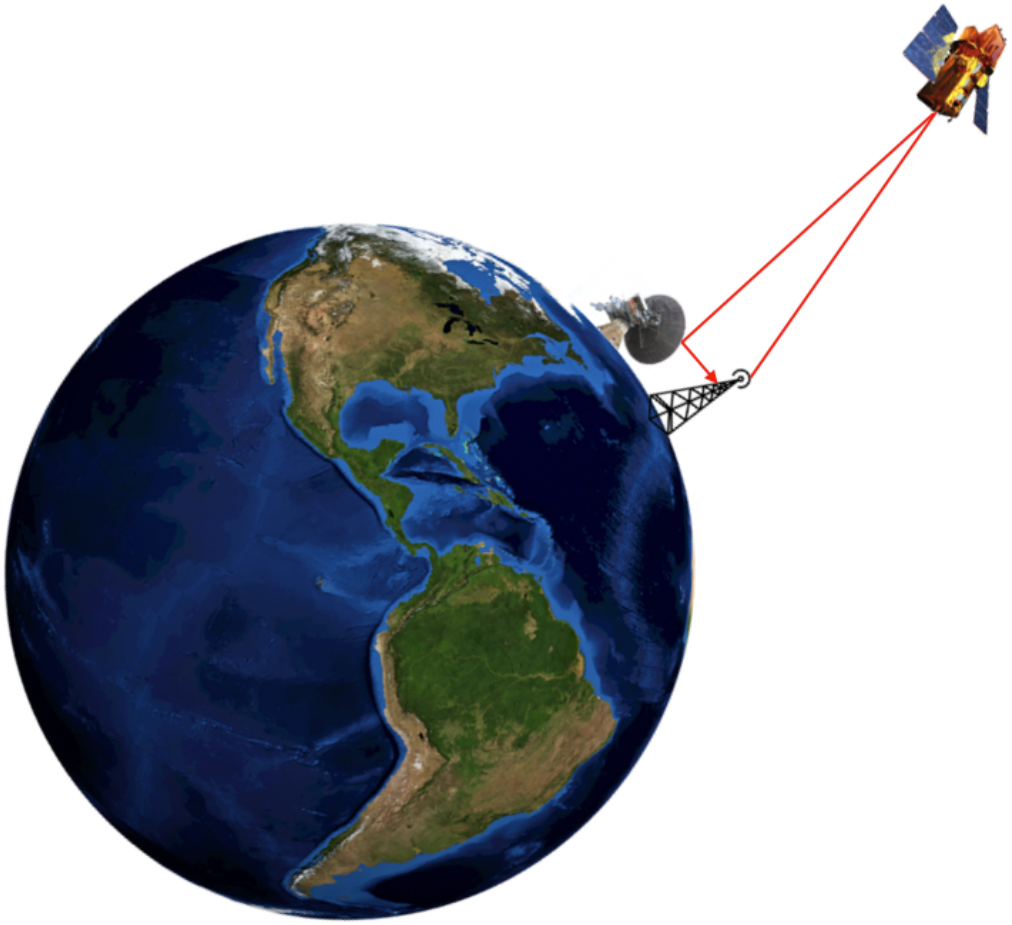

Figure 11.: Depiction of the first scheme: Quantum optical signals (the red line) are emitted from a station on Earth to a satellite which reflects them back to Earth, to another lab. On Earth, they are reflected to the initial laboratory in order to close the path loop. The picture's plane is a $\phi = cst.$ plane.

Two reflecting satellites

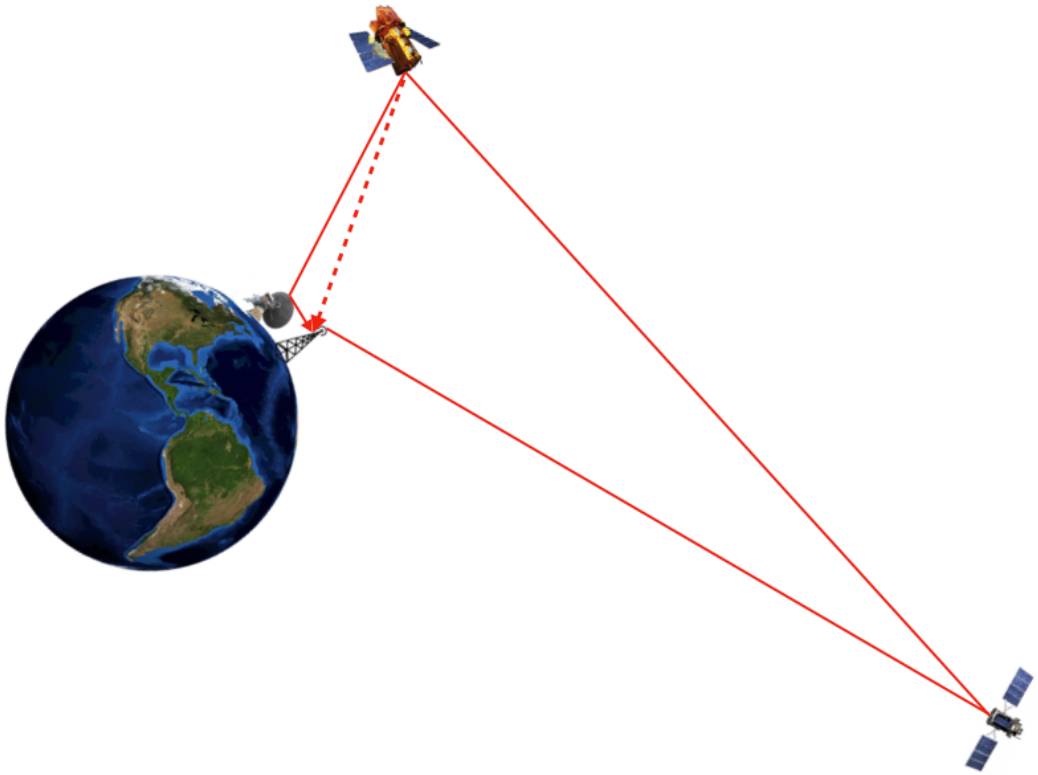

Figure 12.: Depiction of the second scheme: The light ray (the red line) is sent from Earth to a first satellite that reflects it to another satellite, which then reflects it back to Earth either directly to the emitting station (dotted line), or to another laboratory (continuous line). In this latter case, the signals are then finally sent back to the initial lab to form a closed path. Here again, the picture's plane is a $\phi = cst.$ plane for consistency with our calculations.

Another scheme (see Fig. 12) we can consider consists in a station on Earth emitting photonic signals to a satellite, which then reflects them to another satellite, with the second satellite then reflecting the signals back to the emitter's laboratory. Alternatively, the downlink from the second satellite to Earth could also reach another station that would then send the photons back to the emitter's lab, as shown in Fig. 12. Since the light ray's radial

coordinate stays approximately constant along the null geodesic in such an extra Earth-Earth segment, there is no Wigner phase (213) contribution from it, and the two variants for this second scheme are equivalent mathematically. In practice, we consider this scheme in a configuration using a low Earth orbit (LEO) and a GEO satellite.

8.3.2 *Wigner phase*

After having described the physical implementation of the two schemes in the previous subsection, we here give the explicit expression for the total Wigner phase accrued along these closed paths. Making use of (213) for each geodesic segment of the closed trajectory, we find for the first scheme:

$$\Psi_1 = \sqrt{2}\left[\sqrt{\frac{R_E}{R_s}}\left(\sqrt{\frac{\kappa}{R_s^2-\kappa}}-\sqrt{\frac{\kappa'}{R_s^2-\kappa'}}\right)+\sqrt{\frac{\kappa'}{R_E^2-\kappa'}}-\sqrt{\frac{\kappa}{R_E^2-\kappa}}\right]\epsilon+O(\epsilon^3), \tag{214}$$

and R_s denotes the satellite's radius. The last segment of the light's propagation, from the receiver's laboratory back to the emitter's station, does not contribute to the phase since its endpoints are at the same altitude: the Wigner phase (213) vanishes in this case. Notice that if the receiver's laboratory was at the same location as the emitter's one, we would have $\kappa' = \kappa$ and Ψ_1 would therefore vanish. This is the reason why we need the emitter and the receiver at different locations, i.e. at different latitudes.

To obtain some extra physical insights, we can expand the expression of the phase (214) in $\kappa^{(\prime)} \ll R_E^2$, in the same fashion as we previously did to obtain the approximate expression of the rescaled Carter constant (210) in the special case of small angular deviations. We then have:

$$\Psi_1 \approx \sqrt{2}(|\Delta\theta'|-|\Delta\theta|)\frac{1-\left(\frac{R_E}{R_s}\right)^{\frac{3}{2}}}{1-\frac{R_E}{R_s}}\epsilon+O(\epsilon^3). \tag{215}$$

From this simple explicit formula, we can notice that if $|\Delta\theta'| = |\Delta\theta|$, then there is no Wigner phase for this scheme. This feature is due to the symmetry of the spacetime, and it is merely a more explicit way of saying that (214)

vanishes for $\kappa = \kappa'$. The expression (215) is however not a good approximation in most realistic cases, for which one should preferably use (214). Equation (215) can be used with a decent accuracy when the two labs are close to the equator and exchange signals with a geostationary satellite.

Now turning to the second scheme, we obtain a sum of three contributions for the total Wigner phase:

$$\begin{aligned}\Psi_2 = \sqrt{2}\Bigg[&\sqrt{\frac{R_E}{R_{s_2}}}\left(\sqrt{\frac{\kappa'}{R_{s_2}^2-\kappa'}}-\sqrt{\frac{\kappa''}{R_{s_2}^2-\kappa''}}\right)\\&+\sqrt{\frac{R_E}{R_{s_1}}}\left(\sqrt{\frac{\kappa}{R_{s_1}^2-\kappa}}-\sqrt{\frac{\kappa'}{R_{s_1}^2-\kappa'}}\right)\\&+\sqrt{\frac{\kappa''}{R_E^2-\kappa''}}-\sqrt{\frac{\kappa}{R_E^2-\kappa}}\Bigg]\epsilon+O(\epsilon^3),\end{aligned} \tag{216}$$

where R_{s_1} and R_{s_2} denote the radii of the first and second satellite to reflect the light pulses, respectively. Here, we do not expand this expression as it is not likely to find extra physical insights that have not been already seen in (215). It is also more difficult to find an interesting configuration with two satellites that fulfils the validity condition at each path segment contributing to the Wigner phase (216).

Both total phases (214) and (216) do not seem to vanish in general, which can be seen even more explicitly in the approximate formula (215). This seems to contradict the statement found in the literature that the total Wigner phase acquired along a closed path in Schwarzschild spacetime would always vanish regardless of the gauge convention [96, 95].

The latter statement was a consequence of the general claim made by the authors, that the Wigner phase remains gauge invariant under changes of reference frames along closed trajectories. In Schwarzschild spacetime, if one works within the Newton gauge, there is no rotation of polarisation along arbitrary null geodesics. The authors concluded that this absence of effect would remain along closed paths for any choice of reference frame. Yet, we have just shown in our derivation that a different choice of frame does not necessarily yield a zero result along a closed trajectory. One can

argue that the claim in [96, 95] should hold only for closed paths in phase space, which is a much stronger restriction. The paths we consider are not closed in phase space, although they form a closed trajectory in position space. In [109] the authors first say that the geodetic effects of gravity on polarisation rotation are zero along a closed trajectory. However, in the same work they also say that this is true for closed phase space trajectories. From our result, it seems that the geodetic effects vanish for closed paths in phase space only. An example of such paths would be given by photons following circular geodesics on the photon sphere of a black hole at $r_{\text{ps}} = 3M_{\text{bh}}$. In this case, the path is closed in both position and momentum spaces. One can expect the absence of Wigner phases for such configurations in Schwarzschild spacetime. However, if the path is closed by judiciously positioned mirrors, like in this work, then the claim made in [96, 95] does not seem to hold. This occurs because the mirrors change the light's null vector in a discontinuous way, which therefore opens the path in momentum space. The arguments made by the authors in those works can no longer be applied, and the gauge-invariance is lost even if the photons are measured at the same location by the same observer who initially emitted them. This supports our nonzero result.

In the next section 8.4.1, we will give the numerical values for the parameters appearing in (214) and (216) in order to estimate the amplitude of the total Wigner phases obtained here for the two schemes. Before that, let us review the effects due to the reflections by the satellites in the next subsection.

8.3.3 *Changes due to reflections on mirrors*

In the schemes described in 8.3.1, the propagating light pulses are reflected by the satellite(s), and prior to measurement by the static observer on Earth in order to align the received light rays with the emitted ones. This last reflection doesn't change the energy of the received photons as seen by the

static observer that will perform the measurement, because the mirror is static itself and located at the same radius. It solely changes the directional parameters $\epsilon_r, \epsilon_\theta$ and κ of the null vector (208) back to the initial values that the emitted light rays had.

Yet, the orbiting satellite does communicate some of its energy to the photons at the reflection event, which changes the value of E_p for the new geodesic segment(s) after the reflection. The Wigner phases are however energy independent, therefore the helicity states are not affected by such energy shifts, only the momentum states are.

The light ray's reflections on the mirrors change its direction, and as a consequence, its polarisation vector. This may induce extra Wigner phases, although we here ignore these effect because of the considerations in [109], where it was found that the relativistic corrections on the polarisation vector due to reflections on the mirrors are one order higher in the relativistic perturbation than the polarisation rotation due to propagation in the curved spacetime which we are studying here.

8.4 TOTAL WIGNER PHASE

Here we give numerical values for the parameters that appear in the expression of the Wigner phase (213), in order to give the phase's value for the different configurations described in 8.3.1.

8.4.1 *Parameters*

The Wigner phases (214) and (216) encode physical parameters of the Earth and some parameters of the light's trajectory. We consider three orbits for the satellites: a GEO i.e. at $R_s(\text{GEO}) = R_E + 35784\text{km}$, a LEO at $R_s(\text{LEO}) = R_E + 2000\text{km}$, which is the highest orbit to be considered as LEO, and a VLEO at $R_s(\text{VLEO}) = R_E + 255\text{km}$, which is the radius at which the Gravity

field and steady-state Ocean Circulation Explorer (GOCE) satellite orbited the Earth.

Quantity (natural u.)	Quantity (S.I. u.)	Position	Light ray trajectory	Value
M/R_E	$\frac{GM}{R_E c^2}$	Earth	/	6.95×10^{-10}
M/R_s	$\frac{GM}{R_s c^2}$	GEO	/	1.05×10^{-10}
		LEO	/	5.29×10^{-10}
		VLEO	/	6.69×10^{-10}
κ	κ	/	Earth $\rightarrow$ GEO	$2.73 \times 10^{13}\mathrm{m}^2$
			GEO $\rightarrow$ Earth	$2.66 \times 10^{13}\mathrm{m}^2$
			Earth $\rightarrow$ LEO	$3.75 \times 10^{13}\mathrm{m}^2$
			LEO $\rightarrow$ Earth	$3.80 \times 10^{13}\mathrm{m}^2$
			Earth $\rightarrow$ VLEO	$4.03 \times 10^{13}\mathrm{m}^2$
			VLEO $\rightarrow$ Earth	$4.46 \times 10^{13}\mathrm{m}^2$
			GEO $\rightarrow$ LEO	$6.98 \times 10^{13}\mathrm{m}^2$
			LEO $\rightarrow$ GEO	$6.98 \times 10^{13}\mathrm{m}^2$

Table 5.: Physical parameters in the Wigner phase's expression.

In the table 5, we give the numerical values of the quantities appearing in the expressions of the Wigner phases. We compute the values for the rescaled Carter constant κ by integrating numerically the constraint equation (209). We used the parameters given in the previous paragraph together with the latitudes $\theta_e = 42^\circ$ and $\theta_o = 43^\circ$ respectively for the emitting and receiving stations on Earth, $\theta_s(\mathrm{VLEO}) = 30^\circ$ and $\theta_s(\mathrm{LEO}) = 15^\circ$ respectively for the reflecting VLEO and LEO satellites, and the GEO satellite lies in the equatorial plane $\theta_s(\mathrm{GEO}) = 90^\circ$.

Notice that the rescaled Carter constants in the table above have the same value when the light propagates in one way or in the opposite way. This doesn't seem to be true *a priori* for the Earth-satellite exchanges in the table

above, yet this difference in value is only due to our set up choice of having the receiver's lab at a slightly different latitude than the emitter's station.

8.4.2 *Wigner phases*

We now have all the numerical values required to evaluate the Wigner phases (214) and (216). We give their amplitudes for the different schemes and satellites' configurations in the table 6 below:

Scheme	Satellites' orbits	Ψ (rad)
1	VLEO	1.97×10^{-4}
	LEO	1.32×10^{-5}
	GEO	-2.09×10^{-6}
2	LEO $\rightarrow$ GEO	-5.56×10^{-4}
	GEO $\rightarrow$ LEO	5.67×10^{-4}

Table 6.: Wigner phase for different satellite configurations in both schemes.

Unsurprisingly, the magnitude of the effect is larger in the second scheme, where the light pulses propagate along larger distances in the curved spacetime surrounding the Earth. Yet we can notice that for the first scheme, higher values are obtained for lower orbits. This is due to the angular constants κ having larger values when the photons are sent to such low orbits, because their $\theta(\lambda)$ angular coordinate varies faster along the ray.

As explained in 3.3.4, we can facilitate the detection of such phases by using more refined helicity states like GHZ states. Nevertheless, the values we obtained for the Wigner phases are larger than what one finds in the litterature for other scenarios studying light's rotation of polarisation, see for example [103, 104, 106, 98]. This result also seems to invalidate the statement that there would be no Wigner phase for a closed trajectory in Schwarzschild spacetime [95, 96, 109], even when it is due to judiciously positioned mirrors and not because of initial conditions [96].

8.5 conclusion

We have considered beams of polarised light that travel closed paths in the Schwarzschild spacetime around the Earth, and we found that the photon helicity states pick up a non zero Wigner phase. For the configurations we looked at, the amplitudes of the Wigner phases we found are, to our knowledge, larger than what can be found in the litterature for different scenarios probing the light's polarisation rotation. Our result also questions the statement found in the litterature that there is no Wigner phase accrued by photons propagating along a closed path in the Schwarzschild spacetime.

We presented a theory for realistic schemes involving reflecting satellites in the near Earth environment. This proposal should lead to new quantum measurements of general relativistic effects induced on polarised photons. We find that the amplitude of the effect is higher when considering lower orbits for schemes with a single satellite. With multiple reflecting satellites, the configurations with longer path length together with greater angular differences between path segments would provide the largest effect. The effect can also be enhanced by using more refined helicity states, such as GHZ states.

The experiment we propose in this chapter is achievable with current technology. The measurement of the phase we predict would help deepen our understanding of the influence of the polarisation rotation in curved spacetime on the quantum state of photons, and therefore of the interplay between quantum physics and relativity.

9

HELICITY STATES OF PHOTONS IN A CENTRIFUGE

Entangled states of photons have been used extensively to show how exact were the predictions made by quantum theory. Bell test experiments using polarisation entangled photons [12] are a striking example. On another side, the theory of relativity has been necessary to explain effects due to acceleration, such as in particle accelerators, where the lifetime of created particles is longer due to the time dilation induced by the particles' relativistic velocities [13]. The question we address in this chapter is the following: How shall we describe the quantum state of polarised light, that is the helicity states of photons, as seen by accelerated observers?

There are several motivations for looking at the influence of observers' acceleration on the outcome of a usual quantum optics experiment: the first one would be that both relativity and quantum theory give an important, yet different role to the observer regarding the outcome of an experiment. Seeking for observer dependent effects arising from both theories should help get new insights on the interplay between these theories. Another reason is that despite a wide range of relativistic tests in different regimes, relativistic effects directly related to acceleration of motion haven't been tested much on quantum states. However, a recent experiment by Fink *et al.* [43] gave bounds for the invariance of a (rotationally invariant) Bell state of photons under uniform acceleration in a centrifuge. We explore the theory to find different configurations where this invariance could break down and give a possibly measurable effect, in particular by making other choices for the

type of acceleration and for the quantum state to be probed. Finally, quantum technologies will indubitably be increasingly used in the future, for example in space in order to provide better services and security. Whether in the case of quantum experiments in space or for future all day life quantum technologies, resilience under acceleration seems to be an essential feature. In general, knowing the impact of relativistic effects on quantum properties is very important as quantum technology will develop to be increasingly elaborate and therefore sensitive to such effects.

In this chapter we will look at different configurations where polarised photons propagate between centrifuged observers. Relativistic treatments of light's polarisation in Minkowski spacetime has been carried out in several works [89, 87, 91, 90, 92, 88, 93, 63, 64]. In the present work, we mainly use the theory developed in [60, 62] to investigate the possible effects of the observers' acceleration on photonic quantum helicity states. The structure of the chapter is as follows: in section 9.1 we introduce the mathematical tools necessary to describe the observers and the light rays in the centrifuge. In section 9.2, we calculate the Wigner phase factors acquired by the helicity states, first for photons propagating radially, then for photons with angular momentum. Section 9.3 proposes an experimental scheme to measure such Wigner phases. In section 9.4, we discuss the results we have obtained and we compare them with the outcome of the experiment [43]. Finally, we conclude in our results in section 9.5.

9.1 MATHEMATICAL FORMALISM

9.1.1 *Centrifuged observers*

In this chapter, the spacetime background is considered to be the Minkowski spacetime in cylindrical (actually polar) coordinates $(t, r, \theta, z = 0)$. The matrix representation of the spacetime's metric is $g = \mathrm{diag}(-1, 1, r^2, 1)$.

At event $(t, r, \theta, z = 0)$, an observer rigidly attached to the arm of a centrifuge has 4-velocity [49]:

$$\boldsymbol{v} = \gamma(t, r)\,(\,\partial_t + \omega(t)\,\partial_\theta)\,, \tag{217}$$

with $\omega(t) = \frac{d\theta}{dt}$ the coordinate angular velocity of the centrifuge and $\gamma(t, r) = (1 - r^2\,\omega(t)^2)^{-\frac{1}{2}}$. The emitter, the receiver and the quantum optical tools (like the mirrors) are all rigidly attached to the centrifuge and therefore have a velocity of the form (217).

We introduce the tetrad $\boldsymbol{e}$ that will translate the expressions of physical quantities from the global polar Minkowski coordinates to local Cartesian coordinates adapted to our accelerating observer. A tetrad field for the familly of centrifuged observers will be defined at each point along the geodesic followed by the light beam from emission to reception (or reflection to another geodesic segment). This will allow us to track the change in the light's polarisation as measured by our accelerating observers. Following the procedure described previously, we set the timelike component of the tetrad as $\boldsymbol{e}_{\hat{0}} = \boldsymbol{v}$ at each event along the path of the light ray. As in the previous chapter, the remaining tetrad components are obtained using the adaptation procedure and the orthonormalisation relations.

9.1.2 *The light's null vector*

We consider beams of light propagating in the polar plane of a centrifuge between two accelerating observers (see figure 13). A light ray propagating in the (r, θ) polar plane in Minkowski spacetime has null vector [49]:

$$\boldsymbol{k} = E_p \left(\partial_t + \eta_r \sqrt{1 - \frac{\kappa^2}{r^2}}\,\partial_r + \frac{\kappa}{r^2}\,\partial_\theta \right), \tag{218}$$

where $\eta_r = \text{sign}(k^r) = \pm 1$, $E_p = \hbar\Omega > 0$ is the photon's energy as measured by an inertial observer and $\kappa = K/E_p$, with $K = r^2(d\theta/d\lambda)$ the photon's constant polar angular momentum as seen by an inertial observer.

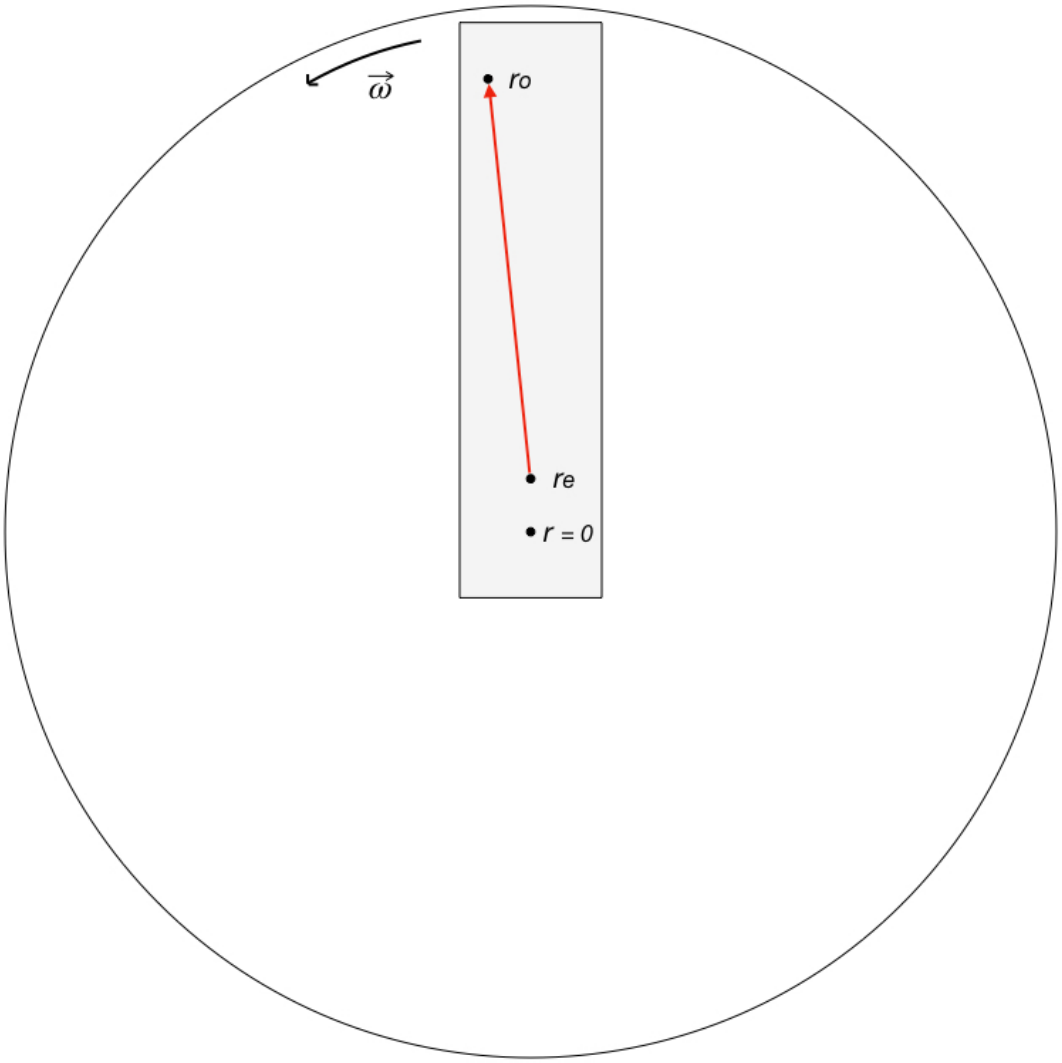

Figure 13.: The centrifuge's arm rotates with angular velocity ω and is represented here by the greyed rectangle. Within the arm of the centrifuge, a polarised light beam (in red on the figure) propagates between the source and the detector that are located at $r_1 = r_e$ and $r_2 = r_o$, respectively.

We can relate the photon's timelike constant of motion E_p to the photon's frequency Ω_{acc} as measured by an accelerated observer, using that [49]:

$$\hbar\Omega_{acc} = -k^\mu v_\mu = E_p\,\gamma(t,r)\,(1-\kappa\,\omega(t)). \tag{219}$$

Similarly, we can obtain an explicit expression for κ, for example by integrating $k^\theta/k^r = d\theta/dr$. We get:

$$\kappa = \frac{r_2\, r_1 \sin\Delta\theta}{\sqrt{r_2^2 + r_1^2 - 2\, r_2\, r_1 \cos\Delta\theta}}, \tag{220}$$

where $\Delta\theta = \theta_2 - \theta_1$ denotes the angular coordinate's deflection between the two endpoints of the null geodesic followed by the light ray. Combining these two expressions, we obtain the following explicit expression:

$$E_p = \frac{\gamma^{-1}(t,r)\,\hbar\Omega_{acc}}{1 - \frac{\omega(t)\, r_2\, r_1 \sin\Delta\theta}{\sqrt{r_2^2+r_1^2-2\, r_2\, r_1 \cos\Delta\theta}}}, \tag{221}$$

which holds for any event along the null geodesic between the endpoints (t_1, r_1, θ_1) and (t_2, r_2, θ_2). All our formulas are now expressed in terms of known quantities that are measured either at the beginning or at the end of the light's null geodesic.

9.2 POLARISATION ROTATION OF LIGHT AND WIGNER PHASE

In this section, we compute the Wigner rotation experienced by the light's polarisation vector when the photons propagate. We first consider light pulses propagating radially, then photons with an arbitrary propagation direction within the polar plane of the centrifuge.

9.2.1 *Radial photons*

Radial light rays, namely null geodesics with $\theta_1 = \theta_2$, have tangent null vectors that reduce to $\boldsymbol{k} = E_p\,(\,\partial_t + \eta_r\,\partial_r)$, with $E_p = \gamma^{-1}(t,r)\,\hbar\Omega_{acc}$. The

tetrad field for our accelerated observers, once adapted to radial photons, is given by $\boldsymbol{e}_{\hat{0}} = \boldsymbol{v}$ and:

$$\boldsymbol{e}_{\hat{1}} = -\eta_1\eta_2\sqrt{1-r^2B^2}\left(r\,\omega(t)(\eta_r\,\partial_t + \partial_r) + \frac{\eta_r}{r}\,\partial_\theta\right) + \eta_1 rB\,\partial_z \tag{222}$$

$$\boldsymbol{e}_{\hat{2}} = r^2\omega(t)B(\,\partial_t + \eta_r\,\partial_r) + B\,\partial_\theta + \eta_2\eta_r\sqrt{1-r^2B^2}\,\partial_z \tag{223}$$

$$\boldsymbol{e}_{\hat{3}} = \gamma(t,r)\left(-r^2\omega(t)^2\,\partial_t + \eta_r(1-r^2\omega(t)^2)\,\partial_r - \omega(t)\,\partial_\theta\right). \tag{224}$$

where $B = e_{\hat{2}}^{\theta}$ is a free tetrad component encoding most of the gauge freedom from the choice of the frame, with also $\eta_1, \eta_2 = \pm 1$ encoding the rest of the gauge. Notice that the parameter B is not completely arbitrary since it needs to have the dimension of the inverse of a distance. It also needs to obey some constraints, for example in this radial case $|B| \leq r^{-1}$ so that all the tetrad components remain real valued.

Computing explicitly the Wigner rotation while keeping the gauge quantities free, we obtain:

$$\tilde{\Psi} = -\eta_1\eta_2\frac{B + r\left(\frac{\partial B}{\partial r} + \eta_r\frac{\partial B}{\partial t}\right)}{\gamma(t,r)\sqrt{1-r^2B^2}}. \tag{225}$$

The Wigner phase for a radial path from r_1 to r_2 is then:

$$\Psi = \int_{\lambda_1}^{\lambda_2}\tilde{\Psi}\,d\lambda = \int_{r_1}^{r_2}\frac{\tilde{\Psi}}{u^r}dr \tag{226}$$

$$\Psi = -\eta_1\eta_2\int_{r_1}^{r_2}\frac{B + r\left(\frac{\partial B}{\partial r} + \eta_r\frac{\partial B}{\partial t}\right)}{\sqrt{1-r^2B^2}}\,dr. \tag{227}$$

This phase is clearly independent of the parameters of the centrifuge. It is a purely gauge phase due to the choice of the frame, it encodes no information from the accelerating nature of our observers. One can pick a frame where such a trivial phase vanishes, by setting $B = C_0/r$, with $C_0 \in [-1, 1]$. Notice that despite the presence of an apparent singularity in the expressions (225) and (227) when we make the choice $B = \pm 1/r$, which amounts to use the tetrad components $\boldsymbol{e}_{\hat{1}} = \pm\eta_1\,\partial_z$ and $\boldsymbol{e}_{\hat{2}} = \pm r\,\omega(t)(\,\partial_t + \eta_r\,\partial_r) \pm \frac{1}{r}\,\partial_\theta$, this choice gives an identically zero Wigner rotation as well.

We have just seen that radial photons do not give any interesting phase when measured by centrifuged observers. In the next subsection, we consider photons with angular momentum in order to obtain a better result.

9.2.2 *Angular photons*

In the case of non radial light beams, we follow the same procedure as in the previous subsection but now using the complete null vector (218). The photon's angular constant of motion $\kappa \neq 0$ induces several extra terms, and B can now be a function of (t, r, θ). The tetrad for our accelerating observers and adapted to the light beam considered here is given in appendix C.1. The obtained Wigner rotation $\tilde{\Psi}$ is rather cumbersome and we display it in equation (247) in appendix C.2.

In order to extract physical insights on the effect of the observer's acceleration on the measurement of photon states, we seek for an interesting frame choice that would simplify the expression of the Wigner rotation. Let us first look for a frame in which the Wigner rotation would vanish in the limit of radial photons $\kappa \to 0$. This choice is motivated by the lack of physical meaning the Wigner phase has in the radial case, as we saw in the previous subsection. Such a frame can be chosen by picking an expression for $B(t, r, \theta)$ that solves the differential equation in (225). The solutions can be written as $B(t, r, \theta) = f(\theta)/r$, where f is for now an arbitrary differentiable function. Using this family of tetrad frames and after a lengthy computation we obtain the new expression for the Wigner rotation (248) (in appendix C.2). In order to obtain a simple analytical expression, let us look at the case where the beam is only slightly angular. To do so, we use the explicit expressions for the constants of motion (220) and (221), and we expand the Wigner rotation up to first order in $\Delta\theta = \theta_2 - \theta_1$, which gives:

$$\tilde{\Psi} = \frac{r_2\, r_1}{r_2 - r_1} \frac{f(\theta)\, r^2 \omega'(t) - f'(\theta)}{\gamma(t, r)\, r^2 \sqrt{1 - f(\theta)^2}} \Delta\theta + O\big(\Delta\theta^2\big), \tag{228}$$

where we have set $\eta_1 = \eta_2 = 1$ to further simplify the formula. We have now an expression simple enough to get some physical insights. First, notice that the Wigner rotation (228) is independent on the energy of the photons $\hbar\Omega_{acc}$, as it should [87]. Also notice that f has to be a bounded function: $|f(\theta)| < 1$ for all θ, otherwise the Wigner rotation (228) would become imaginary due

to some components of the tetrad taking complex values. A simple choice like $f(\theta) = 0$ clearly yields an identically zero Wigner rotation. This is true in the general case as well, as can be seen by setting $B(t, r, \theta) = 0$ in the general formula (247). Despite the apparent singularity, the simple choice $f(\theta) = \pm 1$ gives a perfectly regular yet vanishing result if it is made before the derivation of the Wigner rotation. To obtain a non trivial result, namely a phase which genuinely depends on the rotation of the centrifuge, one thus needs to make some other frame choice. We can now have a closer look at the two different regimes for the acceleration of the centrifuge: uniform and non-uniform acceleration.

Uniform acceleration

If the centrifuge is in uniform acceleration, namely when $\omega(t) = \omega_0 = cst.$, only the centripetal acceleration $\boldsymbol{a}_c(v) = -\frac{r\,\omega_0^2}{1-r^2\omega_0^2}\,\partial_r$ is left. The Wigner phase (228) then simplifies to:

$$\tilde{\Psi} = -\frac{r_2\, r_1}{r_2 - r_1}\frac{f'(\theta)}{\gamma(r)\, r^2\sqrt{1 - f(\theta)^2}}\Delta\theta + O\big(\Delta\theta^2\big), \tag{229}$$

where here $\gamma(r) = (1 - r^2\omega_0^2)^{-\frac{1}{2}}$. The choice $B = f(\theta)/r$ that we made therefore gives a non zero result in the uniform acceleration case. However we notice that the Wigner rotation would completely vanish in this uniform acceleration case if we were to choose $f(\theta) = cst$. We can specify a function f to simplify (229) further. A natural choice seems to be $f(\theta) = \cos\theta$, then:

$$\tilde{\Psi} = \eta_\theta \frac{r_2\, r_1}{r_2 - r_1}\frac{\Delta\theta}{\gamma(r)\, r^2} + O\big(\Delta\theta^2\big), \tag{230}$$

where $\eta_\theta = \mathrm{sign}(\sin\theta)$. Let us consider the case where η_θ remains constant along the beam's trajectory. The Wigner phase is then easily computed:

$$\begin{aligned}
\Psi &= \int_{\lambda_1}^{\lambda_2} \tilde{\Psi}\, d\lambda \\
&= \eta_\theta\, \Delta\theta \frac{r_2\, r_1}{r_2 - r_1}\int_{r_1}^{r_2} \frac{1}{\gamma(r)\, r^2}\frac{dr}{u^r} + O\big(\Delta\theta^2\big) \\
&= \eta_r\, \eta_\theta\, \Delta\theta \frac{r_2\, r_1}{r_2 - r_1}\int_{r_1}^{r_2} \frac{dr}{r^2} + O\big(\Delta\theta^2\big) \\
\Psi &= \eta_r\, \eta_\theta\, \Delta\theta + O\big(\Delta\theta^2\big).
\end{aligned} \tag{231}$$

This neat expression shows a Wigner phase that only depends on the direction of the beam. The result is independent of the radial distance covered by the beam, and more importantly, of the angular velocity ω_0 of the centrifuge. This phase is therefore not directly related to the acceleration, in a similar way as with the radial photons result (227). Notice that using the more general expression of (229) would not change this dependence. Therefore, to find a genuine effect due to acceleration we need to consider non uniform accelerations.

Non uniform acceleration

Let us now consider a centrifuge accelerating non uniformly. In order to have a phase due purely to the non uniform nature of the acceleration, let us choose a frame that would make the phase vanish in the uniform acceleration scenario. From the considerations below (229), we know that we need to take $f(\theta) = f_0 = cst$. Furthermore, we know that we need to choose $0 < |f_0| < 1$ in order to have a real valued and non zero Wigner rotation. Let us then take an intermediate value: $f_0 = 1/\sqrt{2}$ will turn out to be convenient. We then obtain a Wigner rotation that vanishes for uniformly accelerating observers and radial light rays. It reads:

$$\tilde{\Psi} = \Delta\theta \frac{r_2\, r_1}{r_2 - r_1} \frac{\omega'(t)}{\gamma(t)} + O\big(\Delta\theta^2\big). \tag{232}$$

The Wigner phase accumulated along the light's path then reads:

$$\begin{aligned}
\Psi &= \int_{\lambda_1}^{\lambda_2} \tilde{\Psi}\, d\lambda \\
&= \Delta\theta \frac{r_2\, r_1}{r_2 - r_1} \int_{t_1}^{t_2} \frac{\omega'(t)}{\gamma(t)} \frac{dt}{u^t} + O\big(\Delta\theta^2\big) \\
&= \Delta\theta \frac{r_2\, r_1}{r_2 - r_1} \int_{t_1}^{t_2} \omega'(t)\, dt + O\big(\Delta\theta^2\big), \\
\Psi &= \Delta\theta \frac{r_2\, r_1}{c\,(r_2 - r_1)} \left(\omega(t_2) - \omega(t_1)\right) + O\big(\Delta\theta^2\big).
\end{aligned} \tag{233}$$

We have restored the speed of light c in this last equality for clarity. The phase we obtain depends on the trajectory of the beam, and it is proportional to the difference in the angular velocities measured by the centrifuged

emitter and receiver. The phase we obtained is small because of two perturbative quantities: the angular deviation $\Delta\theta$ that we chose to be perturbative for convenience in the calculations (but which doesn't have to be in principle) and the relativistic terms of the form $r\,\omega/c$ which are expected to be small in realistic experiments. In the next section we will propose an experimental scheme where the light beam travels a closed path.

9.3 PROPOSED SCHEME

The Wigner phases we obtained in (231) and (233) are acquired by the quantum state of the photons when these are prepared and measured in the specific observer frames that we have defined. The expression of the Wigner phases we obtained work for a definite angular momentum constant κ, i.e. along a single null geodesic. However, when the light beam eventually encounters a mirror or any other device that changes its direction, κ then takes a different value. The phase for the new geodesic segment then needs to be computed separetely with the new value for κ (namely with the new values for r_1, r_2 and $\Delta\theta$). The final result is the sum of the phases acquired along such portions.

The reflections on mirrors also change the light's polarisation vector. Such reflection events may therefore induce extra Wigner phases to the quantum state. In this chapter we ignore such phases and leave this problem for further work. However, such phases are relevant for the complete theory and they would need to be taken into account in a realistic experiment.

We now describe the experimental scheme we consider to be the most relevant to measure the effect. A closed loop seems to be indicated as the most interesting path to be followed by the photons, for several reasons: firstly, we can compare polarisation states only from light rays with parallel null vectors. In a closed path, the null vector at the end of the loop is reflected such that it takes again the direction it had at emission, which therefore enables a legitimate comparison of the polarisation states. Sec-

ondly, the result we have obtained in (233) indicates that the value of the phase is rather small. A closed path would enable the light to propagate again and again in the loop and therefore to cumulate phases until the total phase becomes measurable. Lastly, in [95, 96] it is claimed that one can obtain a completely gauge-independent phase in a static spacetime (like in the Minkowski spacetime considered here) by measuring the phase after the photons have travelled a closed path in space. We will thus be able to probe this claim by using a closed path propagation of the light.

Let us consider the following closed path scheme (see figure 14): a beam of polarised light is prepared and emitted along the arm of the centrifuge with a small angular momentum at event $(t_e, r_e, 0)$. The emission's radius r_e is close to the center of the centrifuge and the beam propagates towards the end of the centrifuge's arm. A mirror reflects the light beam at event (t_i, r_i, θ_i) and the photons are finally reflected back to their emission point without angular momentum from event $(t_{i'}, r_{i'}, 0)$ to $(t_o, r_o = r_e, 0)$ using another mirror. Just before the measurement takes place at the latter location, we reflect one last time the beam in order to close the light's path in phase space: this last reflections uses a mirror that we have placed close to the source and appropriately oriented in order for the measured photons to have a parallel momentum as the emitted ones. This is a required condition to compare polarisation states and for the claim made in [95, 96] to hold.

The total Wigner phase acquired is then the sum of the Wigner phases acquired in each segment of the closed path: $\Psi = \Psi_{e\to i} + \Psi_{i\to i'} + \Psi_{i'\to o}$. Assuming the centrifuge is in a non uniformly accelerating motion, these individual phases read:

$$\Psi_{e\to i} = \theta_i \frac{r_i\, r_e}{c\,(r_i - r_e)}\,(\omega(t_i) - \omega(t_e)) + O(\theta_i^2) \tag{234}$$

$$\Psi_{i\to i'} = -\,\theta_i \frac{r_{i'}\, r_i}{c\,(r_{i'} - r_i)}\,(\omega(t_{i'}) - \omega(t_i)) + O(\theta_i^2) \tag{235}$$

$$\Psi_{i'\to o} = 0. \tag{236}$$

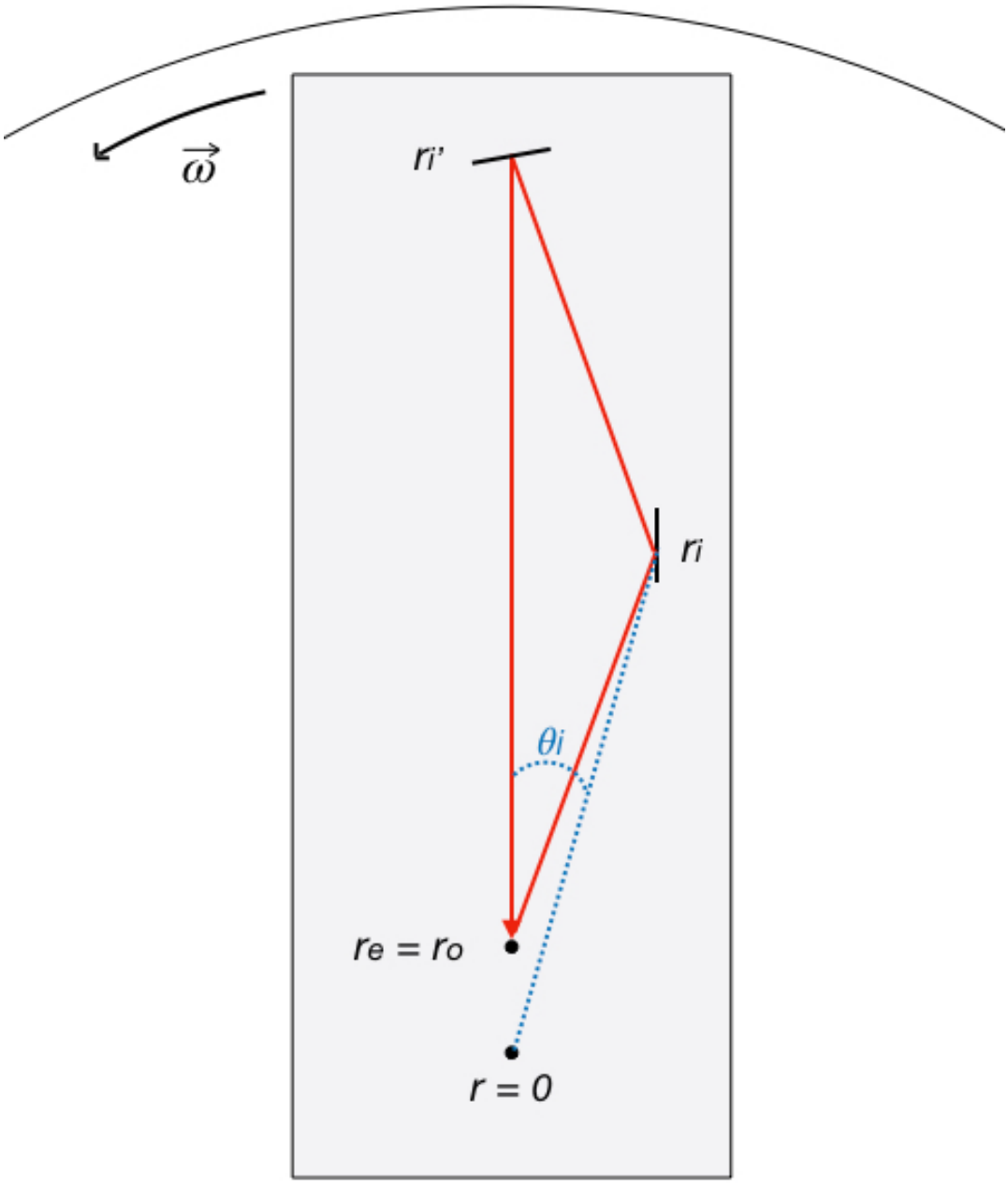

Figure 14.: A beam of light (in red solid lines) travels a closed path within the centrifuge's arm (greyed rectangle). The centrifuge's arm width and the angle θ_i have been drawn large for clarity only.

Therefore, the total phase acquired by the helicity states is:

$$\Psi = \theta_i \frac{r_{i'} + r_e}{r_{i'} - r_e} \frac{(r_{i'} + r_e)\,\omega(t_i) - r_{i'}\,\omega(t_{i'}) - r_e\,\omega(t_e)}{c} + O(\theta_i^2), \tag{237}$$

where it has been used that $r_i = \frac{r_{i'}+r_e}{2} + O(\theta_i^2)$. This phase is small, in particular due to the little change in angular velocity $\omega(t)$ experienced by the centrifuge during the photons' propagation between the different observers and mirrors. However, one can let the light go through the loop again and again, until it picks up a measurable phase. In the uniformly accelerating case, the total phase vanishes up to first order in θ_i, as can be seen using (231). According to the results of [95, 96] these phases should be gauge-independent. However we can see from (228) that there would be no Wigner rotation for the choice of a frame with $f = 0$, which seems to contradict the claim, here again, since with the other frame choice we have made we obtained the result (237). The scheme we are proposing thus offers a way to test this prediction, together with providing a way to measure the effect of (non uniformly) accelerating observers on quantum states.

9.4 DISCUSSION ON RECENT EXPERIMENTAL RESULTS

In the experiment [43], the quantum state that probed the effects of the centrifuge's acceleration was a rotationally invariant polarisation entangled Bell state $|\Psi^-\rangle = (|H_1V_2\rangle - |V_1H_2\rangle)/\sqrt{2}$. This state is rewritten in terms of helicities as $|\Psi^-\rangle = (|+_1-_2\rangle - |-_1+_2\rangle)/\sqrt{2}$. Such a state prevents the effects described in this chapter: using this state, Wigner phase factors cancel due to paired particles with same momentum but opposite helicities [64, 63]:

$$\hat{U}|\Psi^-\rangle = \frac{1}{\sqrt{2}}\left(e^{i\Psi}|+_1\rangle \otimes e^{-i\Psi}|-_2\rangle - e^{-i\Psi}|-_1\rangle \otimes e^{i\Psi}|+_2\rangle\right) = |\Psi^-\rangle \quad (238)$$

Such invariant states are therefore recommended for quantum tasks such as quantum cryptography or quantum teleportation. In order to probe relativistic effects on quantum systems we however need to use other kinds of quantum states. An interesting state to select for this purpose would be one

of the other Bell states of the form $|\Phi^{\pm}\rangle = (|+_1+_2\rangle \pm |-_1-_2\rangle)/\sqrt{2}$. Such states would cumulate two Wigner phases after propagation:

$$\hat{U}|\Phi^{\pm}\rangle = \frac{1}{\sqrt{2}}\left(e^{i\Psi}|+_1\rangle \otimes e^{i\Psi}|+_2\rangle - e^{-i\Psi}|-_1\rangle \otimes e^{-i\Psi}|-_2\rangle\right). \tag{239}$$

That means that the phase difference in the superposition is actually of 4 times the Wigner phase. One can further increase this factor by using a N particles GHZ state $|\text{GHZ}\rangle = |+\rangle^{\otimes N} + |-\rangle^{\otimes N}$, which will give a phase difference of $2N\Psi$.

Still, the use of another kind of quantum state in the experiment [43] would have probably not been enough to find a measurable effect. The Wigner phases we found have small values, and they would require much larger path lengths together with non uniform acceleration of the centrifuge in order to become measurable. In our study, the uniformly accelerating case probed in [43] seems to give only a gauge phase, which is independent on the acceleration of the observers and therefore not relevant for the present study. The smallness of the Wigner phases we found confirms the resilience of entangled states of light under acceleration observed in [43]. Yet, our theoretical work offers predictions that haven't been rulled out by the results of this experiment.

9.5 CONCLUSION

In this chapter, we first derived the general yet cumbersome expression for the Wigner rotation of the light's polarisation vector as seen by accelerating observers. We have obtained explicit expressions for the Wigner phases acquired by momentum-helicity states of photons after propagation between accelerating observers in a centrifuge. We found that photons propagating radially (that is, perpendicularly to the centrifuge's angular velocity) cannot pick up any Wigner phase related to the acceleration of the centrifuge. For photons with angular momentum, we found a Wigner phase which does

depend on acceleration but only for non uniformly accelerating observers. Namely, the effect we found appears through changes of acceleration only.

We have then provided the theory for a scheme designed to measure this effect. In this scheme, the polarised light beam follows a closed path, for which previous theoretical works [95, 96] predict the gauge invariance of the total Wigner phase acquired along the loop. The experiment we propose here gives a way to check this result. But most importantly, it would enable to probe the changes acceleration induces on quantum states of light. Such closed path schemes can be implemented in the form of a cavity experiment where the light propagates for a longer time in order for the initially small phase to grow larger. Although the phase would be measurable in such schemes, the smallness of the Wigner phases we found along short distances seems to indicate in general a strong resilience of photons' polarisation states under acceleration. Quantum technologies based on such quantum features should therefore be robust to acceleration as long as there is no cumulative effect coming into play.

Part V.

Conclusion and annexes

10

CONCLUSION

In this thesis we have studied and given predictions for relativistic effects induced on quantum states. We have focused on bosonic systems such as phonons, scalar frequency modes of light, and spin-1 polarised photons. We have investigated relativistic effects arising from both the propagation of these quantum fields and the motion of the observers measuring them in curved spacetimes. We worked in a variety of spacetimes such as the Minkowski, gravitational waves, Schwarzschild and Kerr spacetimes. Within each of these spacetimes, we have considered several type of observers, such as static, circularly geodesic and centrifuged observers. The various configurations lead to different effects that can in principle be probed using current or near-future technologies.

Phonon creation by gravitational waves in a Bose-Einstein condensate is the first relativistic effect on a quantum system that we thoroughly discussed in this thesis, in part II. We began by reviewing the theory developed in the initial proposal [41] in order to then refine it and derive new results. We obtained the Bogolyubov transformation for a discrete step in the metric for an arbitrary boundary condition of the cavity. We then reviewed the validity of such a discrete transformation by checking if it would lead to a leak of the quantum field of the cavity, and we found that to the order of the computation no such problem arises. Working in the symmetric case (with the center of the cavity unaltered by the gravitational wave), we derived the explicit Bogolyubov coefficients for the phonon field under the presence of a

continuous gravitational wave, including the contribution from the change in the mode frequencies that was neglected in the earlier derivation. We then characterised four different resonance scenarios, three of them for the first time, where, in each, different pairs of modes resonate with the gravitational wave either by a mode-mixing or a particle creation resonance.

In the following chapter we looked at the influence of noise in the Bose-Einstein condensate where the effect induced by the gravitational wave is to be measured. We have obtained the Bogolyubov transformation induced on the phonon field due to the shaking of the cavity where the Bose-Einstein condensate is trapped. Provided with the noise spectrum obtained experimentally, one would be able to plug it in the latter Bogolyubov transformation and therefore characterise the influence of such noise on the phonon field and thus on the measurement outcome. Then, we carried out the computation for the discrete Bogolyubov transformation due to both a discrete change in the metric and a displacement of the cavity caused by noise. We could then characterise up to which point such a noisy displacement competes with the gravitational wave's distortion of the metric. Another noise study we regarded was thermal noise. In a simplified model, we analysed how two phonon modes become altered in the presence of thermal noise, whether during the passage of a gravitational wave or not. All these studies refined the model initially proposed in [41] in order to make the theory more acute and to characterise undesirable effects that will inevitably show up in the actual experiment.

In the next part of the thesis, part III, we developed the theory for quantum measurements of spacetime parameters using satellites around the Earth within quantum communcation schemes. We followed the theory initially developed in [34, 35], here again in order to refine and extend it. The first chapter of this part of the thesis accounts for the new results we have published in [1]. We first extended the theory from [34, 35] developed in the Schwarzschild spacetime to a Kerr spacetime picture, that is we took into account the Earth's rotation about its axis. We were therefore able

to provide an estimation of the precision bound one can attain on a quantum measurement of the Earth's angular velocity. Another improvement from the earlier computations was to take into account special relativistic effects. The purely gravitational frequency shift turns out to compete with the Doppler shift caused by the observers' motion. This observation lead to the finding of a special family of orbits on which gravitational and special relativistic effects exactly compensate. For quantum metrology purposes, schemes with satellites orbiting at such altitudes should be proscribed since they would yield very low precisions on the measurement of spacetime parameters. However, such orbits provide communication channels with Earth that are free from any relativistic noise, they are therefore very relevant for quantum tasks such as quantum communication, quantum key distribution or quantum teleportation. A last feature that we introduced in this chapter is the transposition of the already described Earth to satellite scheme to a satellite to satellite scheme. In such schemes, we found results close to the previous ones, but which are free from the problematic atmospheric noise present in the Earth to satellite case.

The following chapter went back to the Schwarzschild picture, but generalising the schemes considered in [34, 35]. In this chapter, the observer was assumed to stand anywhere on Earth and was allowed to communicate with any satellite circularly orbiting around the Earth. Furthermore, two different families of schemes were considered: the first one, the link communications, includes uplinks studied in the previous chapter, but also downlinks where optical pulses are sent from the satellites towards a station on Earth. The other family of schemes we considered are reflection schemes, where the photons emitted from Earth are reflected by a passing satellite equipped with a mirror. The photons received back on Earth then encode parameters from the velocity of the satellite, which itself encodes physical parameters such as the mass of the Earth and the altitude of the orbit. We then performed metrology techniques on some chosen configurations of these schemes and we found results much improved compared

to earlier ones [35, 1]. Our theoretical results now even outbound the current state of the art precision on the Schwarzschild radius that was obtained through classical measurements. We also demonstrated that in such configurations quantum communications and therefore other quantum tasks such as quantum key distribution protocols would be extremely noisy due to relativistic effects if these are not properly corrected. The results of this chapter showed why relativity and quantum physics are relevant to each other for quantum experiments using satellites: we found that relativistic effects cannot be neglected in general in quantum communication. We also discovered a way to outperform classical measurements of physical quantities like the mass of the Earth by using quantum states. This is a very exciting result that should renew the interest of taking advantage of both quantum and relativistic features in order to improve the current technology.

In the previous parts of the thesis we mostly focused on scalar fields, whether with phonon fields or frequency modes of photons. In part IV, we shifted our attention to the spin degree of freedom of photons. We first looked at schemes similar to the reflecting satellite schemes developed in the previous chapter in the Schwarzschild spacetime. Using communication channels linking Earth to a satellite, with optical pulses propagating back to the emission point on Earth through satellite and Earth station nodes, we found that helicity states of photons acquire Wigner phases in such closed paths. This result questions previous claims which can be found in the litterature [95, 96]. Also, the Wigner phases we found have larger values than, to our knowledge, what can be found in the litterature for other schemes. We showed that a measurement of general relativistic effects on spin features of light is at reach with current technology in space.

The subsequent chapter applies the same theoretical framework, but within a centrifuge in Minkowski spactime. The motivation for this research was the measurement of the invariance of polarisation entangled states of light as measured by accelerating observers made in [43]. What we found is that there are many reasons to account for this absence of observed effect. The

first one is the use of a rotationally invariant polarisation entangled Bell state as a quantum probe. We showed how such state cannot acquire any Wigner phase due to acceleration. Considering another quantum state that is not invariant under the effect at play we found further results: there is no effect for a light beam propagating radially in the centrifuge. There is also no effect when the centrifuge accelerates uniformly, which was the case in the experiment [43]. In other words, to find an effect one needs to shoot photons with some angular momentum in a non-uniformly accelerating centrifuge. However, even so, the amplitude of the Wigner phase we predicted is rather small. In order to find a measurable effect, we suggested to implement a cavity scheme where the light propagates within a path loop for a finite amount of time. We predict that by following such directions one would be able to measure a relativistic effect due to acceleration on the quantum state of polarised photons.

In this thesis we developed the theory for new experimental proposals and we improved existing ones. We refined the theory for the phononic gravitational wave detector by taking into account the changes in the frequency modes, by considering new resonances and by checking the effects of both sismic and thermal noise. We then extended a theory for quantum communications and quantum metrology with satellites by including the Earth's rotation and special relativistic effects. We then proposed new schemes such as satellite to satellite communications, and satellites retroreflecting towards the Earth. We found configurations for which quantum measurement techniques outbound optimal classical results. Finally, we developed a theory to study relativistic effects on helicity states of photons, due to acceleration in a centrifuge and due to the curved spacetime surrounding our planet. All these studies combine relativistic effects and quantum features, and they have no classical equivalent (classical can here mean either non relativistic or non quantum). Therefore, experiments based on the effects described in this thesis should lead to new insights in the interplay between the quantum and the relativity theories.

A

GENERAL FREQUENCY SHIFTS

A.1 IN KERR SPACETIME

In chapter 6, in order to keep workable formulas we designed a scheme with radial quantum optical communication channels restricted to the equatorial plane of the Earth. Here we derive frequency shift formulas that relax these constraints.

A.1.1 *Earth-satellite schemes*

In this section, we still consider the satellite to be confined within the equatorial plane in order to keep working with a circular geodesic orbit [110]. However, we consider an arbitrary position for the station on Earth, which means that we do not restrict the communication to radial channels anymore and this provides a much wider range of possible configurations. Furthermore, instead of considering only uplinks from the Earth to the satellite we now leave free the choice of either up or down link communication channels. The 4-velocity of the observer on Earth is given in (21), the 4-velocity of the equatorial satellite in (22), and the general null vector in Kerr spacetime was displayed in (23). From that we can follow the same procedure as in section 6.2 in order to derive the frequency shift $f = \Omega_B/\Omega_A$ for this config-

uration where photons are exchanged between an almost arbitrary station on Earth (we need a line of sight!) and a circular equatorial geodesic:

$$f = \frac{1+\epsilon_\zeta \frac{a-l_\phi}{R_s}\sqrt{\frac{M}{R_s}}}{1-\frac{a\,l_\phi\,M}{I}} \sqrt{\frac{1-\frac{a^2M^2(a^2+R_E^2)\sin^2\theta}{I^2}-\frac{2MR_E(I^2-a^2M\sin^2\theta)^2}{I^2(R_E^2+a^2\cos^2\theta)}}{1-\frac{3M}{R_s}+2\epsilon_\zeta\frac{a}{R_s}\sqrt{\frac{M}{R_s}}}} \tag{240}$$

where we used that the Earth's longitudinal coordinate velocity $\zeta_0 = aM/I$, with I the Earth's moment of inertia about its axis.

A.1.2 *Satellite-satellite schemes*

In the satellite to satellite scheme, we here still consider the geodesic circularly orbiting satellites confined within the equatorial plane. However, we relax the radial assumption to consider any possible trajectory for the light rays between the two communicating satellites. The frequency shift $f_{\text{sat}} = \Omega_B/\Omega_C$ in Kerr spacetime between two of such satellites reads:

$$f_{\text{sat}} = \frac{1+\epsilon_B\frac{a-l_\phi}{r_B}\sqrt{\frac{M}{r_B}}}{1+\epsilon_C\frac{a-l_\phi}{r_C}\sqrt{\frac{M}{r_C}}}\sqrt{\frac{1-\frac{3M}{r_C}+2\epsilon_C\frac{a}{r_C}\sqrt{\frac{M}{r_C}}}{1-\frac{3M}{r_B}+2\epsilon_B\frac{a}{r_B}\sqrt{\frac{M}{r_B}}}}. \tag{241}$$

We can note that the non radial contribution is very simple: the light's azimuthal angular momentum l_ϕ is simply subtracted to the specific angular momentum of the Earth in the first quotient term.

A.2 IN SCHWARZSCHILD SPACETIME

In the Schwarzschild picture, where the Earth is static, we can relax most of the assumptions: we here consider an observer on Earth standing anywhere on the planet that exchanges photons with the satellite in any direction, provided that there is a line of sight. The satellites are again in geodesic circular orbit but here in any of the planes containing the center of the Earth. Because of the spherical symmetry of the Schwarzschild spacetime, any of these planes are equivalent.

A.2.1 *Earth-satellite scheme*

In this general Schwarzschild picture, the frequency shift between an observer on Earth and an observer comoving with the orbiting satellite reads:

$$f = \left(1 - \epsilon_\zeta \frac{l_\phi}{R_s}\sqrt{\frac{M}{R_s}}\frac{\sin\alpha}{\sin^2\theta_s} - \epsilon_\theta\,\epsilon_\omega\sqrt{\frac{M(\kappa - l_\phi^2\cot^2\theta_s)}{R_s^3}}\sqrt{1 - \frac{\sin^2\alpha}{\sin^2\theta_s}}\right) f_{\text{rad}}. \quad (242)$$

We labeled $f_{\text{rad}} = \sqrt{\frac{1-\frac{2M}{R_E}}{1-\frac{3M}{R_s}}}$ the frequency shift for radial rays that was already given in (156). Notice that the angular contribution scales in $\sqrt{M/R_s}$, i.e. when the angular parameters l_ϕ and κ are not negligible then the perturbative terms in the parenthesis are the largest contributions to the shift.

A.2.2 *Satellite-satellite schemes*

Here each of the two satellites follow a geodesic circular path. The frequency shift between the two observers then reads:

$$f_{\text{sat}} = \frac{1 - \epsilon_{\zeta 2}\frac{l_\phi}{R_{s2}}\sqrt{\frac{M}{R_{s2}}}\frac{\sin\alpha_2}{\sin^2\theta_{s2}} - \epsilon_\theta\,\epsilon_{\omega 2}\sqrt{\frac{M(\kappa - l_\phi^2\cot^2\theta_{s2})}{R_{s2}^3}}\sqrt{1 - \frac{\sin^2\alpha_2}{\sin^2\theta_{s2}}}}{1 - \epsilon_{\zeta 1}\frac{l_\phi}{R_{s1}}\sqrt{\frac{M}{R_{s1}}}\frac{\sin\alpha_1}{\sin^2\theta_{s1}} - \epsilon_\theta\,\epsilon_{\omega 1}\sqrt{\frac{M(\kappa - l_\phi^2\cot^2\theta_{s1})}{R_{s1}^3}}\sqrt{1 - \frac{\sin^2\alpha_1}{\sin^2\theta_{s1}}}} f_{\underset{\text{rad}}{\text{sat}}}, \quad (243)$$

with the radial shift $f_{\underset{\text{rad}}{\text{sat}}} = \sqrt{\frac{1-\frac{3M}{R_{s1}}}{1-\frac{3M}{R_{s2}}}}$, which is the Schwarzschild limit of the radial frequency shift in Kerr spacetime displayed in (168).

B

ADAPTED TETRAD FOR STATIC OBSERVERS IN SCHWARZSCHILD SPACETIME

B.1 GENERAL TETRAD

We give here the general first and second triad components for a static observer (12), adapted to an arbitrary null vector (15). Using the expressions of the zeroth $e_{\hat{0}} = v_E$ and third (211) tetrad components, together with the orthonormalisation relations, we have $e^t_{\hat{1}} = e^t_{\hat{2}} = 0$ and:

$$e^r_{\hat{1}} = -\eta_1 \epsilon_r f(r) \sin\theta \frac{l_\phi B - \eta_2 \epsilon_\theta \sqrt{1 - f(r)\frac{\kappa + l_\phi^2}{r^2}} \sqrt{\frac{\kappa - l_\phi^2 \cot^2\theta}{r^2}} \sqrt{Q - r^2 B^2 \sin^2\theta}}{Q}, \tag{244a}$$

$$e^\theta_{\hat{1}} = -\eta_1 \eta_2 \frac{\sqrt{Q - r^2 B^2 \sin^2\theta}}{r \sin\theta}, \tag{244b}$$

$$e^\phi_{\hat{1}} = \eta_1 \frac{rB \sin^2\theta \sqrt{1 - f(r)\frac{\kappa + l_\phi^2}{r^2}} + \eta_2 \epsilon_\theta f(r) \frac{l_\phi}{r} \sqrt{\frac{\kappa - l_\phi^2 \cot^2\theta}{r^2}} \sqrt{Q - r^2 B^2 \sin^2\theta}}{r \sin\theta\, Q}, \tag{244c}$$

$$e^r_{\hat{2}} = -\epsilon_r f(r) \frac{\epsilon_\theta rB \sin^2\theta \sqrt{1 - f(r)\frac{\kappa + l_\phi^2}{r^2}} \sqrt{\frac{\kappa - l_\phi^2 \cot^2\theta}{r^2}} + \eta_2 \frac{l_\phi}{r} \sqrt{Q - r^2 B^2 \sin^2\theta}}{Q}, \tag{244d}$$

$$e^\phi_{\hat{2}} = \frac{-\epsilon_\theta rBf(r) \frac{l_\phi}{r} \sqrt{\frac{\kappa - l_\phi^2 \cot^2\theta}{r^2}} + \eta_2 \sqrt{1 - f(r)\frac{\kappa + l_\phi^2}{r^2}} \sqrt{Q - r^2 B^2 \sin^2\theta}}{r\, Q}, \tag{244e}$$

where we defined $Q = \left(1 - f(r)\frac{\kappa + l_\phi^2}{r^2}\right) \sin^2\theta + \frac{l_\phi^2}{r^2} f(r)$ for compactness, and we denoted again $f(r) = 1 - \frac{2M}{r}$. The quantity $B = e^\theta_{\hat{2}}$ is the gauge component of the tetrad. Like the gauge signs $\eta_1 = \pm 1$ and $\eta_2 = \pm 1$, the tetrad component B is arbitrary, provided that it is of dimension $[r^{-1}]$ and fulfils $Q - r^2 B^2 \sin^2\theta > 0$. These three parameters encode all the gauge from the freedom of choice of our adapted frame.

B.2 CHOSEN TETRAD

In 8.2.1, we focused on light rays with vanishing azimuthal angular momentum l_ϕ, and we fixed the gauge parameters $B = \frac{1}{r}\sqrt{1-\frac{\kappa}{r^2}}$ and $\eta_1 = \eta_2 = +1$ in order to simplify the expression of the Wigner rotation. Plugging these values in (244), we obtain the triad:

$$e_{\hat{1}} = \epsilon_r\,\epsilon_\theta\,\frac{\kappa}{r^2}\sqrt{\frac{2M}{r}}\,\frac{f(r)}{\sqrt{1-f(r)\frac{\kappa}{r^2}}}\,\partial_r - \frac{1}{r}\sqrt{\frac{2M\kappa}{r^3}}\,\partial_\theta + \frac{\csc\theta}{r}\,\frac{\sqrt{1-\frac{\kappa}{r^2}}}{\sqrt{1-f(r)\frac{\kappa}{r^2}}}\,\partial_\phi, \tag{245a}$$

$$e_{\hat{2}} = -\epsilon_r\,\epsilon_\theta f(r)\,\frac{\sqrt{\frac{\kappa}{r^2}}\sqrt{1-\frac{\kappa}{r^2}}}{\sqrt{1-f(r)\frac{\kappa}{r^2}}}\,\partial_r + \frac{1}{r}\sqrt{1-\frac{\kappa}{r^2}}\,\partial_\theta + \frac{\csc\theta}{r}\,\frac{\sqrt{\frac{2M\kappa}{r^3}}}{\sqrt{1-f(r)\frac{\kappa}{r^2}}}\,\partial_\phi, \tag{245b}$$

$$e_{\hat{3}} = \sqrt{f(r)}\left(\epsilon_r\sqrt{1-f(r)\frac{\kappa}{r^2}}\,\partial_r + \frac{\epsilon_\theta}{r}\sqrt{\frac{\kappa}{r^2}}\,\partial_\theta\right). \tag{245c}$$

C

ADAPTED TETRAD FOR CENTRIFUGED OBSERVERS IN MINKOWSKI SPACETIME

C.1 GENERAL TETRAD

We display here the expression for the triad of an accelerating observer in a centrifuge, as obtained from the orthonormalisation relations after the adapting procedure. The adapted $\boldsymbol{e}_{\hat{3}} = \frac{\boldsymbol{k}}{k^{\hat{0}}} - \boldsymbol{e}_{\hat{0}}$ is obtained with $\boldsymbol{e}_{\hat{0}} = \boldsymbol{v}$ given in (217). The gauge quantities are again the triad component $e_{\hat{2}}^{\ \theta} = B(t,r,\theta)$ and the arbitrary signs $\eta_1 = \pm 1$ and $\eta_2 = \pm 1$. The triad reads:

$$\boldsymbol{e}_{\hat{1}} = -\eta_1\eta_2\eta_r \frac{r\,\omega(t)\,\partial_t + \eta_r \frac{r\,\omega(t)-\frac{\kappa}{r}}{\sqrt{1-\frac{\kappa^2}{r^2}}}\,\partial_r + \frac{1}{r}\,\partial_\theta}{1-\kappa\,\omega(t)} \sqrt{Q} + \eta_1\, rB \frac{1-\kappa\,\omega(t)}{\sqrt{1-\frac{\kappa^2}{r^2}}}\,\partial_z \tag{246a}$$

$$\boldsymbol{e}_{\hat{2}} = r^2\omega(t)B\,\partial_t + \eta_r\, rB \frac{r\,\omega(t)-\frac{\kappa}{r}}{\sqrt{1-\frac{\kappa^2}{r^2}}}\,\partial_r + B\,\partial_\theta + \eta_2\eta_r \sqrt{\frac{Q}{1-\frac{\kappa^2}{r^2}}}\,\partial_z \tag{246b}$$

$$\boldsymbol{e}_{\hat{3}} = \frac{-\gamma(t,r)\,r\,\omega(t)\left(r\,\omega(t)-\frac{\kappa}{r}\right)\,\partial_t + \eta_r \frac{\sqrt{1-\frac{\kappa^2}{r^2}}}{\gamma(t,r)}\,\partial_r - \gamma(t,r)\frac{r\,\omega(t)-\frac{\kappa}{r}}{r}\,\partial_\theta}{1-\kappa\,\omega(t)}, \tag{246c}$$

where we dropped the (t,r,θ) dependence of the gauge term B and we introduced $Q = 1 - \frac{\kappa^2}{r^2} - r^2B^2\left(1-\kappa\,\omega(t)\right)^2$ in order to ease the reading.

C.2 WIGNER ROTATION FORMULAS

We give here the general formula for the Wigner rotation $\tilde{\Psi}$ using the general tetrad adapted to a centrifuged observer (246):

$$\tilde{\Psi} = -\eta_1\eta_2 \frac{B(t,r,\theta)\left(\frac{1-2\frac{\kappa^2}{r^2}}{\sqrt{1-\frac{\kappa^2}{r^2}}} - \eta_r \frac{\kappa\, r\, \omega'(t)}{1-\kappa\,\omega(t)}\right) + \eta_r r \frac{\partial B}{\partial t} + r\sqrt{1-\frac{\kappa^2}{r^2}}\frac{\partial B}{\partial r} + \eta_r \frac{\kappa}{r}\frac{\partial B}{\partial \theta}}{\gamma(t,r)\sqrt{1-\frac{\kappa^2}{r^2} - (1-\kappa\,\omega(t))^2\, r^2 B(t,r,\theta)^2}}. \quad (247)$$

To remove the radial part of the phase, we can specify the following constraint on the free tetrad component: $B(t,r,\theta) = f(\theta)/r$, with f a differentiable function verifying $|f(\theta)| < 1$ for all θ. The Wigner rotation then slightly simplifies to:

$$\tilde{\Psi} = \frac{\eta_1\eta_2}{r} \frac{\left(\frac{\frac{\kappa}{r}}{\sqrt{1-\frac{\kappa^2}{r^2}}} + \eta_r \frac{r^2\,\omega'(t)}{1-\kappa\,\omega(t)}\right) f(\theta) - \eta_r f'(\theta)}{\gamma(t,r)\sqrt{1-\frac{\kappa^2}{r^2} - f(\theta)^2\,(1-\kappa\,\omega(t))^2}}\,\frac{\kappa}{r}. \quad (248)$$

BIBLIOGRAPHY

[1] Jan Kohlrus, David Edward Bruschi, Jorma Louko, and Ivette Fuentes. Quantum communications and quantum metrology in the spacetime of a rotating planet. *EPJ Quantum Technology*, 4(1):7, Apr 2017.

[2] Jan Kohlrus, David Edward Bruschi, and Ivette Fuentes. Quantum metrology of spacetime parameters of the Earth beating classical precision. arXiv:1811.07322, 2018.

[3] Jan Kohlrus, Jorma Louko, Ivette Fuentes, and David Edward Bruschi. Wigner phase of photonic helicity states in the spacetime of the Earth. arXiv:1810.10502, 2018.

[4] Carlos Sabín, Jan Kohlrus, David Edward Bruschi, and Ivette Fuentes. Thermal noise in bec-phononic gravitational wave detectors. *EPJ Quantum Technology*, 3(1):8, May 2016.

[5] Dominik Safranek, Jan Kohlrus, David Edward Bruschi, Antony R. Lee, and Ivette Fuentes. Ultimate precision: Gaussian parameter estimation in flat and curved spacetime. arXiv:1511.03905, 2015.

[6] A. Einstein. Die Grundlage der allgemeinen Relativitätstheorie. *Annalen der Physik*, 354(7):769–822, 1916.

[7] Sir F.W. Dyson, A. S. Eddington, and Mr. C. Davidson. A determination of the deflection of light by the Sun's gravitational field, from observations made at the total eclipse of May 29, 1919. *Philosophical Transactions of the Royal Society of London A: Mathematical, Physical and Engineering Sciences*, 220(571-581):291–333, 1920.

[8] B. P. Abbott *et al.* (LIGO Scientific Collaboration and Virgo Collaboration). Observation of gravitational waves from a binary black hole merger. *Phys. Rev. Lett.*, 116:061102, Feb 2016.

[9] Max Planck. Zur Theorie des Gesetzes der Energieverteilung im Normalspectrum. *Verhandlungen der Deutschen Physikalischen Gesellschaft*, 2:237, 1900.

[10] C. J. Davisson and L. H. Germer. Reflection of electrons by a crystal of nickel. *Proceedings of the National Academy of Science*, 14:317–322, April 1928.

[11] Alain Aspect, Philippe Grangier, and Gérard Roger. Experimental tests of realistic local theories via Bell's theorem. *Phys. Rev. Lett.*, 47:460–463, Aug 1981.

[12] Alain Aspect, Jean Dalibard, and Gérard Roger. Experimental test of Bell's inequalities using time-varying analyzers. *Phys. Rev. Lett.*, 49:1804–1807, Dec 1982.

[13] J. Bailey, K. Borer, F. Combley, H. Drumm, F. Krienen, F. Lange, E. Picasso, W. von Ruden, F. J. M. Farley, J. H. Field, W. Flegel, and P. M. Hattersley. Measurements of relativistic time dilatation for positive and negative muons in a circular orbit. *Nature*, 268:301–305, July 1977.

[14] Pekka Pyykkö. Relativistic effects in chemistry: More common than you thought. *Annual Review of Physical Chemistry*, 63(1):45–64, 2012. PMID: 22404585.

[15] Peter Asenbaum, Chris Overstreet, Tim Kovachy, Daniel D. Brown, Jason M. Hogan, and Mark A. Kasevich. Phase shift in an atom interferometer due to spacetime curvature across its wave function. *Phys. Rev. Lett.*, 118:183602, May 2017.

[16] G. Rosi, G. D'Amico, L. Cacciapuoti, F. Sorrentino, M. Prevedelli, M. Zych, Č. Brukner, and G. M. Tino. Quantum test of the equiva-

lence principle for atoms in coherent superposition of internal energy states. *Nature Communications*, 8:15529 EP –, 06 2017.

[17] C. W. Chou, D. B. Hume, T. Rosenband, and D. J. Wineland. Optical clocks and relativity. *Science*, 329(5999):1630–1633, 2010.

[18] T. Kovachy, P. Asenbaum, C. Overstreet, C. A. Donnelly, S. M. Dickerson, A. Sugarbaker, J. M. Hogan, and M. A. Kasevich. Quantum superposition at the half-metre scale. *Nature*, 528:530 EP –, 12 2015.

[19] Stefan Gerlich, Sandra Eibenberger, Mathias Tomandl, Stefan Nimmrichter, Klaus Hornberger, Paul J. Fagan, Jens Tüxen, Marcel Mayor, and Markus Arndt. Quantum interference of large organic molecules. *Nature Communications*, 2:263 EP –, 04 2011.

[20] Richard Howl, Lucia Hackermüller, David Edward Bruschi, and Ivette Fuentes. Gravity in the quantum lab. *Advances in Physics: X*, 3(1):1383184, 2018.

[21] David Rideout, Thomas Jennewein, Giovanni Amelino-Camelia, Tommaso F Demarie, Brendon L Higgins, Achim Kempf, Adrian Kent, Raymond Laflamme, Xian Ma, Robert B Mann, Eduardo Martín-Martínez, Nicolas C Menicucci, John Moffat, Christoph Simon, Rafael Sorkin, Lee Smolin, and Daniel R Terno. Fundamental quantum optics experiments conceivable with satellites—reaching relativistic distances and velocities. *Classical and Quantum Gravity*, 29(22):224011, 2012.

[22] Giuseppe Vallone, Davide Bacco, Daniele Dequal, Simone Gaiarin, Vincenza Luceri, Giuseppe Bianco, and Paolo Villoresi. Experimental satellite quantum communications. *Phys. Rev. Lett.*, 115:040502, Jul 2015.

[23] Giuseppe Vallone, Daniele Dequal, Marco Tomasin, Francesco Vedovato, Matteo Schiavon, Vincenza Luceri, Giuseppe Bianco, and

Paolo Villoresi. Interference at the single photon level along satellite-ground channels. *Phys. Rev. Lett.*, 116:253601, Jun 2016.

[24] Daniele Dequal, Giuseppe Vallone, Davide Bacco, Simone Gaiarin, Vincenza Luceri, Giuseppe Bianco, and Paolo Villoresi. Experimental single-photon exchange along a space link of 7000 km. *Phys. Rev. A*, 93:010301, Jan 2016.

[25] Luca Calderaro, Costantino Agnesi, Daniele Dequal, Francesco Vedovato, Matteo Schiavon, Alberto Santamato, Vincenza Luceri, Giuseppe Bianco, Giuseppe Vallone, and Paolo Villoresi. Towards quantum communication from global navigation satellite system. *Quantum Science and Technology*, 4(1):015012, dec 2018.

[26] Kevin Günthner, Imran Khan, Dominique Elser, Birgit Stiller, Ömer Bayraktar, Christian R. Müller, Karen Saucke, Daniel Tröndle, Frank Heine, Stefan Seel, Peter Greulich, Herwig Zech, Björn Gütlich, Sabine Philipp-May, Christoph Marquardt, and Gerd Leuchs. Quantum-limited measurements of optical signals from a geostationary satellite. *Optica*, 4(6):611–616, Jun 2017.

[27] Zhongkan Tang, Rakhitha Chandrasekara, Yue Chuan Tan, Cliff Cheng, Luo Sha, Goh Cher Hiang, Daniel K. L. Oi, and Alexander Ling. Generation and analysis of correlated pairs of photons aboard a nanosatellite. *Phys. Rev. Applied*, 5:054022, May 2016.

[28] Rakhitha C. M. R. B. Chandrasekara, Robert Bedington, Xueliang Bai, Karthik Ilangovan, Yau Yong Sean, Denis Naughton, Simon Barraclough, Douglas Griffin, Russell Boyce, and Alexander Ling. Demonstrating miniaturised, entangled photon-pair sources on board nano satellites to enable future QKD missions. Oct 2017.

[29] C. Bonato, A. Tomaello, V. Da Deppo, G. Naletto, and P. Villoresi. Feasibility of satellite quantum key distribution. *New Journal of Physics*, 11(4):045017, 2009.

[30] Robert Bedington, Juan Miguel Arrazola, and Alexander Ling. Progress in satellite quantum key distribution. *npj Quantum Information*, 3(1):30, 2017.

[31] Sheng-Kai Liao, Wen-Qi Cai, Wei-Yue Liu, Liang Zhang, Yang Li, Ji-Gang Ren, Juan Yin, Qi Shen, Yuan Cao, Zheng-Ping Li, Feng-Zhi Li, Xia-Wei Chen, Li-Hua Sun, Jian-Jun Jia, Jin-Cai Wu, Xiao-Jun Jiang, Jian-Feng Wang, Yong-Mei Huang, Qiang Wang, Yi-Lin Zhou, Lei Deng, Tao Xi, Lu Ma, Tai Hu, Qiang Zhang, Yu-Ao Chen, Nai-Le Liu, Xiang-Bin Wang, Zhen-Cai Zhu, Chao-Yang Lu, Rong Shu, Cheng-Zhi Peng, Jian-Yu Wang, and Jian-Wei Pan. Satellite-to-ground quantum key distribution. *Nature*, 549:43 EP –, 08 2017.

[32] Juan Yin, Yuan Cao, Yu-Huai Li, Sheng-Kai Liao, Liang Zhang, Ji-Gang Ren, Wen-Qi Cai, Wei-Yue Liu, Bo Li, Hui Dai, Guang-Bing Li, Qi-Ming Lu, Yun-Hong Gong, Yu Xu, Shuang-Lin Li, Feng-Zhi Li, Ya-Yun Yin, Zi-Qing Jiang, Ming Li, Jian-Jun Jia, Ge Ren, Dong He, Yi-Lin Zhou, Xiao-Xiang Zhang, Na Wang, Xiang Chang, Zhen-Cai Zhu, Nai-Le Liu, Yu-Ao Chen, Chao-Yang Lu, Rong Shu, Cheng-Zhi Peng, Jian-Yu Wang, and Jian-Wei Pan. Satellite-based entanglement distribution over 1200 kilometers. *Science*, 356(6343):1140–1144, 2017.

[33] Sheng-Kai Liao, Wen-Qi Cai, Johannes Handsteiner, Bo Liu, Juan Yin, Liang Zhang, Dominik Rauch, Matthias Fink, Ji-Gang Ren, Wei-Yue Liu, Yang Li, Qi Shen, Yuan Cao, Feng-Zhi Li, Jian-Feng Wang, Yong-Mei Huang, Lei Deng, Tao Xi, Lu Ma, Tai Hu, Li Li, Nai-Le Liu, Franz Koidl, Peiyuan Wang, Yu-Ao Chen, Xiang-Bin Wang, Michael Steindorfer, Georg Kirchner, Chao-Yang Lu, Rong Shu, Rupert Ursin, Thomas Scheidl, Cheng-Zhi Peng, Jian-Yu Wang, Anton Zeilinger, and Jian-Wei Pan. Satellite-relayed intercontinental quantum network. *Phys. Rev. Lett.*, 120:030501, Jan 2018.

[34] David Edward Bruschi, Ivette Fuentes, Thomas Jennewein, and Mohsen Razavi. Spacetime effects on satellite-based quantum communications. *Phys. Rev. D*, 90:045041, 2014.

[35] David Edward Bruschi, Animesh Datta, Rupert Ursin, Timothy C. Ralph, and Ivette Fuentes. Quantum estimation of the Schwarzschild spacetime parameters of the Earth. *Phys. Rev. D*, 90:124001, 2014.

[36] G.M. Tino, F. Sorrentino, D. Aguilera, B. Battelier, A. Bertoldi, Q. Bodart, K. Bongs, P. Bouyer, C. Braxmaier, L. Cacciapuoti, N. Gaaloul, N. Gürlebeck, M. Hauth, S. Herrmann, M. Krutzik, A. Kubelka, A. Landragin, A. Milke, A. Peters, E.M. Rasel, E. Rocco, C. Schubert, T. Schuldt, K. Sengstock, and A. Wicht. Precision gravity tests with atom interferometry in space. *Nuclear Physics B - Proceedings Supplements*, 243-244:203 – 217, 2013. Proceedings of the IV International Conference on Particle and Fundamental Physics in Space.

[37] David Edward Bruschi, Carlos Sabín, Angela White, Valentina Baccetti, Daniel K.L. Oi, and Ivette Fuentes. Testing the effects of gravity and motion on quantum entanglement in space-based experiments. *New J. Phys.*, 16:053041, 2014.

[38] Abhay Ashtekar. Singularity resolution in loop quantum cosmology: A brief overview. *Journal of Physics: Conference Series*, 189(1):012003, 2009.

[39] Carlo Rovelli and Francesca Vidotto. Planck stars. *International Journal of Modern Physics D*, 23(12):1442026, 2014.

[40] Leonard Parker and David Toms. *Quantum field theory in curved spacetime*. Cambridge University Press, Cambridge, 2009.

[41] Carlos Sabín, David Edward Bruschi, Mehdi Ahmadi, and Ivette Fuentes. Phonon creation by gravitational waves. *New J. Phys.*, 16:085003, 2014.

[42] Ji-Gang Ren, Ping Xu, Hai-Lin Yong, Liang Zhang, Sheng-Kai Liao, Juan Yin, Wei-Yue Liu, Wen-Qi Cai, Meng Yang, Li Li, Kui-Xing Yang, Xuan Han, Yong-Qiang Yao, Ji Li, Hai-Yan Wu, Song Wan, Lei Liu, Ding-Quan Liu, Yao-Wu Kuang, Zhi-Ping He, Peng Shang, Cheng Guo, Ru-Hua Zheng, Kai Tian, Zhen-Cai Zhu, Nai-Le Liu, Chao-Yang Lu, Rong Shu, Yu-Ao Chen, Cheng-Zhi Peng, Jian-Yu Wang, and Jian-Wei Pan. Ground-to-satellite quantum teleportation. *Nature*, 549:70 EP –, 08 2017.

[43] Matthias Fink, Ana Rodriguez-Aramendia, Johannes Handsteiner, Abdul Ziarkash, Fabian Steinlechner, Thomas Scheidl, Ivette Fuentes, Jacques Pienaar, Timothy C. Ralph, and Rupert Ursin. Experimental test of photonic entanglement in accelerated reference frames. *Nature Comm.*, 8:15304, 2017.

[44] Robert M. Wald. *General relativity*. University of Chicago Press, Chicago, 1984.

[45] Asher Peres. Separability criterion for density matrices. *Phys. Rev. Lett.*, 77:1413–1415, Aug 1996.

[46] D. Bini, K. Boshkayev, R. Ruffini, and I. Siutsou. Equatorial circular geodesics in the Hartle-Thorne spacetime. *Il Nuovo Cimento*, 36 C(1 Suppl. 1), 2013.

[47] D. L. Wiltshire, M. Visser, and S. M. Scott. *The Kerr Spacetime*. Cambridge University Press, January 2009.

[48] Fernando de Felice and Giovanni Preti. On the meaning of the separation constant in the Kerr metric. *Classical and Quantum Gravity*, 16(9):2929, 1999.

[49] Fernando de Felice and Donato Bini. *Classical measurements in curved space-times*. Cambridge University Press, Cambridge, 2010.

[50] Gerardo Adesso, Sammy Ragy, and Antony R. Lee. Continuous variable quantum information: Gaussian states and beyond. *Open Systems & Information Dynamics*, 21(01n02):1440001, 2014.

[51] Vittorio Giovannetti, Seth Lloyd, and Lorenzo Maccone. Advances in quantum metrology. *Nature Photonics*, 5:222 EP –, 03 2011.

[52] Mehdi Ahmadi, David Edward Bruschi, and Ivette Fuentes. Quantum metrology for relativistic quantum fields. *Phys. Rev. D*, 89:065028, 2014.

[53] Mehdi Ahmadi, David Edward Bruschi, Carlos Sabín, Gerardo Adesso, and Ivette Fuentes. Relativistic quantum metrology: Exploiting relativity to improve quantum measurement technologies. *Sci. Rep*, 4:04996, 2014.

[54] Paulina Marian and Tudor A. Marian. Uhlmann fidelity between two-mode Gaussian states. *Phys. Rev. A*, 86:022340, 2012.

[55] Harald Cramér. *Mathematical methods of statistics*. Princeton University Press, Princeton, 1999.

[56] O. Pinel, P. Jian, N. Treps, C. Fabre, and D. Braun. Quantum parameter estimation using general single-mode Gaussian states. *Phys. Rev. A*, 88:040102, Oct 2013.

[57] Rosanna Nichols, Pietro Liuzzo-Scorpo, Paul A. Knott, and Gerardo Adesso. Multiparameter Gaussian quantum metrology. *Phys. Rev. A*, 98:012114, Jul 2018.

[58] Magdalena Szczykulska, Tillmann Baumgratz, and Animesh Datta. Multi-parameter quantum metrology. *Advances in Physics: X*, 1(4):621–639, 2016.

[59] F. de Felice and C.J.S. Clarke. *Relativity on Curved Manifolds*. Cambridge University Press, Cambridge, 1992.

[60] Matthew C. Palmer, Maki Takahashi, and Hans F. Westman. Localized qubits in curved spacetime. *Annals of physics*, 327(4):1078–1131, 2012.

[61] Thomas Müller and Frank Grave. Catalogue of spacetimes. arXiv:0904.4184, 2010.

[62] Matthew C. Palmer. *Relativistic quantum information theory and quantum reference frames*. PhD thesis, University of Sydney, School of Physics, 2013.

[63] Stephen D. Bartlett and Daniel R. Terno. Relativistically invariant quantum information. *Phys. Rev. A*, 71:012302, Jan 2005.

[64] Kamil Brádler. Relativistically invariant photonic wave packets. *J. Opt. Soc. Am. B*, 28(4):727–736, Apr 2011.

[65] J. M. Weisberg, J. H. Taylor, and L. A. Fowler. Gravitational waves from an orbiting pulsar. *Scientific American*, 245:74–82, October 1981.

[66] LIGO Scientific Collaboration and Virgo Collaboration. Multi-messenger observations of a binary neutron star merger. *The Astrophysical Journal Letters*, 848(2):L12, 2017.

[67] J. Weber. Gravitational radiation. *Phys. Rev. Lett.*, 18:498–501, Mar 1967.

[68] Francesco Sorge. Do gravitational waves create particles? *Classical and Quantum Gravity*, 17(22):4655, 2000.

[69] S Fagnocchi, S Finazzi, S Liberati, M Kormos, and A Trombettoni. Relativistic Bose–Einstein condensates: a new system for analogue models of gravity. *New Journal of Physics*, 12(9):095012, 2010.

[70] Matt Visser and Carmen Molina-París. Acoustic geometry for general relativistic barotropic irrotational fluid flow. *New Journal of Physics*, 12(9):095014, 2010.

[71] David Edward Bruschi, Jorma Louko, Daniele Faccio, and Ivette Fuentes. Mode-mixing quantum gates and entanglement without particle creation in periodically accelerated cavities. *New Journal of Physics*, 15(7):073052, 2013.

[72] Richard Howl, Carlos Sabín, Lucia Hackermüller, and Ivette Fuentes. Quantum decoherence of phonons in Bose–Einstein condensates. *Journal of Physics B: Atomic, Molecular and Optical Physics*, 51(1):015303, 2018.

[73] Dennis Rätzel, Richard Howl, Joel Lindkvist, and Ivette Fuentes. Dynamical response of Bose–Einstein condensates to oscillating gravitational fields. *New Journal of Physics*, 20(7):073044, 2018.

[74] IEEE International conference on computers, systems and signal processing. *Quantum Cryptography: Public key distribution and coin tossing*, 1984.

[75] T. van Zoest, N. Gaaloul, Y. Singh, H. Ahlers, W. Herr, S. T. Seidel, W. Ertmer, E. Rasel, M. Eckart, E. Kajari, S. Arnold, G. Nandi, W. P. Schleich, R. Walser, A. Vogel, K. Sengstock, K. Bongs, W. Lewoczko-Adamczyk, M. Schiemangk, T. Schuldt, A. Peters, T. Könemann, H. Müntinga, C. Lämmerzahl, H. Dittus, T. Steinmetz, T. W. Hänsch, and J. Reichel. Bose-Einstein condensation in microgravity. *Science*, 328(5985):1540–1543, 2010.

[76] Michael A. Nielsen and Isaac L. Chuang. *Quantum computation and quantum information*. Cambridge University Press, Cambridge, 2000.

[77] Erwin Schrödinger. *Expanding universe*. Cambridge University Press, Cambridge, 2011.

[78] Subrahmanyan Chandrasekhar. *The mathematical theory of black holes*. Oxford University Press, Oxford, 1983.

[79] Henning Vahlbruch, Moritz Mehmet, Simon Chelkowski, Boris Hage, Alexander Franzen, Nico Lastzka, Stefan Goßler, Karsten Danzmann, and Roman Schnabel. Observation of squeezed light with 10-db quantum-noise reduction. *Phys. Rev. Lett.*, 100:033602, Jan 2008.

[80] IERS Numerical Standards, IAG1999. `http://hpiers.obspm.fr/eop-pc/models/constants.html`.

[81] K.U. Schreiber, T. Klügel, J.-P.R. Wells, R.B. Hurst, and A. Gebauer. How to detect the Chandler and the annual wobble of the Earth with a large ring laser gyroscope. *Phys. Rev. Lett.*, 107:173904, 2011.

[82] R. Anderson, H.R. Bilger, and G.E. Stedman. Sagnac effect: a century of Earth-rotated interferometers. *Am. J. Phys.*, 62:975, 1994.

[83] Sebastian P. Kish and Timothy C. Ralph. Estimating spacetime parameters with a quantum probe in a lossy environment. *Phys. Rev. D*, 93:105013, 2016.

[84] Timothy C. Ralph Peter P. Rohde and Michael A. Nielsen. Optimal photons for quantum-information processing. *Phys. Rev. A*, 72:052332, 2005.

[85] GOCE satellite, ESA. `https://www.esa.int/Our_Activities/Observing_the_Earth/GOCE/Satellite`.

[86] Alain Dabas. Observing the atmospheric wind from space. *Comptes Rendus Geoscience*, 342(4):370 – 379, 2010.

[87] Paweł Caban and Jakub Rembieliński. Photon polarization and Wigner's little group. *Phys. Rev. A*, 68:042107, 2003.

[88] Netanel H Lindner, Asher Peres, and Daniel R Terno. Wigner's little group and Berry's phase for massless particles. *Journal of Physics A: Mathematical and General*, 36(29):L449, 2003.

[89] Robert M. Gingrich, Attila J. Bergou, and Christoph Adami. Entangled light in moving frames. In *Frontiers in Optics*, page WAA7. Optical Society of America, 2003.

[90] André G. S. Landulfo, George E. A. Matsas, and Adriano C. Torres. Influence of detector motion in entanglement measurements with photons. *Phys. Rev. A*, 81:044103, Apr 2010.

[91] Paweł Caban. Einstein-Podolsky-Rosen correlations of photons: Quantum-field-theory approach. *Phys. Rev. A*, 76:052102, Nov 2007.

[92] Asher Peres and Daniel R. Terno. Relativistic Doppler effect in quantum communication. *Journal of Modern Optics*, 50(6-7):1165–1173, 2003.

[93] Asher Peres and Daniel R. Terno. Quantum information and special relativity. *International Journal of Quantum Information*, 01(02):225–235, 2003.

[94] G. V. Skrotskii. The influence of gravitation on the propagation of light. *Soviet Physics Doklady*, 2:226, 1957.

[95] Aharon Brodutch, Tommaso F. Demarie, and Daniel R. Terno. Photon polarization and geometric phase in general relativity. *Phys. Rev. D*, 84:104043, Nov 2011.

[96] Aharon Brodutch and Daniel R. Terno. Polarization rotation, reference frames, and Mach's principle. *Phys. Rev. D*, 84:121501, Dec 2011.

[97] Sergei Kopeikin and Bahram Mashhoon. Gravitomagnetic effects in the propagation of electromagnetic waves in variable gravitational fields of arbitrary-moving and spinning bodies. *Phys. Rev. D*, 65:064025, Feb 2002.

[98] A. R. Prasanna and S. Mohanty. Gravitational-wave-induced rotation of the plane of polarization of pulsar signals. *EPL (Europhysics Letters)*, 60(5):651, 2002.

[99] Valerio Faraoni. The rotation of polarization by gravitational waves. *New Astronomy*, 13(3):178 – 181, 2008.

[100] Liang Dai. Rotation of the cosmic microwave background polarization from weak gravitational lensing. *Phys. Rev. Lett.*, 112:041303, Jan 2014.

[101] Juan Antonio Morales and Diego Sáez. Evolution of polarization orientations in a flat universe with vector perturbations: CMB and quasistellar objects. *Phys. Rev. D*, 75:043011, Feb 2007.

[102] Mauro Sereno. Gravitational Faraday rotation in a weak gravitational field. *Phys. Rev. D*, 69:087501, Apr 2004.

[103] Maxim Lyutikov. Rotation of polarization by a moving gravitational lens. *Phys. Rev. D*, 95:124003, Jun 2017.

[104] Ue-Li Pen, Xin Wang, and I-Sheng Yang. Gravitational rotation of polarization: Clarifying the gauge dependence and prediction for a double pulsar. *Phys. Rev. D*, 95:044034, Feb 2017.

[105] Mohammad Nouri-Zonoz. Gravitoelectromagnetic approach to the gravitational Faraday rotation in stationary spacetimes. *Phys. Rev. D*, 60:024013, Jun 1999.

[106] M. L. Ruggiero and A. Tartaglia. Gravitational Faraday rotation in binary pulsar systems. *Monthly Notices of the Royal Astronomical Society*, 374(3):847–851, 2007.

[107] M. Sereno. Detecting gravitomagnetism with rotation of polarization by a gravitational lens. *Monthly Notices of the Royal Astronomical Society*, 356(1):381–385, 2005.

[108] Hideki Ishihara, Masaaki Takahashi, and Akira Tomimatsu. Gravitational Faraday rotation induced by a Kerr black hole. *Phys. Rev. D*, 38:472–477, Jul 1988.

[109] Aharon Brodutch, Alexei Gilchrist, Thomas Guff, Alexander R. H. Smith, and Daniel R. Terno. Post-Newtonian gravitational effects in optical interferometry. *Phys. Rev. D*, 91:064041, Mar 2015.

[110] F. de Felice. On the non-existence of non-equatorial circular geodesics with constant latitude in the Kerr metric. *Physics Letters A*, 69(5):307 – 308, 1979.